**MARYLAND DEPARTMENT OF TRANPORTATION
STATE HIGHWAY ADMINISTRATION**

RESEARCH REPORT

DEVELOPMENT OF A TRAFFIC MANAGEMENT DECISION SUPPORT TOOL FOR FREEWAY INCIDENT TRAFFIC MANAGEMENT (FITM) PLAN DEPLOYMENT
- Phase 3: An Incident Duration and Impact Prediction (IDIP) System -

YEN-LIN HUANG, YAO CHENG, AND GANG-LEN CHANG

UNIVERSITY OF MARYLAND, COLLEGE PARK

FINAL REPORT

May 2023

TECHNICAL REPORT DOCUMENTATION PAGE

1. Report No. MD-22- SHA/UM/6-1	2. Government Accession No.	3. Recipient's Catalog No.
4. Title and Subtitle Development of a Traffic Management Decision Support Tool for **F**reeway **I**ncident **T**raffic **M**anagement (FITM) Plan Deployment *Phase 3: An **I**ncident **D**uration and **I**mpact **P**rediction (IDIP) system*		5. Report Date May 2023.
		6. Performing Organization Code
7. Author(s) Yen-Lin Huang, Yao Cheng, and Gang-Len Chang		8. Performing Organization Report No.
9. Performing Organization Name and Address The University of Maryland, College Park, MD 20742		10. Work Unit No.
		11. Contract or Grant No. SHA/UM/6-1
12. Sponsoring Agency Name and Address Maryland Department of Transportation (SPR) State Highway Administration Office of Policy & Research 707 North Calvert Street Baltimore MD 21202		13. Type of Report and Period Covered SPR-B Final Report (Feb. 2021-May 2023)
		14. Sponsoring Agency Code (7120) STMD - MDOT/SHA
15. Supplementary Notes		

16. Abstract

This phase of the study has finalized the innovative system for real-time prediction of a detected incident's duration and its potential traffic impacts on both the subject freeway and its neighboring local streets due to the queues and resulting detouring off-ramp flows. With such information, highway agencies responsible for incident response and traffic management can inform en-route motorists via any advanced traveler information system or public media of the location and time duration over which the freeway segment will be plagued by nonrecurrent congestion queues. Depending on the severity level of the detected incidents and the estimated traffic impacts, responsible traffic agencies can either concurrently or sequentially respond with appropriate strategies.

17. Key Words Incident duration, incident queue impact, detour operations, Incident response and management.	18. Distribution Statement This document is available from the Research Division upon request.

19. Security Classif. (of this report) None	20. Security Classif. (of this page) None	21. No. of Pages	22. Price

Form DOT F 1700.7 (8-72)   Reproduction of completed page authorize

Table of Contents

List of Figures

List of Tables

Chapter 1
Introduction

1.1 RESEARCH BACKGROUND

To effectively contend with day-to-day non-recurrent congestion due to traffic incidents, the Maryland Department of Transportation State Highway Administration (MDOT SHA) has worked with the research team from the Traffic Safety and Operations Laboratory over the past three years to develop a traffic management decision support tool, known as the Incident Duration and Impacts Prediction (IDIP) system for Freeway Incident Traffic Management (FITM) plan deployment. As with most technological products, the development process for an innovative IDIP system started from its initial phase of concept proof with I-95, followed by the prototype construction in Phase II, based on Coordinated Highways Action Response Team's (CHART) incident records for I-495, I-695, I-70, and US 29. Promising results from the first two phases offer support for the IDIP system's development to progress to its third phase of refinement, generalization, and deployment.

Conceivably, for best use by CHART's response teams to minimize the incident impacts and the resulting traffic delay during their daily operations, it is expected that the proposed IDIP system in the Phase 3 development can expand its prediction function to all highway segments covered by CHART and offer a reliable estimate of the resulting queues' spatial evolution pattern during the predicted incident clearance period. Since the information on traffic queue distance due to incidents and its impacts on the neighboring surface streets is critical to the selection of the best traffic management strategy, the IDIP system in this phase has also been designed with a supplemental function to approximate the freeway volume detouring to the local routes up to the full recovery of the roadway capacity.

With all essential functions developed in this phase for IDIP, CHART's incident response team can conveniently estimate the required clearance duration for a detected incident, reliably project its maximum traffic queue distance during the response operations, and project the likely distribution of the freeway traffic detouring to the local streets during the same period. Note that IDIP's functions are developed with all field operational and information constraints in mind so that they can provide reliable and robust estimation for freeway segments with insufficient or unreliable surveillance systems.

1.2 RESEARCH OBJECTIVE

The primary objective of this study is to finalize the IDIP system's development so that CHART can reliably project the impacts of a detected incident, from detection to clearance, on its target freeway and neighboring local networks. Such an IDIP system, designed to function under an insufficient traffic surveillance system, is comprised of the following three models:

- A generalized incident duration prediction system for the entire network covered by CHART;
- A traffic queue evolution model for estimating the maximum queue distance during the incident clearance period; and
- A robust function for estimating the detouring traffic volumes and their impacts on the neighboring local network during the incident clearance period.

A graphical illustration of the proposed IDIP system and the interrelations between its three key modules is shown in Figure 1-1. The output of an online operated IDIP system can offer all information needed for CHART to best implement the traffic control/management strategies during the incident clearance period and convey the traffic conditions in a timely manner to both drivers and the general public via all available channels.
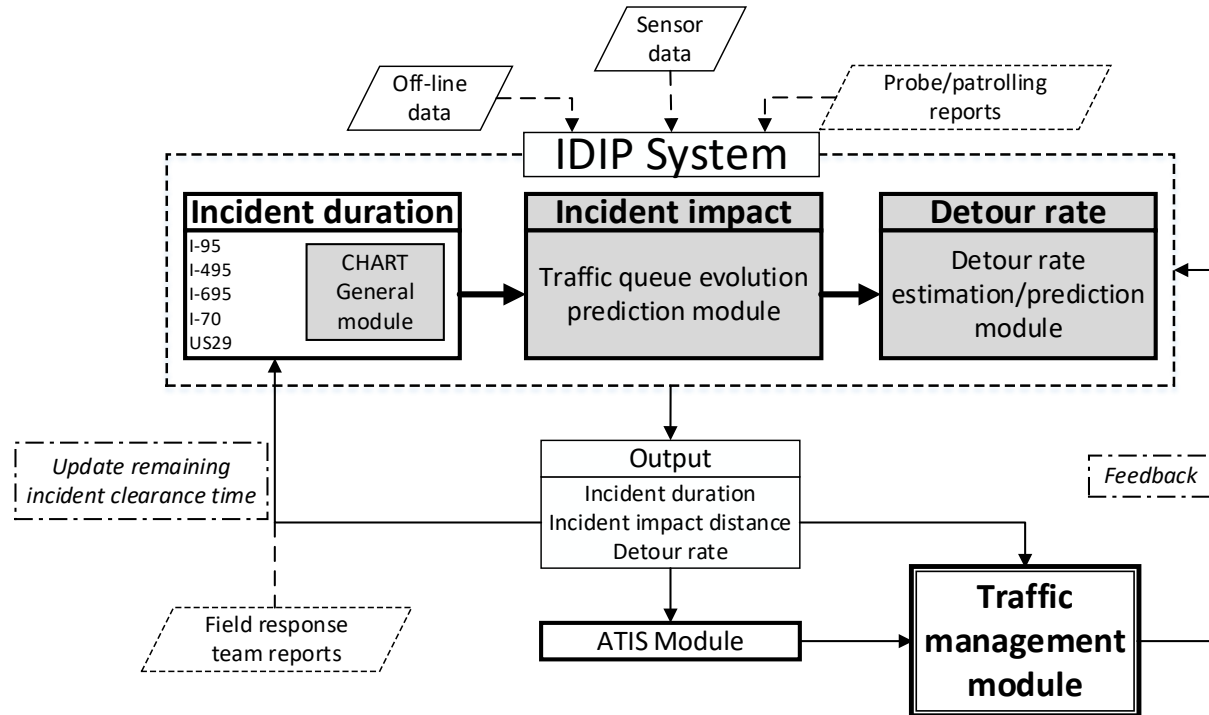
FIGURE 1-1: *Graphical Illustration of the Incident Duration and Impact Prediction (IDIP) System*

1.3 REPORT ORGANIZATION

Based on the above research objective and scope, the research team has organized all research results into six chapters. The principal results discussed in each chapter are summarized below:

Chapter 2 provides a comprehensive review of available studies related to each of the three principal models for the IDIP system, including various state-of-the-art and state-of-the-practice systems for estimating the clearance time of a detected incident, its time-varying queue distance due to roadway capacity reduction, and the impacts to neighboring arterials incurred by the detouring traffic. As the focus of this project is to produce a robust tool for incident response and management under insufficient traffic surveillance environments or in highway networks without reliable detection function, an in-depth investigation of all existing systems' applicability on Maryland's highways, having only sparsely distributed traffic sensors, constitutes the core of this chapter. The enhancement needs for SHA to operate the incident response and management at the desirable level of efficiency within the budget constraints are also discussed in this chapter.

Chapter 3 presents the innovative methodology to generalize the knowledge-based rules for incident duration prediction, developed for I-495, I-695, I-70, and US 29, for all major highways managed by CHART but with insufficient incident data for calibrating their own

2

customized prediction models. The core modeling structure of this system, featuring its innovative circumvention of the demanding development efforts and extensive data needs for calibration, is described first in this chapter, followed by a step-by-step discussion of the automated process for constructing a similar rule-based prediction system for any other highways by intelligently transferring from existing Incident Duration Prediction Model's (IDPM) embedded rules. The effectiveness of the developed knowledge-transferability method has been evaluated with multi-year incident records from other highways managed by CHART. Promising evaluation results along with some recommendations for further enhancements to cope with all data deficiency scenarios are discussed in detail in this chapter.

Chapter 4 reports the models developed for estimating the incident queue impacts on roadway traffic in real-time with and without a reliable traffic surveillance system, including its development process, innovative alternatives to cope with insufficient information from traffic detectors, and the performance evaluation results from both simulation experiments and field data. This chapter starts with a discussion of how to construct a dataset from all available archived data sources that contain the traffic queue distance under different lane-blockage incidents at different volume levels. A prediction model, based on classical traffic flow theory and the assumption of having reliable traffic sensors, is then described for estimating the time-varying traffic impact distance during the duration of incident clearance. This is followed by an extensive review of limitations and constraints often encountered by incident response teams in daily field operations. The remaining of this chapter presents the set of alternative models developed to provide the estimated traffic queues during the incident response period under the constraints of insufficient detection data in real-time operations. Results of extensive evaluations with both simulation experiments and field data are also reported in this chapter.

Chapter 5 focuses on discussing the methodology and the produced model for the traffic control center to estimate the distribution of freeway traffic over the available detouring routes during the incident clearance operations, given the identified incident nature, estimated clearance duration, and the computed maximum queue distance with and without reliable real-time traffic surveillance data. Starting with a brief review of available models for estimating the detour rate under a reliable traffic surveillance environment, this chapter devotes its first two sections to discussing the challenges in developing a robust model for estimating time-varying detouring traffic via off-ramps during incident clearance periods when such real-time traffic detection data is not available in practice. The methodology and calibration process of an innovative model, developed with the needs of incident management and the lack of traffic detection data in mind, constitute the core of this chapter. Performance evaluation results with respect to the developed model from extensive simulation experiments and field-collected data are also documented in this chapter.

Chapter 6 serves to compile all major research findings from this study, including major challenges encountered in developing each of the system's three principal modules and their key features, as well as the main strengths making the system best applicable for use in practice. Primary areas for future system enhancements when more real-time and/or archived data are available, along with the description of training needs as well as potential system deployment issues are also discussed in this chapter.

Chapter 2
System Structure and Literature Review

2.1 SYSTEM STRUCTURE

To mitigate traffic impacts due to incidents, most U.S. highway agencies have established Traffic Incident Management (TIM) programs to support detection, response, and clearance operations. Efficient execution of such vital series tasks can minimize not only the resulting traffic queues on the roadway segment, but also the likelihood of incurring secondary incidents by lane-changing vehicles. Hence, a state-of-the-art TIM program, as shown in Figure 2-1, is expected to have the following essential functions to support different stages of the incident response and operations:

- Provide an estimate of the required incident clearance duration at Stage 1 of the incident detection and response operations;
- Offer the approximate time-varying traffic queues during Stage 2 of incident clearance operations and impact estimate; and
- Assess the potential incident impacts on neighboring surface streets during Stage 3 of incident clearance and deployment of traffic management strategies.

To ensure that the development of robust models and algorithms for the above three principal functions is grounded in the accomplishments of related state-of-the-art works, this study has conducted an extensive literature review and summarized some of those major findings along with critical areas for enhancements in the remaining sections.
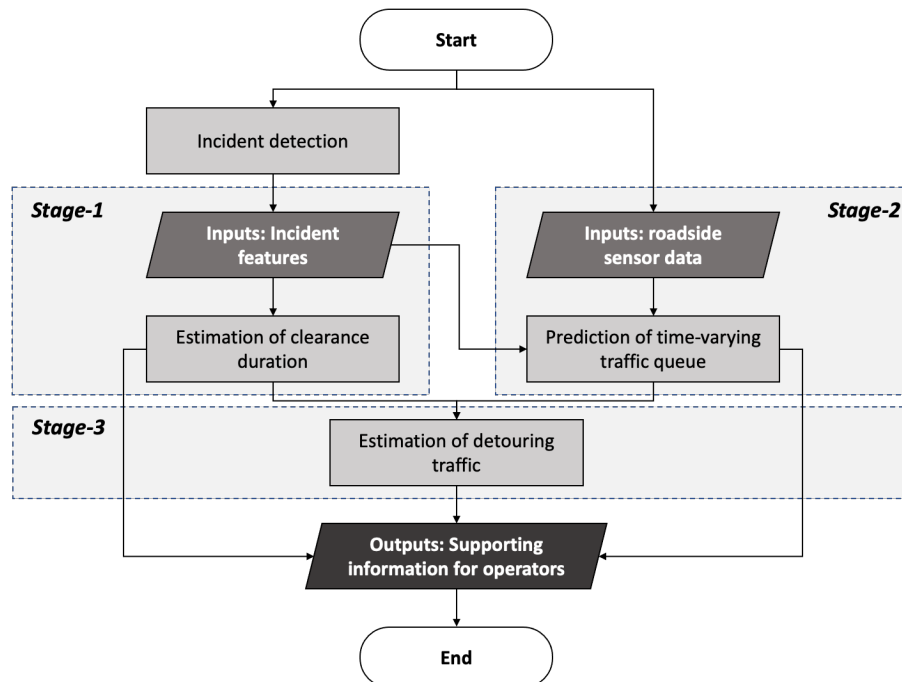
FIGURE 2-1: *Structure of a Traffic Incident Management (TIM) Support System*

2.2 PREDICTION OF THE INCIDENT DURATION

Over the past decades, transportation researchers have devoted significant efforts to developing incident duration prediction models with a variety of techniques, including continuous statistical models (Farradyne, 2000; Golob et al., 1987; Giuliano, 1989; Khattak et al., 1994; Garib et al., 1997; El-Basyouny and Sayed, 2006; Qi and Teng, 2008; Chung, 2010; Khattak et al., 2012; Wang et al., 2013; Wang et al., 2013; Hojati et al., 2013; Li and Shang, 2014; Zou et al., 2016; Khattak et al., 2016; Li et al., 2017; Wang et al., 2018; Laman et al., 2018; Hong et al., 2019), machine learning approaches (Zhang et al., 2021; Wang et al., 2005; Wei and Lee, 2007; Valenti et al., 2010; Guan et al., 2010; Wu et al., 2011; Vlahogianni et al., 2013; Park et al., 2016), discrete/classification methods (Park et al., 2017; Ozbay and Kachroo, 1999; Ozbay and Noyan, 2006; Boyles et al., 2007; Zhao et al., 2009; Chang and Chang, 2013), and hybrid modeling techniques (Ma et al., 2017; Lin et al., 2004; Kim and Chang, 2012; Ji et al., 2011; He et al., 2013; Li et al., 2015; Zhu et al., 2017; Pettet et al., 2017; Won et al., 2018; Won, 2019).

As for the statistical models, a regression model was developed by Garib et al. (1997) to determine the duration of incidents using approximately 2,000 cases. The study revealed several significant factors that affect incident duration, including the number of lanes, the number of vehicles involved, the involvement of trucks, the time of day, the response time of the police, and weather conditions. Using roughly 16,000 incident cases, Khattak et al. (2012) produced a comparable model using Ordinary Least Squares (OLS) regression. Their findings indicated an achievement of approximately 37% for the overall mean absolute percentage error (MAPE) in incidents with durations ranging from 10 to 120 minutes. Chung (2010) developed a log-logit accelerated failure time (AFT) metric model to forecast incident duration on Korean Freeway Systems. The study findings revealed a significant relationship between the duration of incidents and several key factors (e.g., number of vehicles involved, number of injuries, accident types, location, etc.). With the same focus, Hojati et al. (2013) investigated the influence of several factors on the duration of various types of incidents using data on the Australian Freeway Network. Several variables have been identified to significantly affect incident duration, including incident characteristics, location, time of day, and traffic characteristics. Li and Shang (2014) used a series of parametric AFT models and a flexible parametric AFT model to investigate the impact of various factors on different types of incidents. The study found that the general AFT model may not be sufficiently flexible to represent the hazard function adequately, thus could not capture the underlying shape exhibited from the incident duration data due to the diverse distribution of traffic incident durations. Besides, semi-parametric models may not yield the expected performance and often produce large errors for incidents of long duration. Zou et al. (2016) used the finite mixture model to investigate incident clearance time. They applied the g-component mixture model to analyze incident clearance duration using data from freeway segments in Seattle. Their study found that the proposed mixture model better described the survival and hazard probabilities of incident duration and provided more accurate predictions than the AFT model.

In recent years, the method of machine learning has also been adopted in literature to enhance the estimation of incident duration. For example, Wang et al. (2005) compared the performance of two incident duration models calibrated with fuzzy logic (FL) and artificial neural network (ANN), respectively, based on incident data from the Road Network Master

Database in the U.K. They found that both methods have difficulty in identifying outliers. Wei and Lee (2007) developed two ANN models to forecast the incident duration in a sequential manner. The first model predicted the incident duration at the time of notification, while the second model provided updates for the incident duration in the following periods. The study concluded that the developed model performed well in fitting the actual incident duration, and the ANN model was effective in smoothing the data noise. Based on the data from the Netherlands Ministry of Communication, Wu et al. (2011) developed an incident duration model using the Support Vector Regression (SVR) approach to address challenges related to small sample sizes, nonlinearity, and high-dimensional features.

Along the line of applying discrete/classification methods for incident duration estimation, Ozbay and Kachroo (1999) used the decision tree model to predict incident duration by analyzing incident data from Northern Virginia. They first applied linear regression, and then developed a hybrid decision tree for incidents that did not follow lognormal or log-logistic distributions. Ozbay and Noyan (2006) further developed a dynamic incident duration estimation tree using Bayesian Networks (BNs). They highlighted the advantages of using BNs to model and analyze incident duration data because of their ability to consider the stochastic nature of the data. Boyles et al. (2007) used the naive Bayesian classifier to predict the incident duration, which can handle incomplete information received at different times. The model, calibrated with incident data from the Georgia Department of Transportation, showed better prediction performance than the standard linear regression model. The Gradient Boosting Decision Tree (GBDT) method has been adopted by Ma et al. (2017) to address nonlinearity and imbalance issues in incident data with different types of variables. The study results suggested that the GBDT method is superior to existing algorithms, including random forest, artificial neural network, and support vector machine, for predicting incidents with very short and very long durations.

Another category of studies for estimating incident duration is to apply multiple modeling methods and then develop a hybrid model to enhance the estimation results. For example, Lin et al. (2004) developed a model to estimate incident duration by integrating the discrete choice model and the rule-based method. They applied the ordered probit model to incidents with less than 60 minutes duration. For incidents exceeding 60 minutes, they used a rule-based model to capture complex interactions between the contributing factors and the incident duration. Kim and Kim and Chang (2012) developed a model for predicting incident duration by integrating the Rule-Based Tree Model (RBTM) with the Multinomial Logit Model (MNL) or Naive Bayesian Classifier (NBC) as supplemental models. The results showed that the developed model performed well for most incidents, except for those lasting between 60-120 minutes and 240-300 minutes. He et al. (2013) proposed a Hybrid Tree-based Quantile Regression Model that combines the strengths of decision tree and quantile regression methods. They applied the unbiased recursive partitioning algorithm to develop the decision tree. The quantile regression method was then applied to each terminal node of the tree.

Despite the significant progress made by the traffic community in incident duration estimation, field implementation of such an imperative system to contend with non-recurrent congestion remains in the infancy stage. This is due partly to the fact that a large number of factors are critical to an incident's clearance time, but the associated data are difficult to collect

at a desirable level of accuracy for system development. Moreover, the complex nature (e.g., discrete, continuous, or binary) of those critically associated factors and their distributions are inconsistent with the underlying assumptions of many statistical-based methods reported in the literature, thus are mostly difficult to yield robust results for use in practice.

2.3 PREDICTION OF THE INCIDENT QUEUE LENGTH

Queue length prediction has been a widely addressed subject since it is essential information for estimating traffic delays and for the design of relevant traffic control strategies. Most such studies in literature were developed for use under either recurring or non-recurring congestion systems. A large body of works in the literature (Newell, 1968a; Newell, 1968b, Newell, 1068c, Newell, 1982, Hegyi et al., 2005, Carlson et al., 2010; Yang et al., 2016; Cheng et al., 2022) for recurrent congestion applied the input-output based method for various applications. For example, Newell (1968a, 1968b, 1968c, 1982) focused on modeling fluid-based queues in traffic systems that experience time-dependent arrival rates, using linear or quadratic functions. Yang et al. (2016) developed a mesoscopic simulation model to estimate queue lengths under different demand-to-capacity ratio scenarios, using a similar input-output method. Along the same line, Cheng et al. (2022) proposed a spatial queue model for oversaturated traffic systems with time-dependent arrival rates. Their approach involved using polynomial functional approximation to describe the dynamics of oversaturated traffic conditions, and mapping various measurements such as available flow rate, density, and end-to-end travel time to the queue evolution process.

Another common method for queue estimation under recurring congestion is shockwave analysis (Mehran and Nakamura, 2009; Hadiuzzaman and Qiu, 2013; Cao et al., 2015; Vickrey, 1969; Kuwahara and Akamatsu, 1997; Nie and Zhang, 2005; Ban et al., 2012; Han et al., 2013a; Han et al., 2013b. For example, Mehran and Nakamura (2009) employed the shockwave analysis to compute the number of queued vehicles. Nie and Zhang (2005) and Ban et al. (2012) applied the same method in their studies for computing the point-queue length (1969) for freeway traffic flows. To address the inevitable capacity, drop under such queue formation scenarios, Hadiuzzaman and Qiu (2013) proposed an enhanced model with the same shockwave methodology for freeway segments under constant flow rates. Cao et al. (2015) further extended the macroscopic shockwave model to a time-space discrete functional form, allowing the discharge flow rate to be time-dependent and the resulting queues to vary over time as manifested in field observations.

As for predicting traffic queues under non-recurring congestion, the input-output based method was also one of the widely adopted methods (Lawson et al., 1997; Erera et al., 1998; Jiang, 2001; Sheu et al., 2001; Cheevarunothai et al., 2007; Lee et al., 2008; Ullman and Dudek, 2003). For instance, Lawson et al. (1997) and Erera et al. (1998) proposed an input-output diagram approach for calculating the spatial queue length. Sheu et al. (2001) presented a discrete-time nonlinear stochastic model for real-time prediction of queue length using Kalman filtering. Ullman et al. (2003) developed a model that uses fluid-flow analogies to represent interactions between traffic queuing on and diversion from the freeway. Their model provides a rational representation of how traffic queues, upstream of temporary work zones, evolve from propagation to stabilization in urban areas. In addition, Du et al. (2017) and Lee et al. (2018)

applied ANNs to estimate work zone impacts and incident queue length. Ghosh et al. (2017) used regression analysis to predict the queue length for incidents on expressways in Singapore.

Aiming to compare the performance of these two commonly used methods (i.e., input-output and shockwave-based methods) for predicting freeway traffic queues, Nem and Drew (1998) indicated that the input-output based method tends to underestimate the overall delays compared with the shock-wave analysis. However, Hurdle and Son (2001) pointed out that despite the discrepancy in defining queue length, these two methods produce identical estimates of travel time and delay. Similarly, Cao et al. (2014) noted that both methods are compatible and capable of providing accurate estimates of real-time queue length upstream of a bottleneck.

As for the queue prediction at a signalized intersection, Akçelik (1997) proposed a method for such needs by modifying the parameters of the Highway Capacity Manual Queue Estimation Model. Mirchandani and Head (2001) and Sharma et al. (2007) proposed similar methods for approximating intersection queues based on the predicted vehicle arrival and release rates, using the conventional input-output method. Geroliminis and Skabardonis (2005) and Li et al. (2018) applied the Lighthill-Whitham-Richards (LWR) shockwave theory Lighthill and Whitham, 1955; Richards, 1956) to predict the signalized queue length.

In brief, despite the tremendous efforts made in predicting traffic queues using various approaches, the complex and mutually dependent relations between the queue propagation speed and arriving flow rate remain better captured in most existing studies, because drivers, when approaching the bottleneck and perceiving the queue formation in real-time, may slow down their speed. Furthermore, the discharge flow rate under lane-blockage scenarios may vary by which and how many lanes are being blocked and consequently result in different lane-changing and car-following behaviors to form the queue pattern. Besides, most existing studies are grounded in the assumption of having extensively deployed traffic sensors with reliable data quality which, however, often does not hold in most freeway incident response scenarios, thus rendering most existing models not applicable for use in practice.

2.4 ESTIMATION OF THE DETOURING RATE DURING FREEWAY TRAFFIC BLOCKAGE

Detouring rate estimation during recurring and non-recurrent congestions has been extensively investigated for off-line and real-time applications in the literature. Aiming at estimating the detouring rates with historical data, most existing methods for off-line applications belong to either stated preference or revealed preference from field observations.

The former category of methods often adopts surveys or driving simulators to collect travelers' stated preferences and then estimates the percentages of travelers who choose to detour under various scenarios of information availability. For example, Peeta et al. (2000) examined the impact of a Dynamic Message Sign's (DMS) contents and other pertinent factors on the resulting detouring rates, reporting that 53% of drivers would opt for an alternative route if the expected delay on their current route exceeds 10 minutes. Their model has further been adopted by Peeta and Gedela (2001) to construct a DMS control heuristic framework.

With extensive surveys, Huchingson and Dudek (1979) found that a driver's detour decision depends mainly on the displayed time savings, much less on all other factors such as incident type and traffic conditions. Khattak et al. (1993) reported some scenarios during which drivers would be more likely to select a detour route. Examples of such scenarios include when the delay on their commuting routes is expected to increase due to incidents; the delay condition was observed directly versus received from the radio; or whether drivers are heading to work or home.

Along the same line, Kattan et al. (2010) adopted a latent choice model to further identify some hidden factors that may critically affect a driver's detour decision, such as prior driving experience, familiarity with alternative routes, trip purpose, trip time, trip length, and complementary information sources (e.g., the radio). Al-Deek et al. (2009) employed a discrete logit model to estimate diversion behaviors on toll roads in Central Florida, based on variables such as travel time, delay, information source, network familiarity, and specific trip characteristics. Based on stated preference data collected from the driving simulator, Xiong et al. (2016) created a diversion behavior model using naïve Bayes rules. A relatively comprehensive detour rate study with stated preference is available in the work by Abdel-Aty and Abdalla (2004) who collected drivers' responses from driving simulators and applied the maximum likelihood estimation to approximate the detouring rate, taking into account both pre-trip and en-route decisions with or without advice to divert.

Despite the extensive studies with various stated preference methods, most of such estimated diversion percentages were found to be lower than those obtained in the second category of studies based on revealed preference surveys and traffic measurements. For instance, Chatterjee and MacDonald (2004) conducted a comprehensive survey across six European countries to assess the impact of DMS on traffic diversion. Their results indicate that the diversion rates were found to be between zero to 7% for incident messages and zero to 35% for route guidance information. Using data from Bluetooth detectors, a study conducted in Maryland (Haghani et al., 2013) revealed a diversion rate within the range of 5% to 18%. Foo and Abdulhai (2006) computed the diversion rate from traffic detector data after implementing DMS for sharing traffic conditions on Highway 401 in Toronto, Ontario, Canada, and found the average to be around 5.55%. Hadi et al. (2013) concluded that the actual detouring rate may vary between 10% to 35%, depending on the number of blocked and total lanes.

Note that unlike offline applications, most works for real-time detouring rate estimation need to collect real-time traffic data to further enhance the estimation accuracy and to account for day-to-day traffic evolution and complex dynamics, especially during non-recurrent congestion. For example, Essien et al. (2021) presented a traffic prediction model using Long-Short-Term Memory (LSTM), integrated traffic data, and their patterns reported in social media. Some studies along this line rely on the timely acquisition of traffic volume information and then perform the estimation by assessing the instantaneous inflow and outflow rates during incidents (He et al., 2013; He et al., 2016) or utilizing the cumulative statistics to compare the volume on a typical day with the volume during the incident (Hadi et al., 2013). With the same assumption on information availability for all entering volumes, Sadek et al. (1998, 1999) have developed an automated traffic routing decision support system using various artificial intelligence techniques.

In summary, despite the significant contributions of existing studies on estimating detouring rates during congested traffic scenarios, how to effectively update such estimates with real-time information to reflect the local and real-time traffic conditions, especially during incident scenarios, remains a challenge to the traffic community. Some studies that can take advantage of real-time data usually rely on the widely deployed traffic sensors that can provide reliable traffic data at the desirable quality and precision. However, such desirable traffic surveillance environments do not commonly exist in most existing highway networks and in most states, due to various constraints such as deployment costs, technical limitations, and various maintenance as well as operational issues. Moreover, most scarcely deployed freeway detectors are distributed on either mainline segments and/or on-ramps, less likely at off-ramps for computing the detour flow rate. Hence, to obtain accurate time-varying estimates of the detouring rates, it is critical that any proposed method for potential use in practice ought not to rely on the availability of traffic sensors at either the off-ramps or upstream segment of the incident location.

Chapter 3
Extending the I-95 Rule-based Incident Duration System with an Automated Knowledge Transferability Model

3.1 RESEARCH BACKGROUND

It is well recognized that traffic incidents can result in a roadway's capacity reduction and reliability degradation, and significant delays for commuters. Over the past several decades, many U.S. highway agencies have established a Traffic Incident Management (TIM) system to help mitigate such impacts and restore normal traffic conditions. A TIM system typically consists of a coordinated multi-disciplinary process to detect, respond to, and clear traffic incidents. It is expected that such a system can effectively reduce the clearance duration of detected incidents and reduce the resulting impacts on traffic delay and safety. To do so, a TIM system first needs a reliable and robust model to predict the required duration for incident clearance operations, and then to assess its time-varying traffic queues as well as resulting delays, because such information is essential for determining the proper control strategies and the responsive traffic management tasks.

As presented in Chapter 2, despite the significant progress made by the traffic community on this subject, the implementation of such an imperative system to contend with non-recurrent congestion remains in the infancy stage. This is due partly to many factors (see Table 3-1) that are critical to an incident's clearance time, but difficult to collect at a desirable level of accuracy for system development. Moreover, the complex nature (e.g., discrete, continuous, or binary) of those critically associated factors and their distributions are inconsistent with the underlying assumptions of many statistical-based methods reported in the literature. In view of such constraints, Won et al. (2018) explored the methodology of integrating the expertise of field responders and extensive information from the incident records to calibrate a rule-based Incident Duration Prediction Model (IDPM). Their proposed knowledge-based model was first applied to Maryland I-95 and later extended to I-495 and I-695.

Further extension of the flexible and robust method by Won et al. (2018) to other Maryland highways (such as I-70 and U.S. 29), however, inevitably encounters the challenges of insufficient incident records for calibration of prediction rules and demand of significant involvement of experienced incident-response operators. Hence, this chapter presents a Knowledge Transferability Analysis (KTA) model, intending to explore the potential of constructing a new IDPM by transferring some of those prediction rules from existing IDPMs, based on their effectiveness to the new target highway. With such a computerized and effective KTA model, traffic professionals need to apply the resource-demanding method by Won et al. (2018) only to the small set of incidents that exhibit unique patterns and demand local-specific incident response resources.

The next section will provide a brief description of the knowledge-based IDPM by Won et al. (2018). This is followed by a detailed presentation of the proposed KTA method for new system construction. An application of the KTA to developing the IDPM for Maryland I-70 constitutes the core of its following section. Concluding comments and future research tasks are summarized in the last section.

TABLE 3-1: *Factors Associated with the Clearance Time of a Detected Incident*

Category	Variables	Classification
Incident Type	Incident type	Collision with Fatality (CF), Collision with Personal injury (CPI), Collision with Property Damage (CPD)
Time	Hour indicator	AM-peak, Day time, PM-peak, Night
	Weekend indicator	Weekend, Weekday
	Holiday indicator	Holiday, Non-Holiday
	Season indicator	Spring, Summer, Fall, Winter
Location	Direction indicator	Northbound, Southbound, Eastbound, Westbound
	Exit number indicator	Exit 1, Exit 2, …
Environmental Conditions	Pavement condition indicator	Dry, Wet, Snow-ice, Chemical wet
	Hazard material related	Yes, No
Operation Center	Center indicator	AOC, TOC3, TOC4, TOC5, SOC
Lane Blockage Information	# of blocked lanes	1, 2, 3, 4, …
	# of blocked shoulder lanes	0, 1, 2, 3, …
	# of blocked travel lanes	0, 1, 2, 3, …
	# of blocked auxiliary lanes	0, 1, 2, 3, …
	Travel lane blocked in tunnel	Yes, No
	Travel lane blocked in toll	Yes, No
Involved Vehicle Information	Vehicle status	Jack-knifed, Over-turned, Lost-load
	# of total involved vehicles	1, 2, 3, 4, …
	# of involved passenger cars	0, 1, 2, 3, …
	# of involved trucks	0, 1, 2, 3, …
	# of involved motorcycles	0, 1, 2, 3, …
Response Unit Information	# of total response units	1, 2, 3, 4, …
	# of arrived CHART	0, 1, 2, 3, …
	# of arrived police	0, 1, 2, 3, …
	# of arrived fireboard	0, 1, 2, 3, …
	# of arrived medical service	0, 1, 2, 3, …
	# of arrived tow service	0, 1, 2, 3, …
	First responder	CHART, Police, Fireboard, Medical, Tow

3.2 DEVELOPMENT OF A KNOWLEDGE-BASED IDPM

Figure 3-1 illustrates the development process proposed by Won et al. (2018), using the Association Rule Mining method (Agrawal et al., 1993; Hahsler et al., 2005) for rule generation and statistical tests to construct prediction rules for different types of incidents.
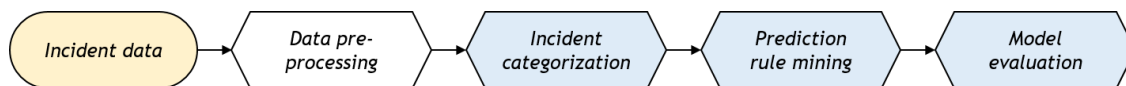
FIGURE 3-1: *Development Process of the Knowledge-Based IDPM (Won, 2019)*

Incident Categorization

 Given the pre-processed incident dataset, all incident records from the target highway will be first classified into several subsets based on incident type and lane blockage information. For instance, all collisions resulting in lane closure, as shown in Figure 3-2, are typically divided into three categories: Collision with personal injury (CPI), collision with property damage (CPD), and collision with fatality (CF). Depending on the available incident records, one may further classify each of the three categories by the number of closed lanes. For instance, due to the small sample size and unique clearance duration pattern, all incidents in CF are grouped in one cluster. The incident records resulting in only shoulder lane blockage are not further decomposed because the clearance times for all such incidents distribute consistently within a relatively stable and short interval.
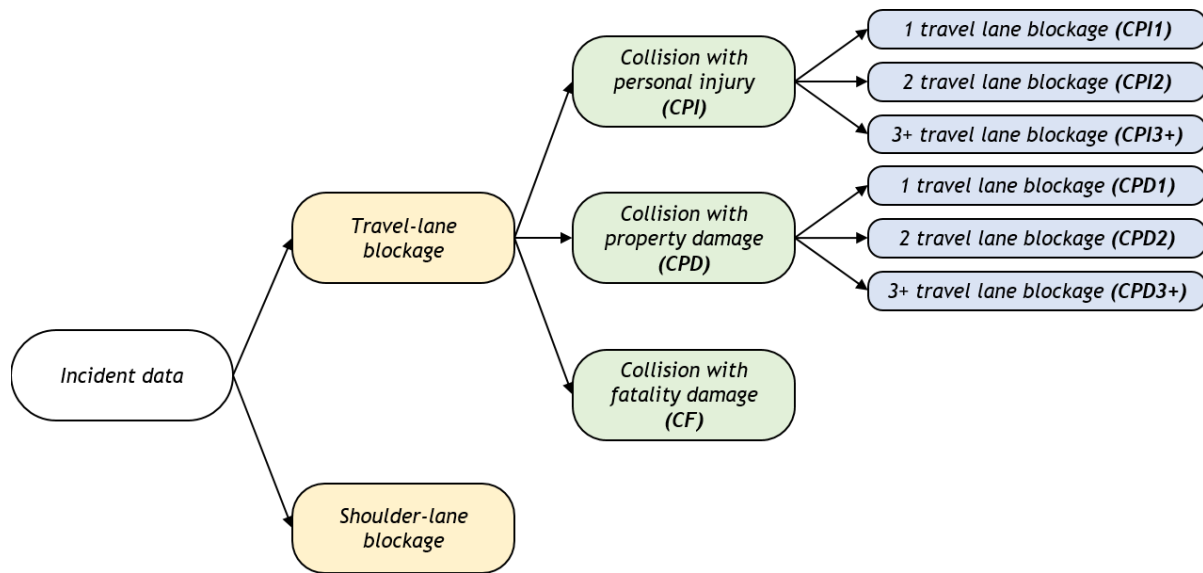
FIGURE 3-2: *Incident Categorization Based on the Incident Type and Lane Blockage Information*

Prediction Rules Mining Process

 After the initial categorization of available incident records, one can then proceed with the following procedures to construct a set of "IF-THEN" rules for the estimated clearance time for each of those finalized subsets of incidents:

Collision with Personal Injury (CPI) and Collision with Property Damage (CPD)

 The incident data in those six subsets of CPI and CPD would be first classified into two classes of "< 30 minutes" and "≥ 30 minutes" by using the Association Rule Mining method. Then, the incident data classified in the class of "≥ 30 minutes" is further divided into two groups of "< 60 minutes" and "≥ 60 minutes" for searching other classification rules. With the same logic, one can then further decompose the incident data group of "≥ 60 minutes" into two clusters of "< 120 minutes" and "≥ 120 minutes." Finally, based on the distribution of the incident clearance durations, three intervals of the estimated clearance duration corresponding to the confidence levels of 60%, 70%, and 80% can be produced from the sequential classification process. Figure 3-3 illustrates such a process by using CPI with two-lane blockage on I-95 from 2012 to 2015 as an example.
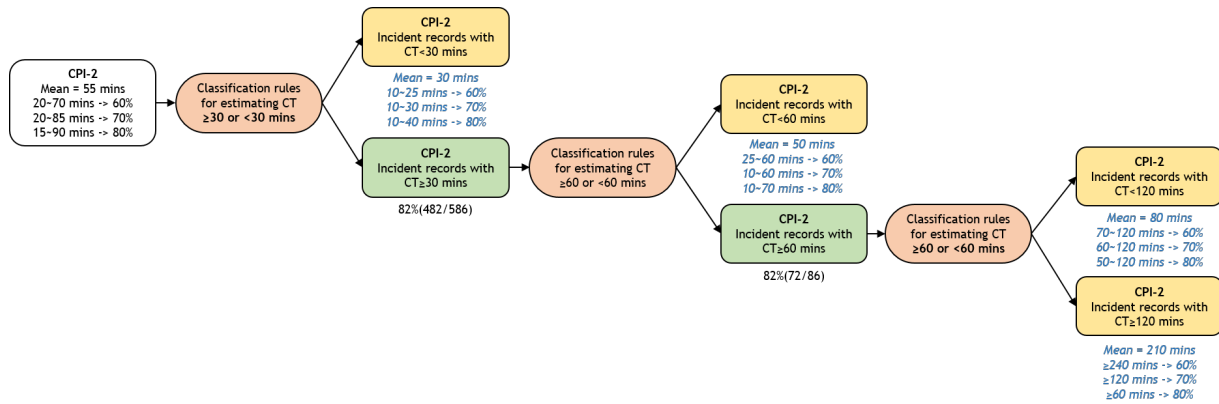
FIGURE 3-3: *An Example of the Sequential Classification Process (2)*

Collision with Fatality (CF)

Notably, compared with CPD and CPI, nearly all highways, by nature, have many fewer incidents resulting in collision with fatality. In view of the very small sample size for CF, Won et al. (2018) suggested adopting a different search process for identifying robust rules to estimate their required clearance durations. A detailed illustration of such a process is available in their works (Won et al., 2018; Won, 2019).

Figure 3-4 presents the application process of the developed IDPM-I-95 software, including its key input data, underlying classification and estimation structure, and the resulting outputs. Note that the system provides an interval-based, rather than a point-based estimate for a detected incident's duration to accommodate the data quality and availability, which are often imperfectly collected during the emergency incident response process. Additionally, such a model was later extended to I-495 and I-695; all three developed models, as shown in Table 3-2, have produced the expected level of performance sufficient for use in daily incident response operations.
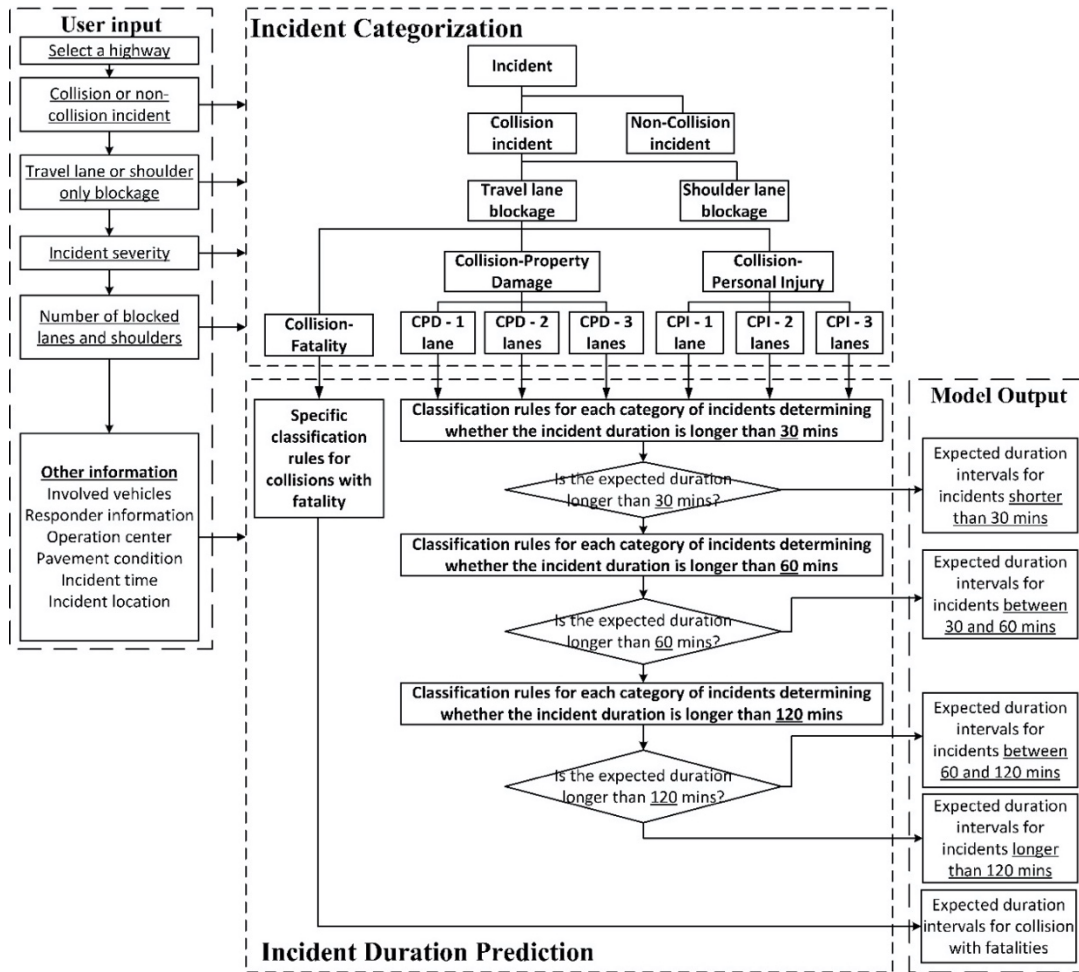
FIGURE 3-4: *The Application Process of the Developed IDPM-I-95 Software (Won, 2019)*

TABLE 3-2: *Performance of IDPMs for I-95, I-495, and I-695 by Incident Type and Blocked Lane*

Highway	Collision with Travel Lane Blockage						
	CPI 1	CPI 2	CPI 3+	CPD 1	CPD 2	CPD 3+	Total
I-95	77.2%[a]	84.6%	78.8%	74.3%	80.5%	83.7%	77.1%
(2012-2017)	(446/578)	(203/240)	(82/104)	(795/1070)	(177/220)	(41/49)	(1744/2261)
I-495	78.7%	78.7%	61.7%	79.8%	81.6%	79.2%	80.0%
(2015-2018)	(392/498)	(295/375)	(113/183)	(631/791)	(301/369)	(95/120)	(2018/2523)
I-695	85.6%	82.4%	78.7%	87.0%	87.6%	82.7%	85.9%
(2016-2019)	(297/347)	(150/182)	(59/75)	(842/968)	(219/250)	(43/52)	(1610/1874)

[a] The percentage represents % of incidents of which durations were captured within the predicted interval with an 80% confidence level

3.3 KNOWLEDGE TRANSFERABILITY ANALYSIS (KTA) METHODOLOGY

The primary functions of the KTA model are to first assess the transferability of available prediction rules and then identify their respective priorities in the transferring sequence. This is

due to the fact that the complex interrelations between the existing prediction rules—such as those mutually exclusive or supplementary in nature—may render the effectiveness dependent on not only which rules to adopt, but also their sequence of execution in the decision structure. Figure 3-5 illustrates the process for the rule transferability analysis including: 1) generation and update of the Rule Box to include available prediction rules from existing systems; 2) ranking of key factors for constructing available prediction rules; 3) identification of the transferring priority for available prediction rules; and 4) effectiveness assessment with respect to all transferred prediction rules.
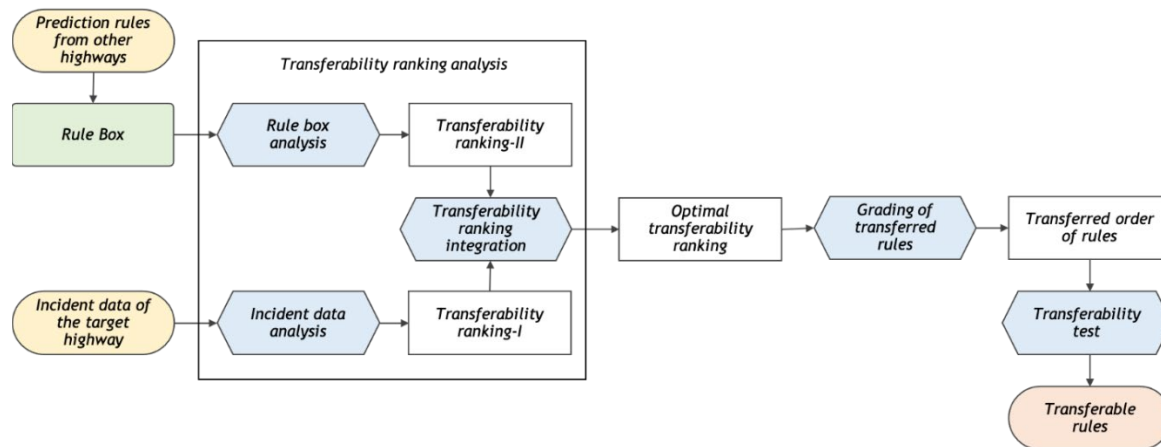
FIGURE 3-5: *Illustration of the Transferability Analysis in the KTA Model*

Rule Box Generation and Update

The primary function of the Rule Box is to house all effective prediction rules from existing IDPMs for assessing their transferability to a highway of similar features and incident patterns. As such, all well-calibrated prediction rules for the IDPMs for I-95, I-495, and I-695 are collected and classified into six categories, as shown in Figure 3-6, based on the incident nature and the resulting number of blocked lanes. Depending on their usage for incident duration prediction, such rules in each category are further divided into six types with three pre-specified thresholds for classifying incident durations (i.e., 30, 60, and 120 minutes).
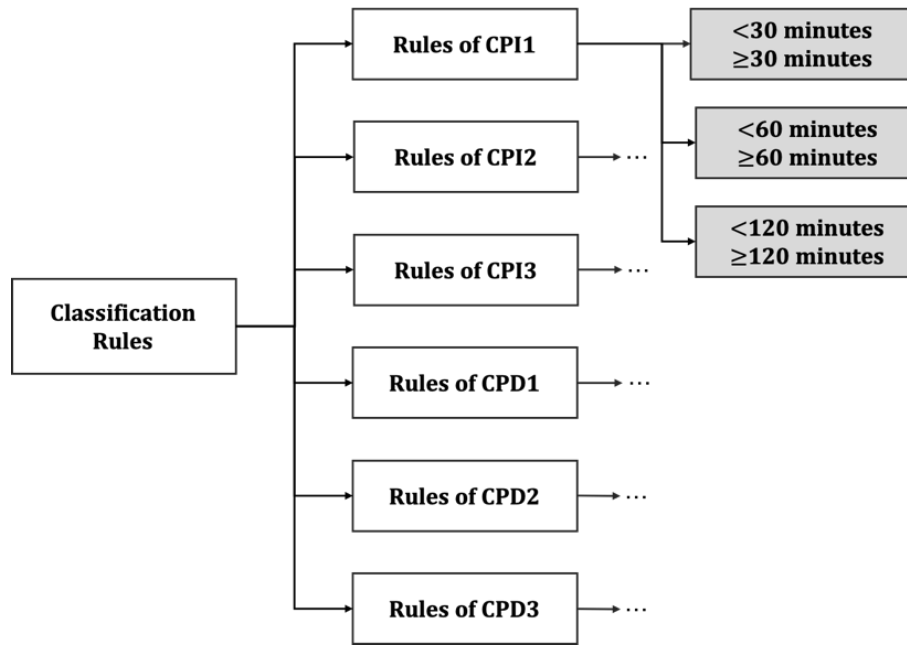
FIGURE 3-6: *Classification of the Prediction Rules in the Rule Box*

Ranking of Key Factors Used in Constituting Prediction Rules

As stated previously, the rule transferring priority concurrently determines not only which rules to transfer, but also the execution structure of the new IDPM. Hence, the set of prediction rules having the highest transferring priority shall have the following properties:

- Their included factors for prediction are also the most critical set of contributors to the incident durations on the target new highway; and
- They have achieved the highest level of prediction effectiveness with respect to incidents on their own highways.

The methodology for assessing the transferability priority for each set of available rules in the Rule Box, based on the above two essential properties, is presented hereafter. First of all, all key factors contributing to the required incident duration are initially classified into the following seven categories, as shown in Table 3-3.

TABLE 3-3: *List of the Incident Duration's Key Contributing Factors Classified by Category*

Category	Description	Item
Category-1 *(# of responders)*	the number of different responders at the incident scene	# of total response units # of arrived CHART # of arrived police # of arrived fireboard # of arrived medical service # of arrived tow service
Category-2 *(First arrived responder)*	type of the first-arriving responders	Police first arrived Medical service first arrived Tow service first arrived CHART first arrived Fireboard first arrived
Category-3 *(Vehicle status)*	the number and the type of vehicles involving in incidents and their damage levels	Overturned, lost-load, jack-knife # of total involved vehicles # of involved passenger cars # of involved trucks # of involved motorcycles
Category-4 *(Pavement conditions)*	indicators for the pavement conditions	Wet, dry, snow-ice, chemical wet, hazard material related
Category-5 *(Lane blockage)*	indicators to denote the lane-blockage conditions	# of blocked lanes # of blocked shoulder lanes # of blocked travel lanes # of blocked auxiliary lanes Travel lane blocked in tunnel Travel lane blocked in toll
Category-6 *(Operation center)*	indicators reflecting different incident response centers	AOC, TOC3, TOC4, TOC5, SOC
Category-7 *(Time)*	temporal-related indicators associated with an incident	AM peak, PM peak, daytime, night weekday, weekend holiday, non-holiday Spring, Summer, Fall, Winter

Transferability Ranking-I Analysis

The purpose of this task is to identify the relative impacts of the above seven categories of factors on the resulting incident durations revealed in the target new system's incident records. To do so, this study has adopted the permutation-based variable-importance measure (Biecek and Burzykowski, 2020) for ranking analysis, and provided a brief description of its core logic below:

Given a set of n incident records for p contributing factors and the incident clearance duration Y, then, let X denotes the matrix of p columns and n rows, and the column vector of $\underline{y}$ shows the observed values of Y. As such, $\hat{\underline{y}} = \left(f(\underline{x}_1), \dots, f(\underline{x}_n) \right)'$ denotes the corresponding vector of predictions from the Random Forest *(46)* for $\underline{y}$ for model $f()$, and $\mathcal{L}(\hat{\underline{y}}, \underline{X}, \underline{y})$ be a loss function to quantify the goodness-of-fit. Then, the core algorithm can be summarized into the following steps:

- **Step 1**: Compute $L^0 = \mathcal{L}(\hat{\underline{y}}, \underline{X}, \underline{y})$ (i.e., the value of the loss function for the original data). Then, for each contributing factor X^j included in the model, repeat steps 2-5.
- **Step 2**: Create a matrix $\underline{X}^{*j}$ by permuting the *j-th* column of $\underline{X}$, i.e., by permuting the vector of observed values of X^j.
- **Step 3**: Compute the model's predicted $\hat{\underline{y}}^{*j}$ based on the modified data $\underline{X}^{*j}$.
- **Step 4**: Compute the value of the loss function for the modified data: $L^{*j} = \mathcal{L}(\hat{\underline{y}}^{*j}, \underline{X}^{*j}, \underline{y}^{*j})$
- **Step 5**: Quantify the importance of X^j (vip_{Ratio}^j) by calculating $vip_{Ratio}^j = L^{*j}/L^0$

With the computed importance of each contributing factor, one can do the ranking analysis based on the highest-importance factor in each category. For instance, if "the total number of responders" is identified to be the most important factor, then the category (i.e., Category 1) having this factor would be assigned the highest rank of 1. By excluding all other factors in Category 1 from the ensuing comparisons, if the next one with the highest importance in the remaining list is "number of trucks involved," then the category (i.e., Category 3) having this factor shall be assigned a rank of 2. The same procedures can be iteratively executed to identify the proper rank for each of the remaining categories.

Transferability Ranking-II Analysis

The core of Ranking-II analysis is to rank the importance associated with each category of factors from the perspective of how often they have been used in the existing IDPMs' prediction rules and the resulting effectiveness. The measurements proposed for such an analysis are defined below:

- **Coverage**: For a given category of factors, its coverage is measured by the total number of incident records in the base dataset (i.e., total incident records from I-495, I-95, and I-495 for their model developments) that have been predicted by any set of rules which contain one or more factors from this category. For instance, the set of 134 rules that contain either one or more factors from the category of "# of responders" has been used to predict the duration for 2,979 incidents in the base dataset.

- **Accuracy**: The total number of correctly predicted incidents out of the total "coverage" associated with each category. For instance, the group "the number of responders" is assessed to yield an "accuracy" level of 83.42%, based on their applications to 2,797 incidents.

- **Proportion of conjunctive rules**: The number of rules constituted with the command of "AND" out of the total rules (defined as frequency) associated with each of those seven pre-classified groups of factors.

With these measurements, one can compute the resulting rank for each category of factors under Rank-II analysis with the following Data Envelopment Analysis (DEA) method (Charnes et al., 1978), in which the objective function is to maximize the total positive measurements for each category:

$$Maximize \qquad E_k = \sum_{r=1}^{s} u_i y_{rk} \qquad (1)$$

$$Subject\ to \qquad \sum_{r=1}^{s} u_r y_{rk} - \sum_{i=1}^{m} v_i x_{ik} \leq 0$$

$$\sum_{r=1}^{s} v_i x_{ik} = 1$$

$$u_r \geq 0,\ r = 1, \dots, s$$

$$v_i \geq 0,\ i = 1, \dots, m$$

where E_k denotes the relative effectiveness of category k among all categories ($k = 1, \dots, 7$), u_r and v_i represent weights for the rth positive measurement (i.e., coverage and accuracy levels) and i^{th} negative measurement (i.e., *proportion of conjunctive rules*), respectively; y_{rk} is the standardized value for the rth measurement in category k, and x_{ik} is the standardized value for its ith negative measurement computed from the base dataset.

The computed effectiveness value for each category will then serve as an indicator for ranking the effectiveness of the seven categories of factors used by the existing IDPMs.

Transferability Ranking Integration
Given the rank assessment from both perspectives, one can then take the following steps to produce the final ranking list for the seven categories of factors:

Let δ_i^* be the optimal rank for category i; r_i^1 denotes the resulting rank from Rank-I test for category i; r_i^2 represents the resulting rank from Rank-II test for category i; and w_i stands for the number of existing rules using one or more factors from category i. Then, with the objective function shown in Equation (2), one can employ the method for rank aggregation by Pihur, Datta, and Datta (Pihur et al., 2009) to produce the final optimized ranking list for all categories.

$$Min \sum_{i=1}^{7} (|\delta_i^* - r_i^1| + |\delta_i^* - r_i^2|) \times w_i \qquad (2)$$

The final ranking for the categories will be in descending order where the category ranked at the top of the list indicates that it contains the set of contributing factors with the most impacts on a detected incident's resulting clearance duration. However, it is noticeable that the Rule Box, due to the contributions from several well-developed IDPMs, may contain multiple

prediction rules for the same category of incidents, but with different categories of factors. Thus, the following process has been proposed in this study to finalize the optimal transferring priority for such rules.

Prioritizing Candidate Rules for Transferability Analysis

For the convenience of assessing the transferring priority, all candidate rules based on their logic structure and target incident types are characterized into four types and assigned a specified score. Now, let Category 1 (i.e., # of responders) be the category with the computed rank of 1 and Category 7 (i.e., time) with the computed rank of 5, the following presents a priority sequence, given by examples, for assigning the weights for each type of rules:

- **Type A rules**: Assigning a score for each of those rules with a simple IF-THEN statement for estimating the lower bound of an incident's clearance duration, based on the rank of the category that includes the factor embedded in the rule. For instance, the rule, *"IF [more than 8 response units arrived], THEN the duration >120 minutes"* will be assigned with a score of "**1**," because the condition variable of "8 response units" is one of the Category 1 factors.

- **Type B rules**: Assigning a score for those with a simple IF-THEN statement for estimating the upper bound of an incident's clearance duration, based on the rank of the group that comprises the factor constituting the rule and an additional status score of **"200,"** to ensure that all such rules will be assessed and transferred after all other types of rules. For instance, the rule, *"IF [no tow service arrived], THEN the duration <30 minutes"* will be assigned the assessment score of **"201,"** because its condition variable of "no tow service," belongs to Category 1 factors.

- **Type C rules**: Assigning a score for those rules constituted with a nest of IF-THEN statements and the relation of "AND," based on the sum of scores computed from the rank of the group associated with the factor constituting each IF-THEN statement in the entire set of rules connected with "AND." For instance, the rule of *"IF on [holiday] AND [tow service arrived], THEN the duration >60 minutes"* will be assigned with the assessment score of **"6,"** because its two condition variables, [holiday] and [tow service arrived], belong to factors in Category 7 and Category 1, respectively.

- **Type D rules**: Assigning the score for those Rules with a nest of IF-THEN statements and the relation of "OR" based on the sum of its assigned priority status score of **"100"** and the lowest rank among those categories which include the factors embedded in all IF-THEN statements connected with "OR." As such, the rule of *"IF on [weekend] OR [police arrived], THEN the duration >30 minutes"* will be assigned with the assessment score of **"101,"** because its two condition variables, [weekend] OR [police arrived], belong to Category 7 and Category 1, respectively. Thus, the final assessment score for this rule shall be the sum of **"100"** plus **"1."**

Transferability Effectiveness Test

As with the standard practice for transferability analysis, this study adopts the following two Measures of Effectiveness (MOEs) for assessing each candidate rule's performance with respect to the incident records from the target roadway: 1) the *confidence level* that demonstrates the accuracy of a candidate rule, and 2) the *support level* that shows the percentage of incident records that are consistent with the set of "IF" conditions in an identified prediction rule.

21

Conceivably, those prediction rules yielding a sufficiently high *confidence level* and having a reasonable *support level* will be deemed transferable. As illustrated in Figure 3-7, the entire process for transferability effectiveness assessment with respect to all candidate prediction rules in the Rule Box can be illustrated with the following steps:

- **Step 1**: Determine the minimum *confidence level* ($X\%$) and the lower bound ($S_L\%$) as well as the upper bound ($S_U\%$) of the *support level*, based on the information in the Rule Box and the available incident records from the target highway.
- **Step 2**: Utilize the incident data in each subset of CPI and CPD on the target highway to verify the effectiveness of each candidate rule with respect to its applicable incident group.
- **Step 3**: Transfer the prediction rule to the new model if it can achieve the *confidence level* and the *support level* specified in Step 1.
- **Step 4**: Filter out the incident records already successfully classified by a prediction rule from the target incident dataset and proceed with the same transferability analysis process with the remaining incident records.
- **Step-5**: Stop the transferring process if no more classification rules can be transferred, otherwise, go to Step 2.
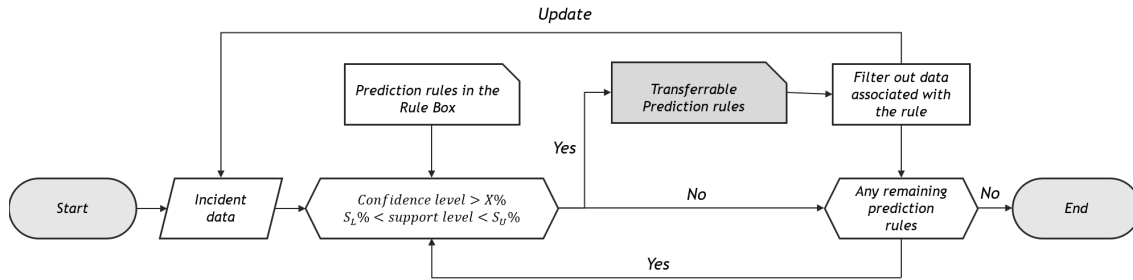
FIGURE 3-7: *Flow Chart of the Transferability Test in the Classification Rules Transferring Process*

3.4 CASE STUDY: I-70 IN MARYLAND

For illustration and evaluation of the proposed KTA method, this study has selected I-70 in Maryland for the case study. The 2016-2018 incident records from the CHART II Database were for model calibration, and those from 2019 served for performance evaluation. As illustrated in Figure 3-8, the system covers I-70 from Exit 1 to Exit 94 in Maryland.
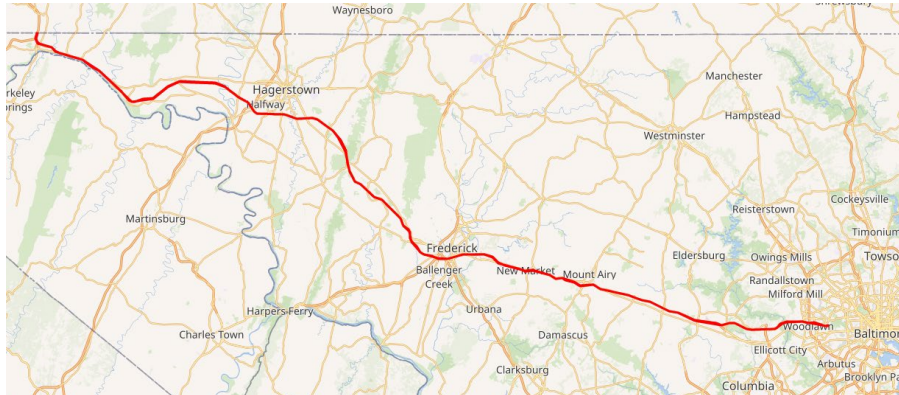
FIGURE 3-8: *Spatial Scope of the IDPM–I-70*

Incident Categorization

Figure 3-9 shows the results of the initial incident categorization, including the mean for each categorized group and the range of its variation within the confidence intervals of 60%, 70%, and 80%. Note that due to the lack of sufficient samples, CPI3 and CPD3 are merged with CPI2 and CPD2, respectively.
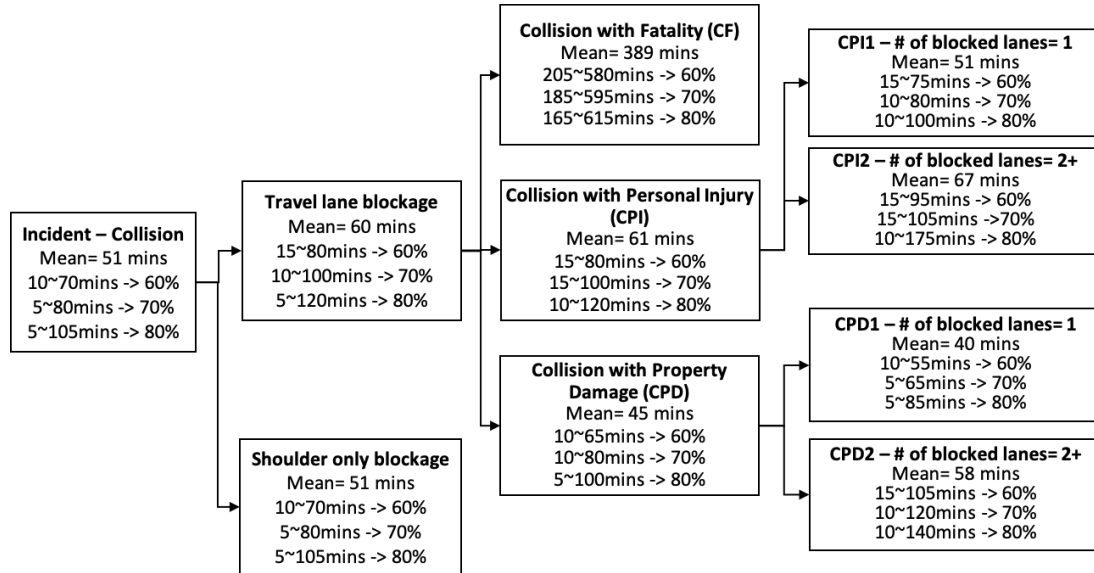
FIGURE 3-9: *Initial Incident Categorization and Estimated Clearance Duration for I-70*

Transferability Ranking-I

Figure 3-10 shows the results of Ranking-I transferability analysis, where the relative importance of the seven categories is based on the factor of the highest rank included in each category. For instance, "# of total responders" is identified to be the most important factor, thus the category (i.e., Category 1: # of responders) including this factor would be assigned with the highest rank of 1. Then, by excluding all other factors in Category 1 from the list for comparison, the next one with the highest importance is "# of involved trucks." Hence, Category 3 (i.e., Vehicle status), containing this factor, shall be assigned the rank of 2.
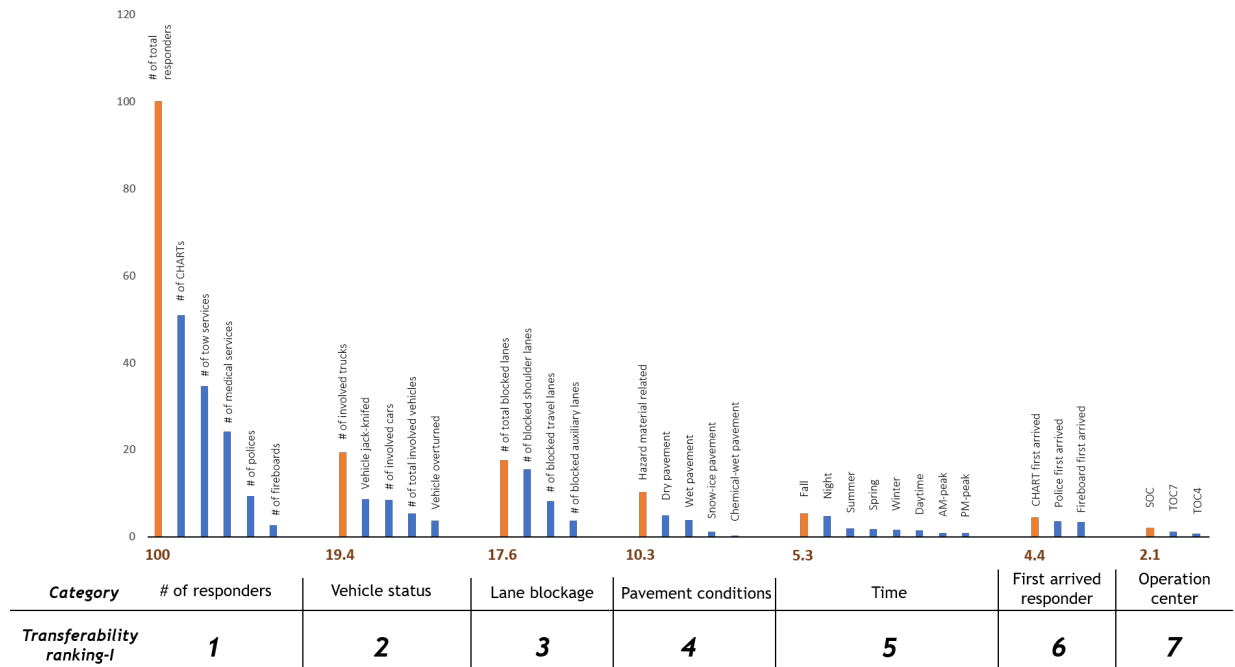
FIGURE 3-10: *Results of Transferability Ranking-I Analysis for I-70*

Transferability Ranking-II

Table 3-4 presents the properties of seven categories of factors used to construct the prediction rules from the existing IDPMs, and the results of transferability ranking analysis with respect to their effectiveness, where those categories with higher E-values are given higher priorities for the transferability assessment.

TABLE 3-4: *Results of Transferability Ranking-II Analysis for I-70*

	# of Responders	First arrived responder	Vehicle status	Pavement conditions	Lane blockage	Operation center	Time
Coverage (# of cases)	2979/0.665[a]	247/0.074	1478/0.640	1220/0.203	343/0.154	596/0.079	684/0.268
Accuracy (mean)	83%/0.377	75%/0.341	85%/0.383	89%/0.404	88%/0.398	82%/0.370	82%/0.371
Proportion of conjunctive rules	0.59/0.331	0.80/0.449	0.64/0.357	0.39/0.246	0.68/0.380	0.69/0.386	0.81/0.457
$E-val$	1.000	0.411	0.642	1.000	0.567	0.521	0.444
Rank	1	7	3	1	4	5	6

Note:
[a] The left-hand side of the number is the measurement (e.g., 2979), while the right-hand side is the normalized measurement (e.g., 0.665).

24

Finalized Ranking for Transferability Assessment

Table 3-5 reports the finalized ranking results, reflecting the relative importance of those categories of factors in the transferability assessment. For instance, those candidate prediction rules, comprising factors from the category "# of responders" should be given the highest priority in the sequence of transferring effectiveness assessment for I-70.

TABLE 3-5: *Final Ranking Analysis Results for all categories of factors*

	# of Responders	First arrived responder	Vehicle status	Pavement conditions	Lane blockage	Operation center	Time
Frequency	134	15	129	41	31	16	54
Transferability ranking-I	1	6	2	4	3	7	5
Transferability ranking-II	1	7	3	1	4	5	6
Optimal transferability ranking	**1**	**7**	**2**	**4**	**3**	**6**	**5**

Transferring and Generation of Prediction Rules

Overall, 36 out of the total 54 prediction rules in the IDPM-I-70 are transferred from existing IDPMs for I-95, I-495, and I-695, and the remaining 18 rules were calibrated with the same method by Won et al. (42) to reflect some local-unique incident patterns. Figure 3-11 illustrates the example of the rule-generation process for CPI2 and its application with all embedded "IF-THEN" rules. Table 3-6 lists the prediction rules of IDPM–I-70 transferred from IDPMs for I-95, I-495, and I-695.

(a)

Collision, CPI2		Transferring Priority Grade	Accuracy	Transferable or not
[Tow service arrived]	≥30 mins	1	86%(24/28)	Yes
[More than 4 response units]	≥30 mins	1	100%(1/1)	Yes
[More than 5 response units]	≥30 mins	1	NaN%(0/0)	No
[Peak hour] AND [More than 4 response units]	≥30 mins	4	0%(0/1)	No
[More than 1 involved vehicles] AND [Motorcycle involved]	≥30 mins	6	NaN%(0/0)	No
[AOC center]	≥30 mins	6	NaN%(0/0)	No
[Weekend] AND [SOC center]	≥30 mins	11	NaN%(0/0)	No
([Auxiliary lane blocked] AND [Pickup involved]) OR [More than 6 response units]	≥30 mins	101	0%(0/1)	No
([More than 3 response units] OR [Police first arrived] OR [Truck involved]) AND [More than 3 involved vehicles]	≥30 mins	103	NaN%(0/0)	No
([Daytime] OR [More than 2 involved vehicles]) AND [Vehicle overturned]	≥30 mins	104	NaN%(0/0)	No
[Winter] OR [Night]	≥30 mins	105	29%(2/7)	No
[Dry pavement]	<30 mins	204	89%(8/9)	Yes

[Tow service arrived] — Yes → ≥30 mins
No ↓
[More than 4 response units] — Yes → ≥30 mins
No ↓
[Dry pavement] — Yes → <30 mins
No ↓
local-unique Prediction rule mining
[Snow-ice pavement] — Yes → ≥30 mins
No ↓
Else then (# of remaining data = 2) → <30 mins

(a)

(b)

If
- [Tow service arrived] — Then >30
- [More than 4 response unit arrived] — >30
- [Dry pavement] — <30
- [Snow-ice pavement] AND [More than 2 response units arrived] — <30

Else then — <30

→ Cases with 0 < CT < 30 minutes
→ **Cases with CT ≥ 30 minutes**

If
- [More than 6 response units arrived] — Then >60
- [More than 1 Fireboard arrived] OR [Snow-ice pavement] — >60
- [No tow service arrived] OR [No truck] — <60
- [More than 1 truck involved] — >60

Else then — <60

→ Cases with 30 ≤ CT < 60 minutes
→ **Cases with CT ≥ 60 minutes**

If
- [More than 7 respond units arrived] OR [More than 5 vehicles involved] — Then >120
- [More than 1 truck involved] OR [More than 3 vehicles involved] OR [Hazard materials related] OR [More than 7 respond units arrived] — >120
- [More than 4 vehicles involved] OR [Wet pavement] — >120
- [Truck involved] — >120

Else then — <120

→ Cases with 30 ≤ CT < 120 minutes
→ Cases with CT ≥ 120 minutes

(b)

FIGURE 3-11: *An Example of an Application for CPI with Two-Travel-Lane Blockage. (a) The generation Process of the Prediction Rules; (b) The Application Process*

TABLE 3-6: *Prediction Rules of the IDPM for I-70 Transferred from I-95, I-495, and I-695*

Transferred Rules Description – CPI1			
IF	[Tow service arrived]	THEN	≥30
IF	[More than 3 vehicles involved]	THEN	≥30
IF	[More than 1 CHART arrived] AND [Police first arrived]	THEN	≥30
IF	[Peak hour] AND [More than 2 vehicles involved]	THEN	≥30
IF	[Car overturned] AND ([Weekend] OR [Tow service arrived])	THEN	≥30
IF	[Fireboard first arrived]	THEN	<30
IF	[Snow-ice pavement] OR [More than 1 truck involved] OR [More than 7 respond units arrived] OR [AOC center]	THEN	≥60
IF	[No tow service arrived] AND [No truck involved]	THEN	<60
IF	[Less than 4 respond units] OR [No truck involved]	THEN	<120
Transferred Rules Description – CPI2			
IF	[Tow service arrived]	THEN	≥30
IF	[More than 4 response units arrived]	THEN	≥30
IF	[Dry pavement]	THEN	<30
IF	[More than 6 response units arrived]	THEN	≥60
IF	[More than 1 Fireboard arrived] OR [Snow-ice pavement]	THEN	≥60
IF	[No tow service arrived] OR [No truck]	THEN	<60
IF	[More than 7 respond units arrived] OR [More than 5 vehicles involved]	THEN	≥120
IF	[More than 1 truck involved] OR [More than 3 vehicles involved] OR [Hazard materials related] OR [More than 7 respond units arrived]	THEN	≥120
IF	[More than 4 vehicles involved] OR [Wet pavement]	THEN	≥120
Transferred Rules Description – CPD1			
IF	[Tow service arrived] AND [Fireboard arrived]	THEN	≥30
IF	[More than 2 CHART arrived] AND [CHART first arrived]	THEN	≥30
IF	[Wet pavement] AND [More than 1 police arrived] AND [Auxiliary lane blocked] AND [Shoulder lane blocked]	THEN	≥30
IF	[More than 2 CHART arrived] OR ([More than 4 respond units arrived] AND [Wet pavement])	THEN	≥30
IF	([Daytime] AND [More than 4 respond units arrived]) OR ([Truck involved] AND [More than 1 police arrived])	THEN	≥30
IF	[Dry pavement]	THEN	<30
IF	[More than 6 response units arrived] OR [Truck overturned] OR [Bus involved] OR [Vehicle lost load]	THEN	≥60
IF	[Truck involved] AND ([More than 5 respond units arrived] OR [Auxiliary lane blocked])	THEN	≥120
IF	[Snow-ice pavement] OR ([Auxiliary lane blocked] AND [Chemical wet pavement])	THEN	≥120
Transferred Rules Description – CPD2			
IF	[Tow service arrived] AND [Fireboard arrived]	THEN	≥30
IF	[Snow-ice pavement] OR [Chemical wet pavement] OR [Truck jackknifed] OR [More than 6 respond units arrived]	THEN	≥30
IF	([Night] OR [More than 4 respond units arrived]) AND [More than 1 police arrived]	THEN	≥30
IF	[Car overturned] OR [More than 1 shoulder lane blocked] OR ([Truck involved] AND [Pickup involved])	THEN	≥30
IF	[More than 1 tow service arrived]	THEN	≥60
IF	[Truck involved] AND [More than 5 response units arrived]	THEN	≥60
IF	([Truck involved] OR [More than 2 vehicles involved]) AND [Night]	THEN	≥60
IF	[More than 1 tow service arrived]	THEN	≥120
IF	[No truck involved]	THEN	<120

Model Evaluation

The evaluation results of the IDPM for I-70 with both transferred and customized local rules are shown in Table 3-7. Noticeably, the IDPM-I-70 constituted mostly transferred rules (i.e., 36 out of 54 rules) that can achieve an accuracy level of 87% with the training dataset (i.e., 2016-2018) and 82% with the test dataset (i.e., 2019). Its level of performance is comparable to existing IDPMs but demands much less resources with an automated computer program and needs not to be constrained by the available size of incident records.

Table 3-8 shows the comparison results between the IDPMs for I-70 with and without the KTA model, where the former yields a better accuracy even though both models have similar training accuracy. This is due to the fact that even if one can find the common prediction rules among incident records in the training dataset to fit with a sufficient level of training accuracy, such rules might be too specific (e.g., overfit), due to the lack of enough data samples, to capture those incident records in the test dataset. The proposed KTA model, in contrast, relies on a great number of empirical rules from previously developed IDPMs which have been proven reliable in estimating incident duration, thus it can be more robust in providing an acceptable and even better accuracy.

TABLE 3-7: *Results of Model Evaluation for IDPM–I-70*

	Evaluated by groups of incident records					
	CPI1	**CPI2**	**CPD1**	**CPD2**	**CF**	**Overall**
Training set (2016-2018)	87.80%	85.37%	86.17%	87.50%	100%	86.94%
	(36/41)	(35/41)	(81/94)	(35/40)	(6/6)	(193/222)
Test set (2019)	100.00%	68.75%	78.26%	90.00%	100%	81.67%
	(10/10)	(11/16)	(18/23)	(9/10)	(1/1)	(49/60)

Note: Numbers in the parenthesis represent "the number of data whose clearance time is correctly estimated by the model/the total number of incident records in the group."

TABLE 3-8 *Comparison Between the Models Developed with and without the KTA Model*

	Model 1	**Model 2**
KTA Model	Yes	No
Training Accuracy	86.94%	83.84%
Testing Accuracy	81.67%	69.05%
Total # of Rules	54	31

3.5 CONCLUSIONS

To circumvent the demanding development efforts and the need for an extensive dataset for calibration of an IDPM's prediction rules, this study has developed an innovative Knowledge Transferability Analysis (KTA) model that allows the construction of a new system to take advantage of existing IDPMs' embedded rules with an automated process. The proposed model

features the use of a series of transferability analysis methods with respect to the existing IDPMs to identify the effectiveness and transferring priority of those adopted prediction rules.

The effectiveness of the proposed model has been evaluated with the incident data from I-70 in Maryland. The result of extensive evaluation with multi-year incident records indicates that the performance of the IDPM for I-70, with 67% of transferred rules, can yield prediction accuracy comparable to existing IDPMs that demand much more development resources. Although a more extensive assessment of the proposed KTA method can be done for other highways in different regions, the preliminary results from the I-70 case study seem to offer a promising avenue for responsible highway agencies to cope with the difficulty of insufficient incident records in the IDPM development for some highways.

Future research along this line includes: 1) extending the KTA model's application to major signalized arterials mostly with a small size of well-documented incident records, and 2) constructing a supplemental module to enhance the efficiency and robustness of the rule-based IDPMs.

Chapter 4
Real-time Incident Queue Propagation (R-IQP) Model for Highways with Insufficient Traffic Surveillance Information

4.1 PROBLEM NATURE

The primary challenge for estimating a major incident's queue impacts in real-time lies mainly in the lack of reliable data to reflect the outflow capacity at the lane blockage location and the incoming flow rate from upstream roadway segments. Such data inadequacy in practice is likely due to various factors, including, but not limited to, no detector deployment, long spacing between detectors, or poor data quality. Hence, to provide a robust estimate of incident queue impacts, a prediction model for use in daily operations shall function effectively under the following traffic surveillance scenarios:

- **Scenario 1**: Sufficient detectors with quality data are available over the target roadway segment.
- **Scenario 2**: Only sparsely distributed detectors on the target roadway segment.
- **Scenario 3**: The real-time data from either well-spaced or sparsely distributed detectors fail to provide information on traffic speed, flow rate, or occupancy.
- **Scenario 4**: No deployment of traffic detectors on the target roadway.

Incident Queue Dynamics

Regardless of available traffic data, the first challenge for developing the R-IQP model is to reliably reflect the complex queue dynamics under various incident lane-blockage scenarios. Figure 4-1 illustrates key factors and their contributions to the formation of incident queue dynamics. For example, the queue discharging rate is time-varying in nature, depending on the number of incident-blocked lanes and the type of lane-changing maneuvers by the open-lane traffic. The resulting shockwave propagation speed is further affected by the ramp volume and the mainline arriving flow rate. Conceivably, the dynamic nature of most such key factors demands that any impact prediction model for use in practice should be capable of performing timely updates with any real-time available information.
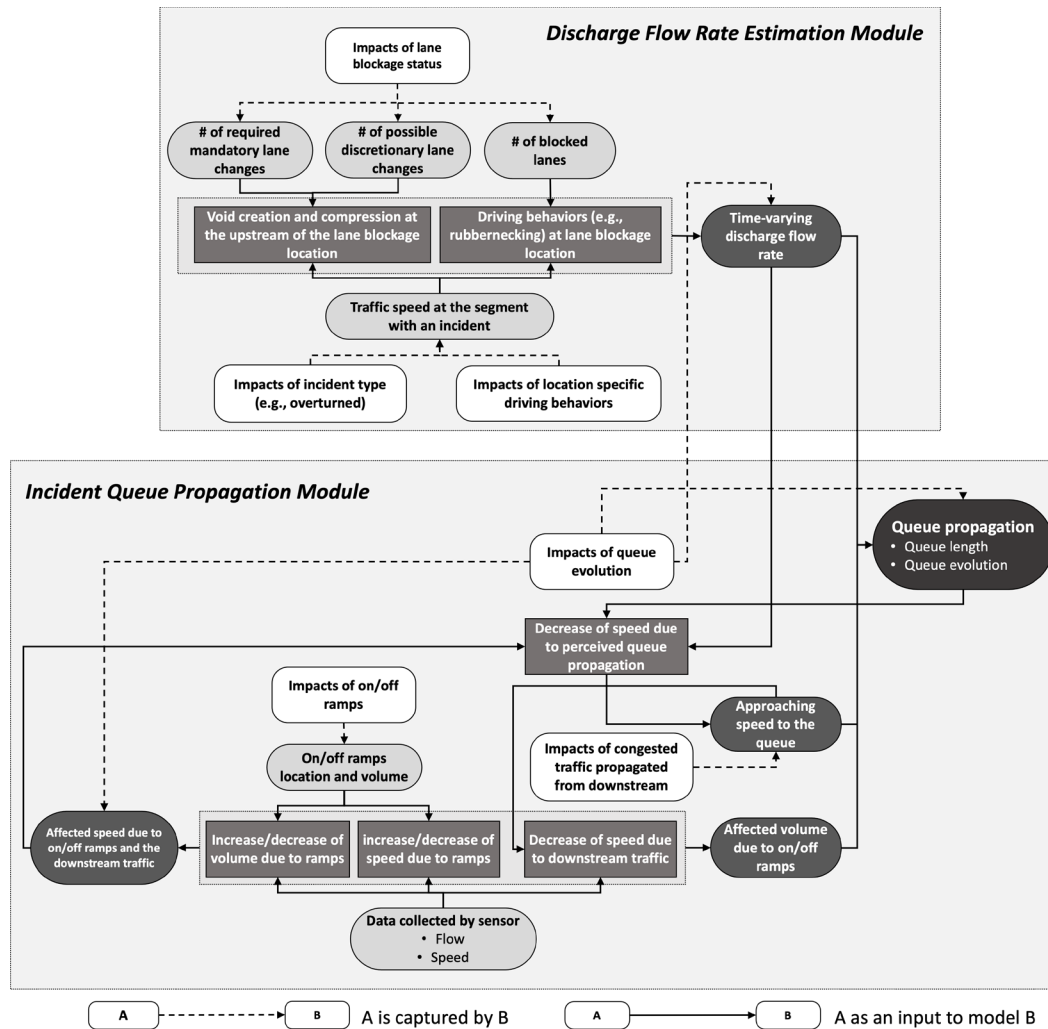
FIGURE 4-1: *The Interrelations Between Critical factors and the Formation of Incident Queue Dynamics*

Estimation of the Discharging Flow Rate

The actual outflow capacity from the lane drop spot is naturally less than the expected capacity of the open lane, known as the capacity drop phenomenon (Weng and Meng, 2013; Yuan et al., 2017). Extensive experimental results confirm that such additional reduction is approximately 5% to 30% below its theoretical capacity (Kerner, 2002; Cassidy and Bertini, 1999; Sarvi et al., 2007; Chung et al., 2007; Elefteriadou et al., 1995; Persaud et al., 1998; and Yi and Mulinazzi, 2007), attributing mainly to the slower lane-changing vehicles that create local voids during the merging process as illustrated in Figure 4-2(a) (Leclercq et al., 2016; Wang and Meng, 2013; and Won, 2019). More specifically, compared with mandatory lane changes, the impacts from discretionary lane changes tend to be less significant because their resulting voids are mostly created by vehicles with less reduced speeds at locations relatively away from the lane blockage spot. Note that such voids, if created concurrently by sequential lane-changing maneuvers are likely to be compressed, as illustrated in Figure 4-2(b).

31
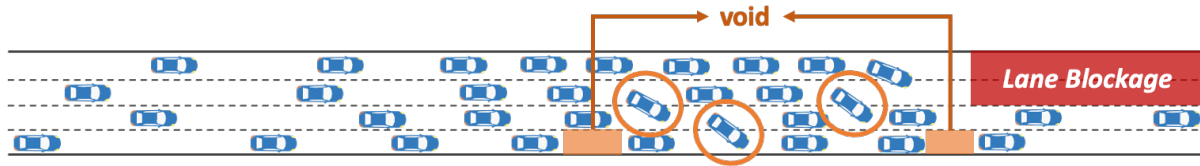
(a) Schematic figure of the slower merging vehicles that create local voids
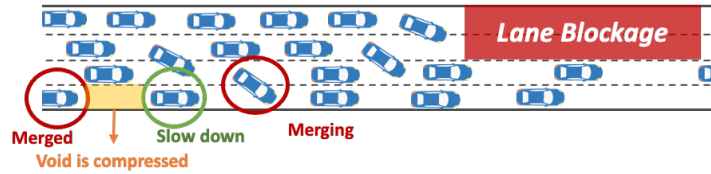
(b) Schematic figure of the multiple lane changes

FIGURE 4-2: *Illustration of Vehicle Discharging Process During Incidents*

In addition, the discharging flow rate may also be affected by the rubbernecking impacts, resulting from drivers' perceptions and responses to the severity at the incident scene.

In summary, the discharge flow rate from a lane-blockage segment is a time-varying variable to be estimated from real-time traffic data, because it varies with incident nature, traffic states, and driving behaviors.

Propagation of the Incident Queues

Assuming the lane blockage status remains unchanged during part of the incident clearance period, the speed of the queue propagation generally increases with the upstream coming traffic speeds and flow rates which may also be affected by weaving vehicles entering and leaving the roadway, and also by the potential spillback from off-ramps.

In addition, vehicles from upstream segments tend to reduce their speeds when approaching and perceiving the incident queue, which further contributes to the complex mutual impacts between the queue propagation speed and the arriving flow rates as well as speeds.

Primary Functions of the Proposed R-IOP

In response to the aforementioned needs, the proposed model for incident queue impacts is designed to flexibly execute the following functions for highways segments from having ideal coverage of reliable traffic detectors to the extreme scenario of no sensor placement at all:

- Reliably reflect the time-varying discharge flow rate under various lane-blockage incident scenarios;
- Robustly capture the incident-incurred queue propagation patterns based on the upstreaming coming traffic and discharging flow rate during incident clearance operations; and
- Dynamically update the estimated impacts to upstream traffic due to the incident queues and resulting shockwaves.

4.2 REAL-TIME INCIDENT QUEUE PROPAGATION (R-IQP) MODEL

Table 4-1 summarizes the key notations for variables used in the R-IQP model under the perfect traffic surveillance scenario (i.e., Scenario 1):

TABLE 4-1: *Key Notations for the Real-Time Incident Queue Propagation (R-IQP) Model*

Freeway-related variables	
i	Segment index
m	On-ramp
n	Off-ramp
k	Time index
v_i^k	Recorded speed from the sensor on segment i at time interval k (mph)
q_i^k	Recorded flow rate from the sensor on segment i at time interval k (veh/hr)
λ_i	Number of lanes at the location of segment i
v_f	Free flow speed
C	Theoretical capacity (veh/hr)
ρ^{jam}	Jam density (veh/mile)
Incident-related variables	
D_i	Distance from the sensor of segment i to the incident spot (mile)
L_p	Length of the TMC segment where the incident occurs
D_p	Distance from the upstream location of the TMC segment where the incident occurs to the incident spot (mile)
v_p^k	Recorded probe speed of the TMC segment where the incident occurs at time interval k (mph)
λ_B^k	Number of blocked lanes at time interval k
$L_q(t)$	Queue length at time t (mile)
CT	Estimated lane clearance duration (mins)
q_k^d	Discharge flow rate at time interval k (veh/hr)

Incident Queue Propagation Model under Scenario 1

Under Scenario 1, the arriving flow rate and speed data are available from sensors upstream of the incident scene for computing the queue propagation process.

Figure 4-3 illustrates the queue propagation process due to an incident, where shockwaves at different speeds may occur between traffic at subsequent detectors, because drivers may begin to reduce speeds at different rates depending on the distance to the perceived queue spot, and thus contribute to the formation of different speeds of waves in the traffic stream between detectors.

33

FIGURE 4-3: *The Spatial Recursive Evolution of the Queue Dynamics*

More specifically, let the entire time needed for vehicles, detected by the sensor on segment i at interval k to join the queue, be denoted as T_i^k, and decomposed it into the following three-time intervals:

$$T_i^k = T_{i,a}^k + T_{i,b}^k + T_{i,c}^k \tag{1}$$

where, $T_{i,a}^k$ is the time duration for vehicles, detected at the sensor on segment i at time interval k, to maintain the same speed (v_i^k) until they are forced to exercise a speed reduction due to encountering of the slow downstream traffic flows. Such traffic state changes will naturally form a wave ($w_{i-1,i}$) in the vehicle stream between two detector stations. Hence it can be expressed as follows:

$$T_{i,a}^k = \begin{cases} \dfrac{D_i - D_{i-1}}{w_{i-1,i} + v_i^k}, & w_{i-1,i} > 0 \\ 0, & \text{otherwise} \end{cases} \tag{2}$$

$$w_{i-1,i} = \frac{q_{i-1}^k - q_i^k}{\left(\dfrac{q_{i-1}^k}{v_{i-1}^k}\right) - \left(\dfrac{q_i^k}{v_i^k}\right)} \tag{3}$$

$T_{i,b}^k$ is the time duration for vehicles, detected at the sensor on segment i at time interval k, to travel with the reduced speed ($\bar{v}_{i,b}^k$) due to the slower downstream traffic until they start to further decelerate when they observe the end of the queue. Such reduced speed ($\bar{v}_{i,b}^k$) shall be lower or equal to the average speed of the downstream traffic, ($\bar{v}_{i-1}^k$). By introducing the parameter k, it can be expressed as follows:

$$\bar{v}_{i,b}^k = \bar{v}_{i-1}^k \times \kappa, \ \text{ for } 0 < \kappa \leq 1 \tag{4}$$

34

$T_{i,c}^k$ is the time duration for vehicles, detected by the sensor on segment i at time interval k, from noticing the incident queues to eventually joining them. Specifically, vehicles often start to reduce their speeds from a proper distance to join the queue safely and smoothly.

As such, let $\bar{v}_{i,c}^k$ be the estimated average speed of vehicles detected by the sensor on segment i at time interval k during the time duration from noticing to eventually joining the incident queues, and q_d^k be the recorded discharge flow rate at the lane blockage spot at time interval k, then one can formulate $T_{i,c}^k$ as follows:

$$T_{i,c}^k = \frac{\tau}{\frac{q_i^k - q_d^k \times \left[1 - \delta_B^{(-CT)}\right]}{\rho^{jam}\lambda_i} + \bar{v}_{i,c}^k} \tag{5}$$

$$\bar{v}_{i,c}^k = \bar{v}_{i,b}^k - \left(\bar{v}_{i,b}^k - v_q^k\right) \times \alpha \tag{6}$$

where τ indicates the distance from the end of the queue when vehicles start braking to join the queue; α indicates the reduction rate for vehicles to reduce the speed from $\bar{v}_{i,b}^k$ to v_q^k; and the term, $\frac{q_i^k - q_d^k \times \left[1 - \delta_B^{(-CT)}\right]}{\rho^{jam}\lambda_i}$, is for computing the queue propagation speed, where $\left[1 - \delta_B^{(-CT)}\right]$ is the function to approximate the reduction in the outflow at the end of the queue under different lane blockage scenarios and incident durations, in which δ_B is the parameter to be calibrated for each lane blockage scenario.

With the computed $T_{i,a}^k$ and $T_{i,c}^k$ and by replacing $T_{i,b}^k$ with $T_i^k - T_{i,a}^k - T_{i,c}^k$, the travel distance for vehicles detected by the sensor on segment i at time interval k to completely joined the queue can be formulated as follows:

$$D_i - \left[L_q\left(T_{i-1}^k\right) + \frac{q_i^k - q_d^k \times \left[1 - \delta_B^{(-CT)}\right]}{\rho^{jam}\lambda_i} \times \left(T_i^k - T_{i-1}^k\right)\right]$$
$$= v_i^k \times T_{i,a}^k + \bar{v}_{i,b}^k \times (T_i^k - T_{i,a}^k - T_{i,c}^k) + \bar{v}_{i,c}^k \times T_{i,c}^k \tag{7}$$

where $L_q\left(T_{i-1}^k\right) + \frac{q_i^k - q_d^k \times \left[1 - \delta_B^{(-CT)}\right]}{\rho^{jam}\lambda_i} \times \left(T_i^k - T_{i-1}^k\right)$ is to compute the resulting queue length after vehicles detected by the sensor on segment i at time interval k have joined the queue.

Based on Eqs. (2)-(7), one can then solve for T_i^k with Eq. (8):

$$T_i^k = \frac{D_i - L_q\left(T_{i-1}^k\right) + \left(\frac{q_i^k - q_d^k \times \left[1 - \delta_B^{(-CT)}\right]}{\rho^{jam}\lambda_i}\right) \times T_{i-1}^k - \left(v_i^k - \bar{v}_{i,b}^k\right) \times T_{i,a}^k - \left(\bar{v}_{i,c}^k - \bar{v}_{i,b}^k\right) \times T_{i,c}^k}{\left(\bar{v}_{i,b}^k + \frac{q_i^k - q_d^k \times \left[1 - \delta_B^{(-CT)}\right]}{\rho^{jam}\lambda_i}\right)} \tag{8}$$

Finally, one can compute the queue length at time T_i^k by Eq. (9) and the average speed of vehicles detected by the sensor on segment i at time interval k to join the queue ($\bar{v}_i^k$) by Eq. (10). The results from both equations then serve as the input for computing the time needed for vehicle detected by the sensor on segment $i + 1$ at time interval k to join the queue.

35

$$L_q(T_i^k) = L_q(T_{i-1}^k) + \frac{\left\{q_i^k - q_d^k \times [1 - \delta_B^{(-CT)}]\right\} \times (T_i^k - T_{i-1}^k)}{\rho^{jam}\lambda_i} \tag{9}$$

$$\bar{v}_i^k = \frac{\bar{v}_i^k \times T_{i,a}^k + \bar{v}_{i,b}^k \times T_{i,b}^k + \bar{v}_{i,c}^k \times T_{i,c}^k}{T_{i,a}^k + T_{i,b}^k + T_{i,c}^k} \tag{10}$$

Notably, if there are ramps between segment i and segment $i-1$, the functions to approximate the traffic flow speed impact by ramps, according to the METANET model (Messmer and Papageorgiou, 1990), can be based on the ratio between the number of vehicles from the ramp and the target mainline segment's volume. In this regard, v_i^k and q_i^k in the above equations can be replaced with $\hat{v}_i^k$ and $\hat{q}_i^k$, as formulated in Eq. (11) and Eq. (12):

$$\hat{q}_i^k = q_i^k + q_{i,m}^k - q_{i,n}^k \tag{11}$$

$$\hat{v}_i^k = \min\left\{v_f, \; v_i^k \times \left[1 - \left(\frac{q_{i,m}^k - q_{i,n}^k}{\bar{q}_i^k}\right)\right]\right\} \tag{12}$$

where v_f is the prespecified free-flow speed; $q_{i,m}^k$ and $q_{i,n}^k$ denote the flow rate of on-ramps and off-ramps between segment i and segment $i-1$ at time interval k, respectively.

The above computations (i.e., Eqs. (1)-(12)) can then be recursively adopted to compute the entire time needed for vehicles detected by the sensor at the next upstream segment (i.e., the sensor on segment $i+1$) at interval k to join the queue (T_{i+1}^k) and the resulting queue length at time T_{i+1}^k, i.e., $L_q(T_i^k)$ until the time the incident has been cleared, that is, when $T_I^k \geq CT$, where $i = 1, ..., I$.

In brief, starting from collecting the recorded flow rate and speed at the onset of the incident from the sensor closest to the far upstream ones, one can recursively compute mutual impacts between the incoming flow and the queue propagation using Eqs. (1)-(8), and Eq. (10), as well as the resulting incident queue length using Eq. (10). Additionally, if the on/off-ramp volumes are available, Eq. (11) and Eq. (12) can be introduced to approximate the speed and the flow rate affected by ramp flows.

Model Enhancements for Highways Without Detectors

For the R-IQP to perform the queue impact estimation on highways without reliable detectors, it needs the following two supplemental models calibrated with real-time speed data from probe vehicles (e.g., RITIS (CATT, 2023)) or other open sources (e.g., Google Map):

- A model for estimating discharge flow rate from the lane-blockage segment using only speed data; and
- A model to approximate the arriving flow rate from upstream segments of the lane-blockage location.

Discharge Flow Rate Estimation Model

Figure 4-4 illustrates the discharge flow rate at an incident lane blockage location and its relations with a Traffic Message Channel (TMC) where the speed from probing vehicles is recorded. This study adopts the method of Support Vector Regression (SVR) (Cortes and Vapnik, 1995) to capture the quantitative relation between the discharge rate and its key

contributing factors, including the time-varying traffic conditions, incident nature (e.g., lane blockage scenarios), and mandatory as well as discretionary lane changing frequencies.
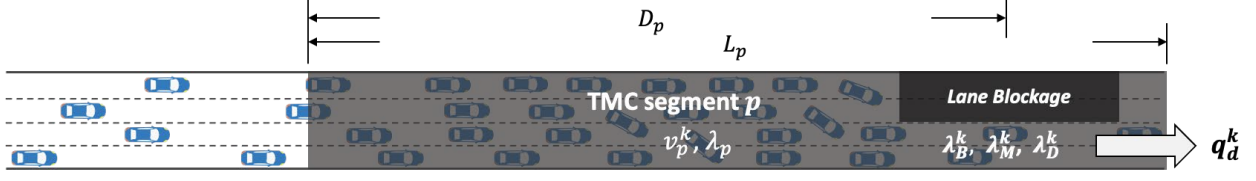

FIGURE 4-4: *Schematic Figure of the Discharge Flow Rate at the Lane Blockage Location*

With only the probe speed data, one needs to first estimate the impact of drivers' rubbernecking behaviors on the discharging flow rate out of the lane-blockage segment, which can be specified as follows:

$$X_1 = \max\left(\theta, \frac{D_p}{\frac{L_p}{v_P^k} - \frac{L_p - D_p}{v_f}}\right) \times \rho^{jam} \times \left(\lambda - \lambda_B^k\right) \tag{13}$$

where θ is the parameter to represent the maximum speed for vehicles traversing the lane-blockage segment to not cause a reduction in the open lanes' capacity and consequently the discharging flow rate; and $\frac{D_p}{\frac{L_p}{v_P^k} - \frac{L_p - D_p}{v_f}}$ denotes the interpolated space mean speed of vehicles traveling to the lane blockage location.

As for the impacts of mandatory lane changes, let λ_M^k be the total number of mandatory lane changes needed for vehicles in the blocked lanes to make lane changes to the open lane at time interval k. For example, Figure 4-5(a) illustrates the three out of four lanes blockage scenario where vehicles in lane 1 need to execute three lane changes to lane 4. Likewise, two lane changes are needed for vehicles in lane 2, and one lane change for those in lane 3. As such, one can specify λ_M^k under such a lane blockage scenario to equal 6.

The mandatory lane-changing frequency can be modeled by its inversely proportional relationship with the space mean speed of vehicles traveling to the lane blockage location (i.e., $\frac{D_p}{\frac{L_p}{v_P^k} - \frac{L_p - D_p}{v_f}}$), because the low speed indicates a larger number of vehicles stuck in the blocked lanes and thus need to execute more mandatory lane changes to the open lanes. Hence, the impacts of mandatory lane changes on the discharge flow rate can be formulated as follow:

$$X_2 = C \times \frac{\varphi v_f}{\max\left(\theta, \frac{D_p}{\frac{L_p}{v_P^k} - \frac{L_p - D_p}{v_f}}\right)} \times \lambda_M^k \tag{14}$$

where $0 < \varphi \leq 1$ is a parameter to be calibrated to compute the speed at the capacity.

Considering the impacts of discretionary lane changes, let λ_D^k be the total number of potential discretionary lane-changing types for vehicles in the open lanes to change from their current lanes to neighboring open lanes at time interval k. For example, Figure 4-5(b) illustrates the blockage of one out of four lanes incident scenario, where vehicles in lane-2 are likely to make a lane change to lane-3 to avoid the impedance by lane-changing vehicles from lane 1 to lane-2. Likewise, those in lane-3 are likely to change to lane-4. Hence, the parameter, λ_D^k, for this scenario is set to equal 2.

The discretionary lane-changing frequency is known to be proportional to the speed difference between the target and subject lanes (Laval and Leclercq, 2008), because vehicles tend to make discretionary lane changes to the adjacent lane when they perceive a higher prevailing speed in that lane. Due to the limitation that the probe speed for each lane is not available, one can approximate the impacts of the discretionary lane changes on the discharge flow rate by using the speed difference between the speed at the capacity (i.e., φv_f) and the estimated space mean speed of vehicles traveling to the lane blockage location (i.e., $\frac{D_p}{\frac{L_p}{v_P^k} - \frac{L_p - D_p}{v_f}}$), which is formulated as follow:

$$X_3 = \max \left\{ \left[\varphi v_f - \max \left(\theta, \frac{D_p}{\frac{L_p}{v_P^k} - \frac{L_p - D_p}{v_f}} \right) \right] \times \rho^{jam} \times \lambda_D^k, \ 0 \right\} \tag{15}$$

$$\lambda_B = 3, \qquad \lambda_M = 6, \qquad \lambda_D = 0$$

(a)

$$\lambda_B = 1, \qquad \lambda_M = 1, \qquad \lambda_D = 2$$

(b)

FIGURE 4-5: *Examples of Lane Changes Patterns under Different Lanes Blockage Scenarios*

By using the above three major parts (Eqs. (13)-(15)) as independent variables and the discharge flow rate as the dependent variable, one can then construct the model for estimating the discharge flow rate with SVR (Cortes and Vapnik, 1995) to reflect their collective impacts and then proceed the parameter estimates with Eq. (17) using data from laboratory experiments or field observations as shown in Eq. (16):

$$q_d^k = f_{SVR}(X_1, X_2, X_3) \tag{16}$$

$$f_{SVR}(\mathbf{x}) = \sum_{i=1}^{N} (\alpha_i - \alpha_i^*)\mathcal{K}(\mathbf{x}, \mathbf{x}_i) + b \tag{17}$$

where α_i and α_i^* are the Lagrange multipliers; $\mathcal{K}(\mathbf{x}, \mathbf{x}_i)$ is the kernel function to transpose into high-dimensional feature space using the low-dimensional space data as the input without knowing the transformation. The calibration procedures for the discharge flow rate estimation model are presented in the numerical experiments.

Flow Rate Estimation Models

For highway segments without traffic sensors to approximate the above traffic queue impacts, one shall need some innovative way to estimate the upstream arriving traffic flows. The set of flow rate estimation models presented below is proposed for doing so, which are based mainly on archived volume data and real-time probe speed information. The core of such models is grounded in the following assumptions:

- Every freeway segment's traffic volume, during the same time of a day and day of a week, shall vary only within a reasonable range;
- Depending on key characteristics and functions associated with the target highway (e.g., the day of a week, geographical locations, geometric conditions, etc.), its volume variation during a given time interval can be generally classified as three levels (i.e., low, medium, and high, based on the distribution of the available archived data; and
- There exists a robust speed-flow rate relation for each classified level of traffic volume.

Based on the above assumptions, the challenge for estimating traffic queue impacts during the period of incident response and management is to estimate the variation range of the arriving flow rate from upstream segments using the proper set of speed-flow relations. With such information, even probabilistic in nature, one can then proceed to approximate the queue impact distance with Eqs. (1)-(10). Hence, the model development process includes the following tasks: 1) constructing a discriminant function to estimate the probability distribution of a target highway segment's traffic volume across the three classified levels during the incident duration, and 2) calibrating a set of speed-flow models for each of those three classified volumes.

The development process, for example, first is to collect four-week data from 25 automatic traffic recorders (ATRs) (MDOT, 2023) (see Figure 4-6) on the freeway networks in Maryland and their corresponding probe speeds over the same period, and then proceed with the following steps:
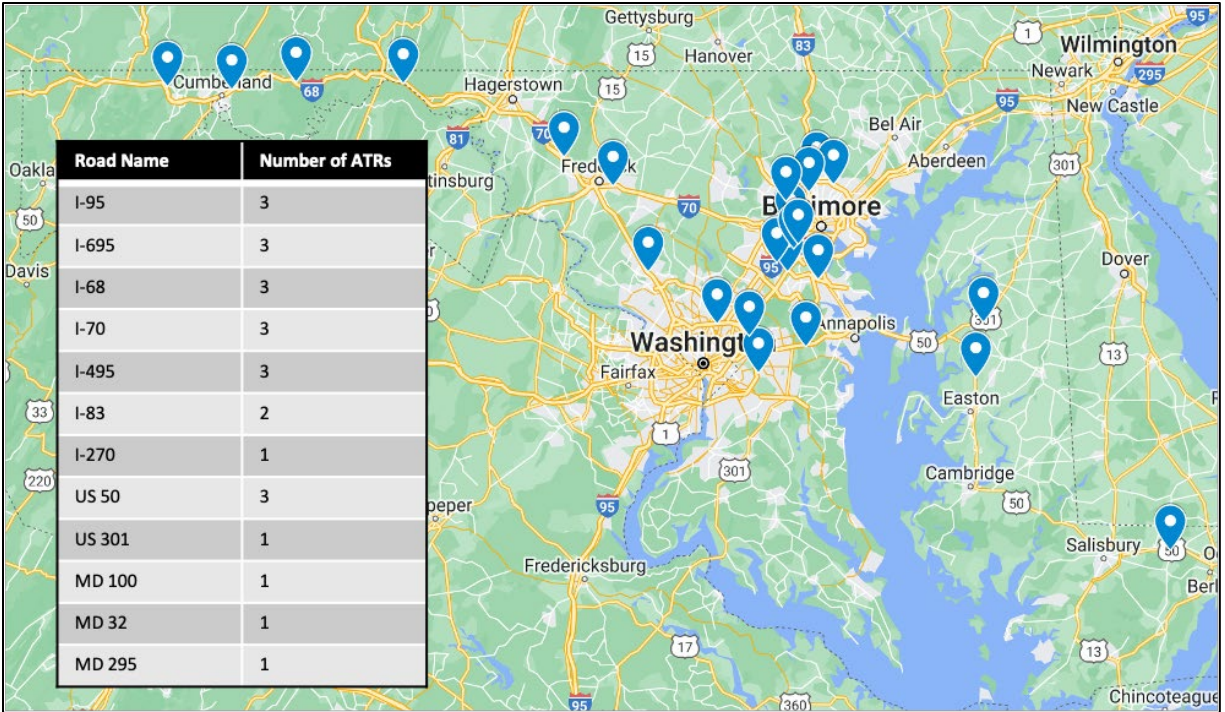
FIGURE 4-6: *Locations of Automatic Traffic Recorders (ATRs) Deployed on Highways*

Step 1: The 24-hour volume data collected from each ATR are first divided into eight different time periods.

Step 2: Classify the volume data associated with each time interval from all ATRs into three distinct levels using the Gaussian mixture density function. By searching the local minima on the density function (see Figure 4-7), the volume data of all ATRs, for example, from 6-9 A.M. can be classified into three levels (i.e., "Low", "Medium", and "High").

FIGURE 4-7: *Gaussian Mixture Density of the Hourly Volume from 6-9 A.M.*

Step 3a: Develop a classification function to classify the probability of each time interval's traffic flow rate into three preset volume levels. Using the classified levels from Step 2 as the

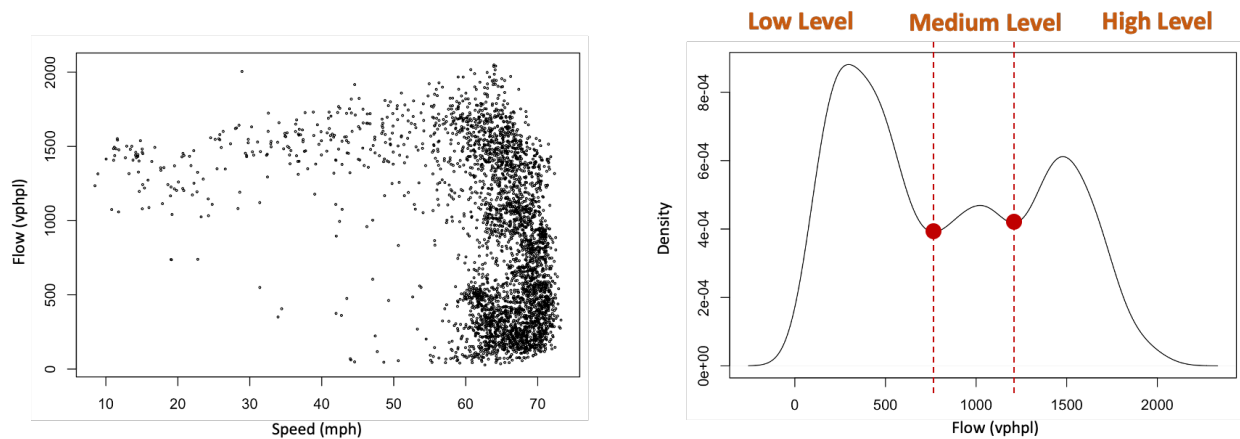dependent variable, one can apply the model by Breiman et al. (1984) to identify the relationship between the classified volume level for a highway segment over a given time interval and their associated characteristic variables such as the following variables: time of a day, day of the week, location (i.e., in the urban area or not), highway classifications (i.e., beltway, intercity highway, the highway between the major city and the residential area, major highway collector, and rural highway), AADT per lane, and the recorded probe speed over the same period.

Note that due to the consequence of underestimating the traffic queue impacts, it is recommended that a higher weight be assigned to the underestimated errors (e.g., 50% as in Figure 4-8) in the classification process of computing the loss function. Figure 4-8 shows the classification results using the volume data from all ATRs between 6-9 A.M. as an example.
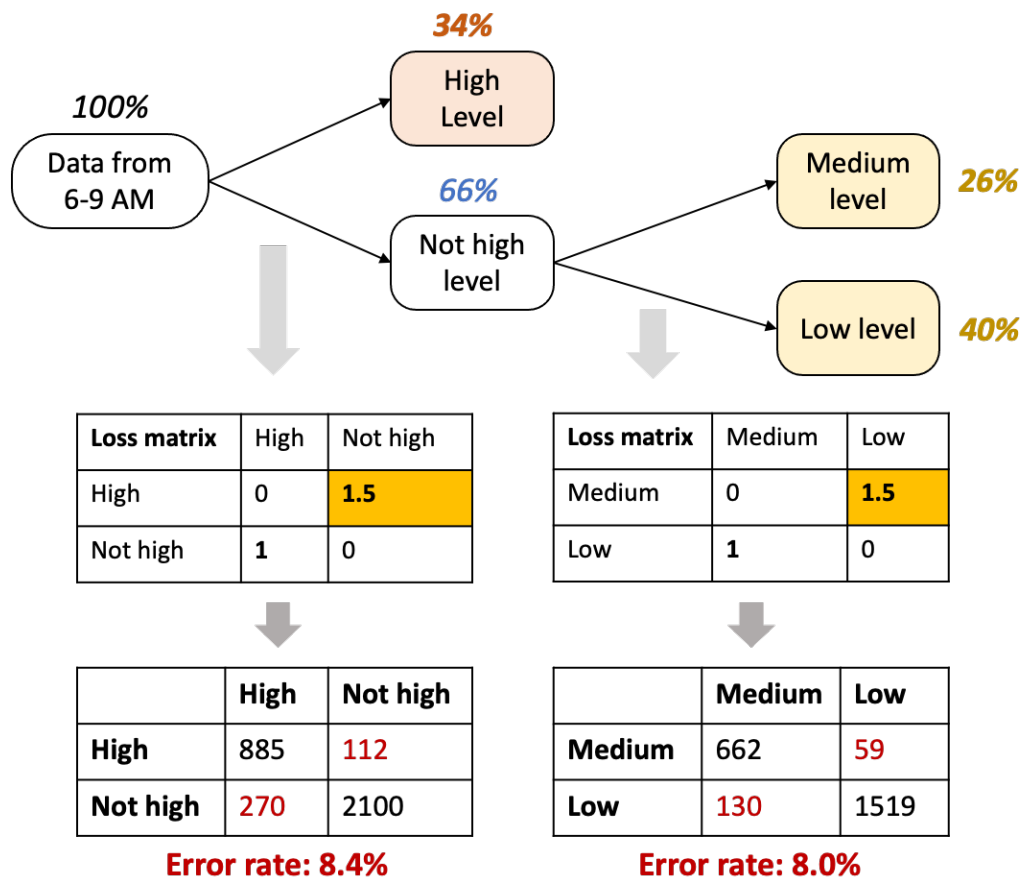
FIGURE 4-8: *Classification Results for Volume Data from all ATRs Between 6-9 A.M*

Step 3b: Develop a speed-flow relation for each classified level of volume. Depending on the scattered pattern of all volume data during the same interval from all ATRs, it is essential that effective modeling concepts be used to reflect their relations with the solely available speed data over the same periods.

Taking the data from 6-9 A.M. as an example, because no obvious pattern can be observed for "Medium Level" and "Low Level" (see Figure 4-9), so one can take the following steps and apply the quantile analysis to produce the practically usable results:

- **Step 1**: Determine the desired confidence interval (θ).
- **Step 2**: Compute the upper bound (q^U) and the lower bound (q^L) of the estimated flow rate by selecting the interval $[a, b]$, where $0 \leq a < b \leq 1$, that can produce the minimum difference between their associated flow rates. That is:

Minimize
$$q^U - q^L$$

Subject to
$$b - a = \theta$$
$$q^U = Q_q(b) \qquad (18)$$
$$q^L = Q_q(a)$$

where $Q_q(x)$ denotes the x-percentile of the flow rate.

For instance, the upper and the lower bounds of the flow rate associated with a 90% confidence interval ($\theta = 0.9$) for "Medium Level," shown in Table 4-2, are computed by using $(a, b) = (0.045, 0.945)$ as they have the minimum flow difference.
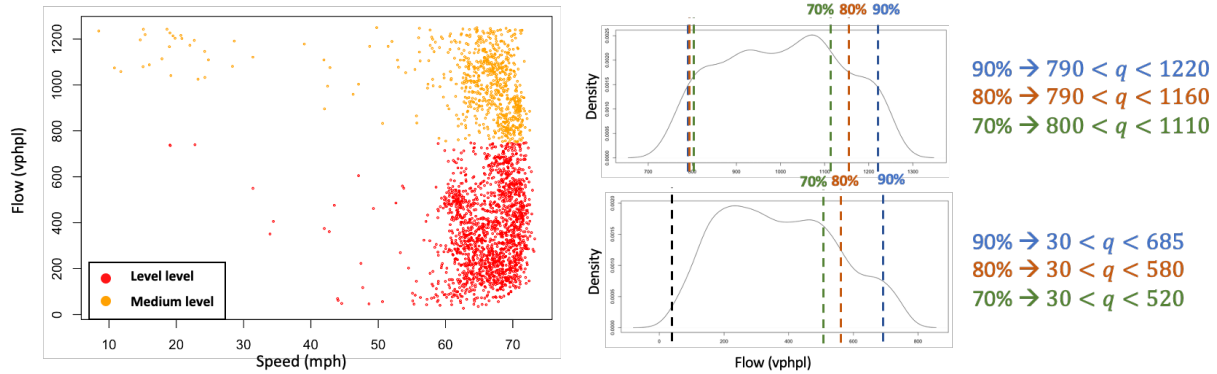
FIGURE 4-9: *Speed-Flow Data for "Medium Level" and "Low Level" from 6-9 A.M.*

As for the volumes in "High Level," their scattered plots exhibit a more complex speed-flow relation (see Figure 4-10). Hence, the method of zone-based control boundaries is adopted to capture such relations and ensure that the control zone can cover the target percentage with the minimum area. A step-by-step description of the development procedures is summarized below:

- **Step 1**: Determine the desired confidence interval (θ), that is, the target percentage of the volume data that the control zone should at least cover.
- **Step 2**: Classify the volume data into two categories: undersaturated and oversaturated conditions. In this case, the speed of 60 mph is used as the boundary between the undersaturated and oversaturated conditions.
- **Step 3**: Develop a set of speed-flow relations for such two conditions by identifying their zone-based control boundaries.

    For the undersaturated condition, the flow rate increases with the decrease in speed, but maintains a maximum value (i.e., capacity) when the speed is sufficiently low.

Hence, one can define the zone-based control boundaries for the undersaturated condition using three unknown points, i.e., (x_1, y_1), (x_2, y_2), $(60, y_2)$ as illustrated in Figure 4-10, where: x_1 defines the maximum speed of the control boundary; y_1 defines the minimum flow rate under the undersaturated condition; x_2 defines the maximum speed of the maximum flow rate; and y_2 defines the maximum flow rate under the undersaturated condition. Based on these three points, one can use the following optimization to identify the best-fit control boundaries:

Minimize $\qquad\qquad\qquad\qquad\qquad\qquad\qquad A$

Subject to $\qquad\qquad\qquad\qquad\qquad\qquad x_1 \geq x_2 \geq 60$

$$y_2 \geq y_1 \qquad\qquad (19)$$

$$A = \frac{1}{2}(x_2 + x_1 - 120) \times (y_2 - y_1)$$

$$n_T \geq \theta \cdot n_W$$

where A is the total area of the control zone for the undersaturated condition; and n_T and n_W denote the total number of data points and the number of points inside the control zone, respectively.

As for the oversaturated condition, since the flow rate decreases with the speed, one can also apply a zone-based to define its control boundaries using three unknown points, i.e., $(60, y_3)$, (x_3, y_4), (x_3, y_5), where x_3 defines the minimum speed; y_3 defines the maximum flow rate under the oversaturated condition; y_4 defines the maximum flow at the minimum speed; and y_5 defines the minimum flow rate under the oversaturated condition. The formulations for such estimation are shown below:

Minimize $\qquad\qquad\qquad\qquad\qquad\qquad\qquad B$

Subject to $\qquad\qquad\qquad\qquad\qquad\qquad x_3 < 60$

$$y_3 \geq y_4 \geq y_5 \qquad\qquad (20)$$

$$B = \frac{1}{2}(y_4 + y_3 - 2y_5) \times (60 - x_3)$$

$$n_{within} \geq \theta \cdot n_{total}$$

where B is the total area of the control zone for the oversaturated condition.

Taking the dataset from 6-9 A.M. as an example and let $\theta = 0.9$, then one can have the optimal values for the set of variables, $(x_1, x_2, y_1, y_2, y_3, y_4, y_5)$ as $(72, 64, 1250, 1900, 2000, 1400, 1300)$. Table 4-2 summarizes the speed-flow relations for "High Level" with this example of data.
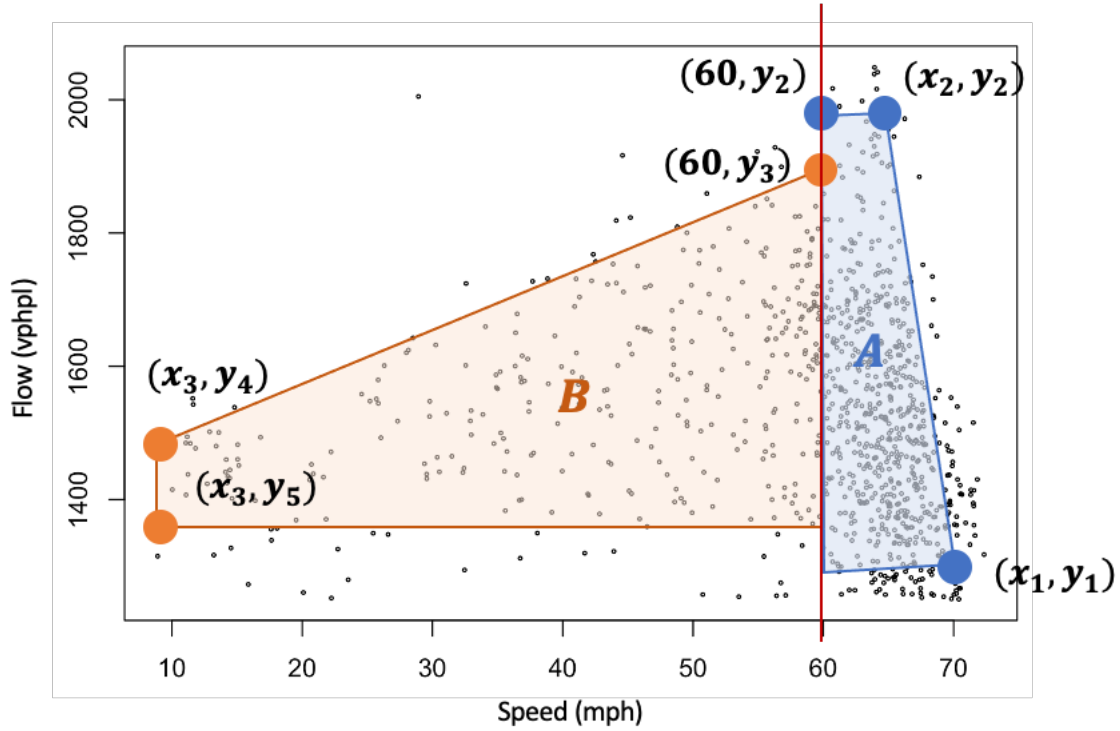
FIGURE 4-10: *Development of Speed-Flow Relation for "High Level" Volume from 6-9 A.M.*

TABLE 4-2: *Speed-Flow Relations for all ATRs from 6-9 A.M. under Different Confidence levels*

Time Period	Level of Flow	Speed-flow relation
6-9 AM	High	For $v > 60\ mph$ 90% → $1250 < q < max(1900,\ 1250 + (72 - v) \times 81.25$ 80% → $1250 < q < max(1750,\ 1250 + (71 - v) \times 83.33$ 70% → $1300 < q < max(1750,\ 1300 + (69 - v) \times 150.0$ For $v \leq 60\ mph$ 90% → $1300 < q < 1400 + (v - 10) \times 12$ 80% → $1350 < q < 1550 + (v - 10) \times 5$ 70% → $1350 < q < 1500 + (v - 10) \times 5$
	Medium	90% → $790 < q < 1220$ 80% → $790 < q < 1160$ 70% → $800 < q < 1110$
	Low	90% → $q < 685$ 80% → $q < 580$ 70% → $q < 520$

Figure 4-11 illustrates the flow chart for adopting the developed models to estimate the flow rate of a segment, given its probe speed and the key characteristics associated with the target highway segment. The segment of interest will be first categorized into its associated time period, and then classified into its corresponding volume level with the developed classification model. Lastly, a unique speed-flow relation will be adopted to estimate the upper and the lower

44

bounds of the flow rate based on the developed speed-flow relations. The obtained upper and lower bounds of the flow rate associated with the desired confidence interval can then be input to Eqs. (1)-(10) to compute the range of the resulting queue.
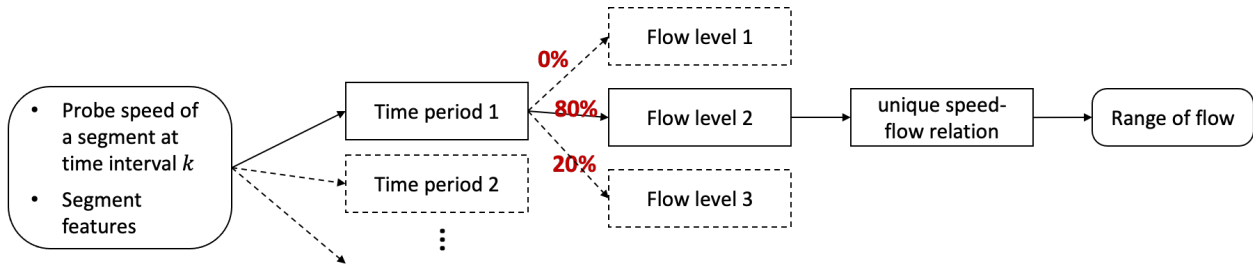
FIGURE 4-11: *The Procedures for Adopting the Flow Rate Estimation Model*

Operation of the Incident Queue Propagation Model

With all principal components in R-IQP and model enhancements, Figure 4-12 illustrates the step-by-step procedures to predict the incident queue in a timely manner.

The target of Step 1 to Step 4 is to identify the data availability and collect the available data. Step 5 and Step 6 record the incoming flow rates, speeds, and discharge flow dates when detector data are available. Otherwise, estimating the incoming traffic volume from Eqs. (1)-(10) and the discharge flow rate from Eqs. (13)-(17) if detector data are not available. Step 7 and Step 14 aim to compute the mutual impacts between incoming flows and queue dynamics. Lastly, Step 15 checks if any new information is available for real-time updates of the predicted incident queue length.
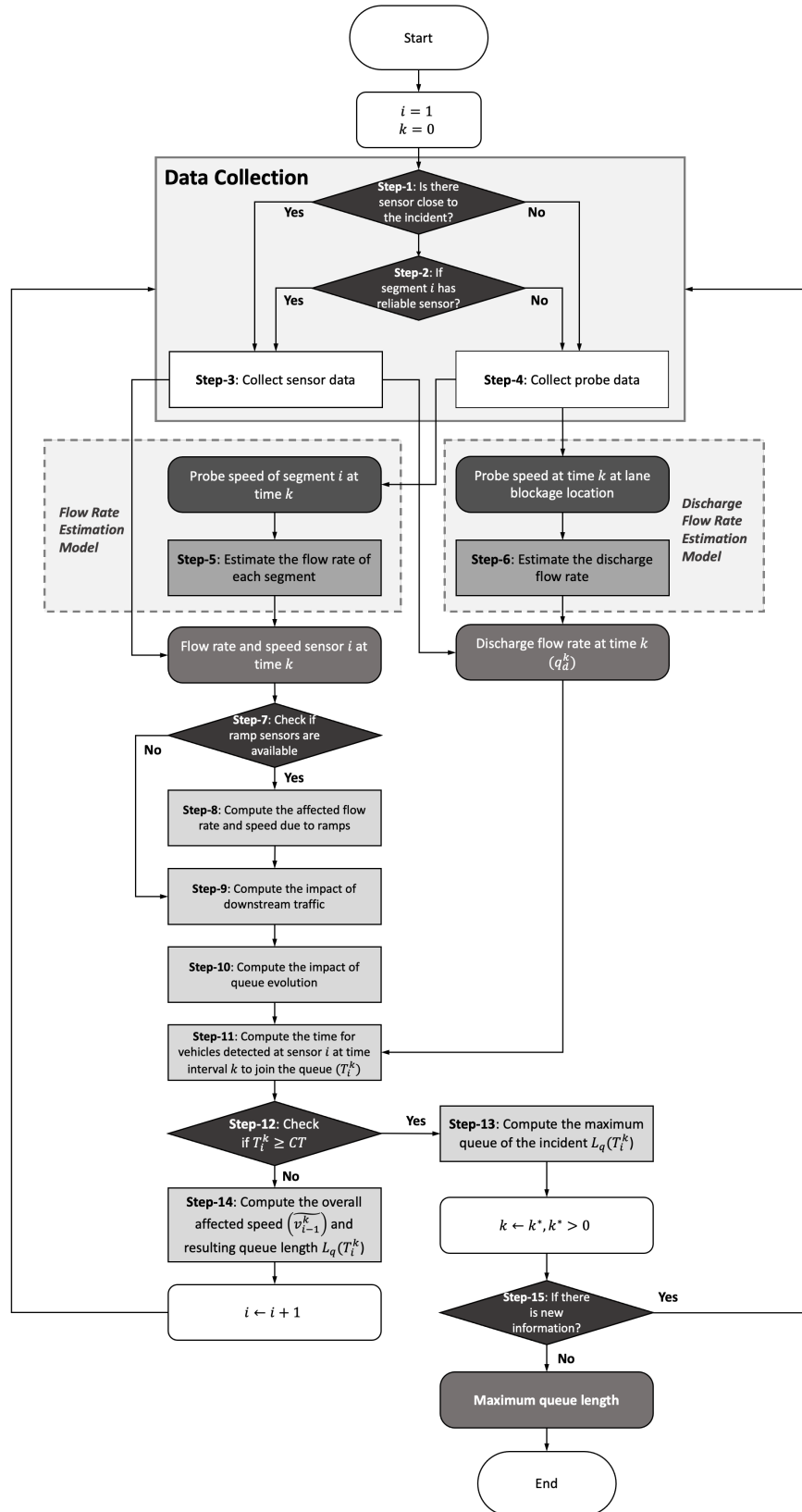
45

FIGURE 4-12: *Real-Time Operation Procedures to Predict the Incident Queue Length*

46

4.3 NUMERICAL EXPERIMENTS

The four sets of numerical experiments presented below are designed to first calibrate key parameters of all developed models, and then conduct extensive evaluations of their performance under both real-world and simulated scenarios:

- **Experiment 1**: Estimating key parameters embedded in the discharge flow rate estimation model for a lane-blockage segment with extensive traffic data generated from a freeway traffic simulator that has been calibrated with the field data.
- **Experiment 2**: Calibration of the proposed R-IQP system with a freeway traffic simulator that has been calibrated with the field data.
- **Experiment 3**: Performance evaluation of the proposed R-IQP system using real-world data.
- **Experiment 4**: Extensive evaluation of the proposed R-IQP system's performance under various lane-blockage scenarios, traffic conditions, and incident natures with a well-calibrated traffic simulator.

This study has adopted VISSIM (PTV, 2023) to construct the traffic simulator. Notably, for the simulator to have sufficient fidelity to generate reliable traffic experimental scenarios, one must first calibrate its key parameters, designed to reflect observed traffic flow characteristics, including car-following and lane-changing patterns and their variations among the driving populations. The fidelity calibration process for the simulator involves field data collection from various incident scenarios, and recursive execution of Simultaneously Perturbation Stochastic Approximation (SPSA) (Spall, 1999) along with the Variation Reduction Technique (VRT) (Law and Kelton, 2007). As a detailed presentation of the calibration process and the adopted optimization algorithm is not the focus of this study, the results are thus reported elsewhere.

Experiment 1: Calibration of the Discharge Flow Rate Estimation Model for Lane-blockage Segments

As shown in Eqs. (13)-(15), there are two parameters, θ and φ, which need to be calibrated to ensure their reliability when only the speed information is available. The designs of experiments for parameter calibration are summarized as follows:

- Nine lane blockage scenarios on a four-lane freeway (see Figure 4-13)
- Six different input volumes (2000, 1800, 1600, 1400, and 1200 veh/hr/ln)
- Five replications of one hour simulation with different random seeds for each simulated scenario, and a data collection interval of every 5 minutes
- Total sample size: 3,240 samples in total (i.e., $9 \times 6 \times 5 \times 12 = 3,240$) for the calibration.

Those two parameters embedded in Eqs. (13)-(15) were calibrated with the gradient decent method, while the hyperparameters for the SVR were based on the grid search method ($\gamma = 0.33, \varepsilon = 0.1$, where γ defines how far the influence of a single training example can achieve and ε has a function to give a tolerable error of the regression model). The dataset for model training consists of 70% of all generated samples, and the remaining 30% of the data were used for performance evaluation.

Table 4-3 summarizes the calibration and test results, where the overall MAE on the training and the testing datasets are within the acceptable range, about 40 veh/hr and 39 veh/hr, respectively.
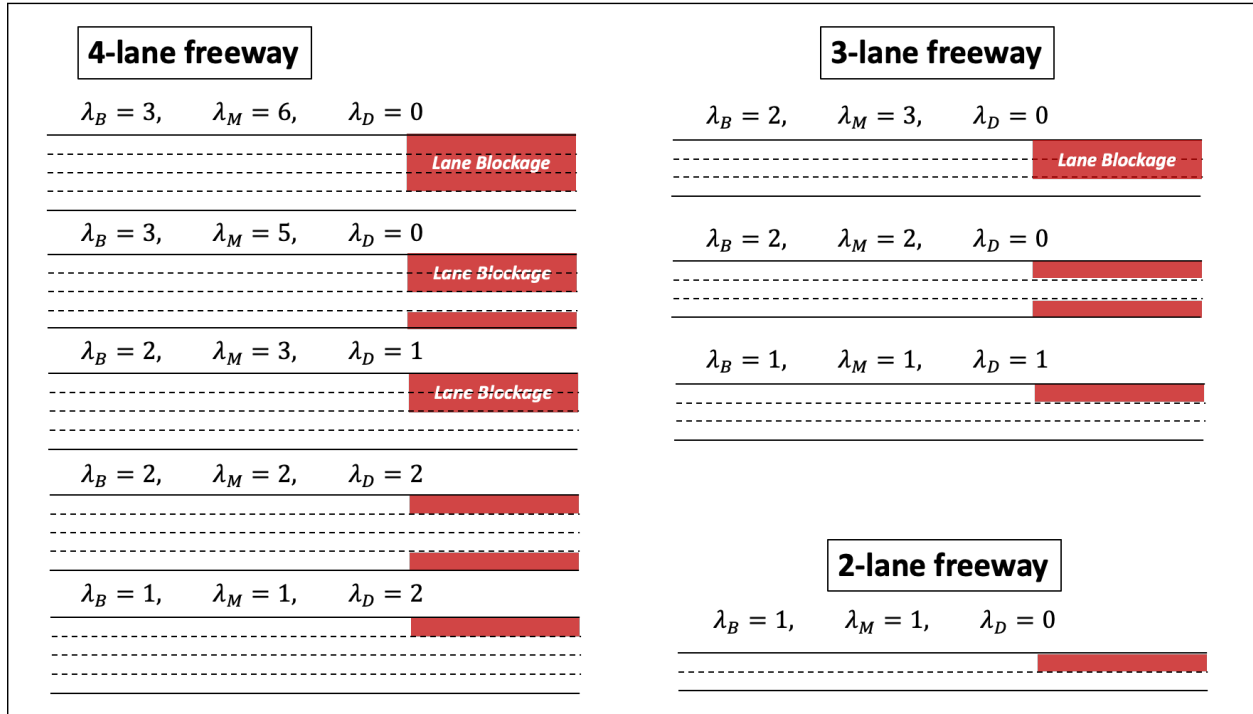
FIGURE 4-13: *The Different Lane Blockage Scenarios Adopted for the Calibration of the Discharge Flow Rate Estimation Model*

TABLE 4-3: *The Calibration Results of the Discharge Flow Rate Estimation Model*

Experiment-1 (sample size: 3240)					
Calibrated parameter values	Lane blockage Scenarios	MAE (veh/hr)		MAPE (%)	
		Training	Testing	Training	Testing
	Overall	39.90	38.43	1.70	1.68
	$\lambda = 4, \lambda_B = 1$	63.09	62.64	1.48	1.47
$\theta = 18.02$	$\lambda = 4, \lambda_B = 2$	54.17	49.35	1.90	1.74
(veh/hr)	$\lambda = 4, \lambda_B = 3$	22.11	20.81	1.55	1.45
$\varphi = 0.84$	$\lambda = 3, \lambda_B = 1$	51.26	48.65	1.78	1.69
	$\lambda = 3, \lambda_B = 2$	25.97	27.90	1.81	1.93
	$\lambda = 2, \lambda_B = 1$	23.36	25.54	1.63	1.79
Overall		**38.43**		**1.67**	

Note: λ denotes the total number of lanes and λ_B denotes the number of blocked lanes

Experiment 2: Calibration of the Proposed R-IQP Model

This set of experiments is designed to calibrate the parameters embedded in Eqs. (1)-(10) (i.e., α, κ, τ, and δ_B). The network used for developing the simulator was based on the 41.5-mile segment of I-495 in Maryland (see Figure 4-14), and the experimental plan to generate the simulated traffic scenarios is summarized below:

- Two incident locations
- Three lane blockage scenarios (i.e., 1 lane blocked, 2 lanes blocked, and 3 lanes blocked)
- Three different incident clearance durations (i.e., 15, 30, and 60 minutes)
- Five mainline traffic volumes ranging from 80% to 120% of the baseline volume
- 90 samples in total (i.e., $2 \times 3 \times 3 \times 5 = 90$) for the model calibration

Table 4-4 shows the set of optimal parameters used in the R-IQP and its performance statistics under those experimental scenarios. Note that the R-IQP has exhibited the expected accuracy and yielded an overall MAE of only 0.267 miles. Its performance, however, seems to degrade with an increase in the number of blocked lanes and the incident clearance duration. For example, under the scenario of a 3-lane blockage, the resulting MAE for incidents of 60 minutes is 0.835 (mile), higher than 0.185 miles for an incident of 30 minutes.

FIGURE 4-14: *Scope of Simulation Experiments for the Calibration of the Incident Queue Propagation Model*
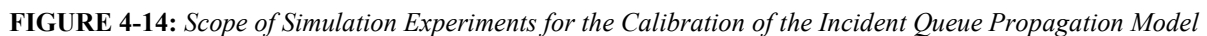
TABLE 4-4: *The Calibration Results of the Incident Queue Propagation Model*

Experiment-2 (sample size: 90)

| Parameters	Lane Blockage Status	Lane Clearance Durations (mins)	MAE (mile)	RMSE
		60	0.835	0.879
	3-lane blocked	30	0.185	0.205
$\alpha = 0.75$		15	0.074	0.083
$\kappa = 0.85$		60	0.459	0.497
$\tau = 0.70$	2-lane blocked	30	0.172	0.197
$\delta_{3\ Lane} = 2.5$		15	0.131	0.145
$\delta_{2\ Lane} = 3.1$		60	0.229	0.273
$\delta_{1\ Lane} = 7.5$	1-lane blocked	30	0.151	0.172
		15	0.167	0.189
	Overall		0.267	0.375

Note: $\delta_{3\ Lane}$ denotes the parameter δ_B in Eqs. (7)-(9) under 3-lane blockage scenario

Those models with optimally calibrated parameters will be adopted in the following experiments for the performance evaluation of the proposed R-IQP system.

Experiment 3: Evaluation of the Proposed R-IQP Model with Field Data

To assess the applicability of the proposed R-IQP model, this study has compared its performance with actual maximum queue lengths observed from the five incidents that occurred on I-495 in Maryland. Figure 4-15 shows a sample incident record with the time-varying queue and the probe speed along the freeway, which exhibits a maximum queue distance of approximately 2.5 to 3.0 miles. Note that since the surveillance system on I-495 in Maryland cannot provide reliable estimates of both the inflows and outflows, the aforementioned models for estimating arriving flow rate from upstream segments and the discharge flow rate out of the lane-blockage location were applied to produce such information.

Table 4-5 presents the predicted queues with the R-IQP system, where its upper and lower bounds are generated based on the upper and lower bounds of the estimated approaching flows associated with a 95% confidence interval (i.e., $\theta = 0.95$ in Eqs. (18)-(20)). Notably, the mean absolute difference between the upper bounds of the actual and predicted queue lengths is 0.36 miles and 0.4 miles for the difference between both lower bounds.
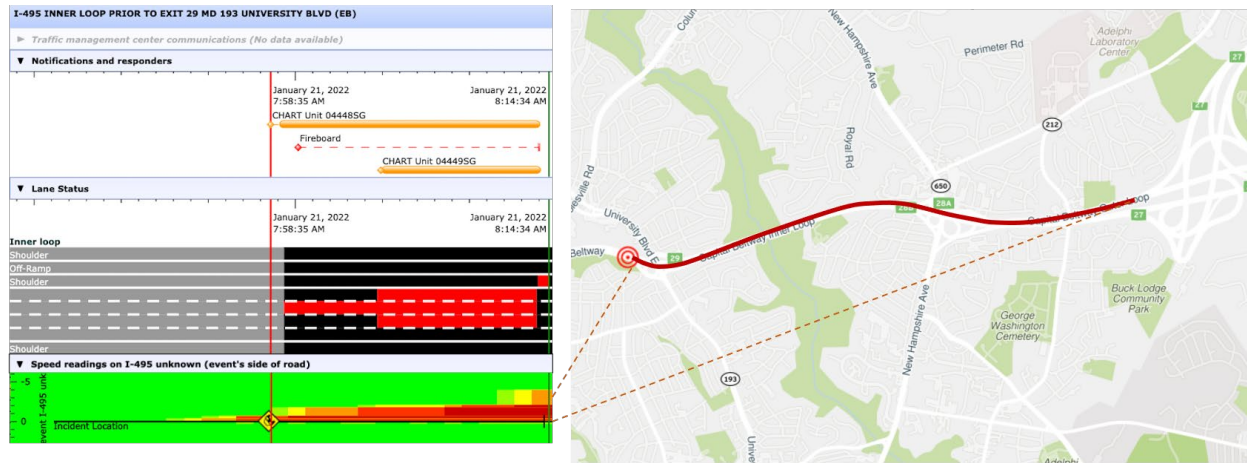
FIGURE 4-15: *An Example of the Incident Query with Lane Status and Probe Speed Information*

TABLE 4-5: *Evaluation Results of the R-IQP Using Real-World Incident Data*

Experiment-3

Incident Location	Lane Blockage Information	Incident Duration (mins)	Actual Queue Length (mile)	Predicted Queue Length with 95% confidence (mile)
I-495 Outer Loop At Exit 34 Md 355 Wisconsin Ave (WB)	3 out of 4 lanes blocked	30	3.6 – 4.3	3.5 – 4.4
I-495 Outer Loop Prior To Exit 34 Md 355 Rockville Pike (WB)	3 out of 4 lanes blocked	20	2.3 – 2.6	2.2 – 2.9
I-495 Outer Loop At Exit 35 I 270 Eisenhower Mem Hwy (WB)	3 out of 4 lanes blocked	29	4.2 – 5.1	3.2 – 5.6
I-495 Outer Loop At Exit 34 Md 355 Rockville Pike (WB)	2 out of 5 lanes blocked	18	2.5 – 3.6	2.3 – 3.2
I-495 Outer Loop After Cedar Ln (WB)	2 out of 4 lanes blocked	12	0.8 – 2.3	1.4 – 1.8

Experiment 4: Evaluation of the Proposed R-IQP Model Using VISSIM Simulation

To ensure the model's performance beyond those limited real-world incident scenarios, this study has further conducted extensive laboratory analyses with the I-495 traffic simulator developed with VISSIM (PTV, 2023). The list of key variables used for generating 18 experimental scenarios are listed below:

- Three lane blockage scenarios (i.e., 1 lane blocked, 2 lanes blocked, 3 lanes blocked)

- Three incident durations (i.e., 15, 30, and 60 minutes)
- Two mainline traffic volumes, ranging from 80% to 120% of the baseline volume
- 18 samples in total (i.e., $3 \times 3 \times 2 = 18$) for experimental analysis

Table 4-6 shows the simulated and the predicted queue lengths under those 18 incident scenarios. Notably, for the predicted queue under Scenario 1 where the flow rate data is collected for each segment, their differences are consistently less than 1 mile, with the MAE of 0.31 miles. As for the predicted queue under Scenario 4, 95% confidence intervals of predicted queues can cover the actual queue lengths in 14 out of 18 incident scenarios, and the other four overestimates are with a mean difference of 0.14 miles.

TABLE 4-6: *The Evaluation Results of the Proposed Model with VISSIM Simulation*

Experiment-4						
	Lane clearance duration (mins)	Lane blockage status	Input volume (veh/hr)	Simulated queue (mile)	Predicted queue under Scenario 1 (mile)[a]	Predicted queue with 95% confidence under Scenario 4 (mile)[b]
1		3 out of 4 lanes blocked	6708	4.92	5.55	4.01 – 6.28
2			6516	4.67	5.72	4.23 – 6.31
3	60	2 out of 4 lanes blocked	6864	4.25	4.71	3.72 – 5.38
4			7164	4.03	4.28	3.61 – 5.33
5		1 out of 4 lanes blocked	7104	3.61	3.86	3.32 – 4.29
6			7200	3.39	3.57	3.14 – 4.18
7		3 out of 4 lanes blocked	6684	2.21	2.52	2.01 – 2.92
8			6708	2.20	2.62	2.03 – 3.02
9	30	2 out of 4 lanes blocked	6372	1.97	2.60	(2.11 – 3.03)[c]
10			6600	2.03	2.07	1.67 – 2.48
11		1 out of 4 lanes blocked	7020	1.65	2.08	(1.75 – 2.42)[c]
12			6684	1.45	1.50	1.36 – 2.11
13		3 out of 4 lanes blocked	3840	0.47	0.79	(0.62 – 0.95)[c]
14			3816	0.50	0.80	(0.64 – 0.96)[c]
15	15	2 out of 4 lanes blocked	3900	0.27	0.44	0.16 – 0.73
16			4020	0.19	0.14	0.00 – 0.43
17		1 out of 4 lanes blocked	4356	0.07	0.00	0.00 – 0.37
18			3852	0.00	0.00	0.00 – 0.37

Note: [a] The predicted queue is computed from the flow rate data recorded at each segment (i.e., Scenario1)
[b] The predicted queue with 95% confidence is computed under the scenario where roadside sensors are not available (i.e., Scenario 4)
[c] The predicted queue with 95% confidence cannot cover the simulated queue

In brief, evaluation results from Experiment 3 and Experiment 4 show that the proposed R-IQP system can robustly reflect the mutual impacts between the queue propagation and the incoming flow from upstream segments. In addition, with the support from two supplemental models (i.e., discharge flow rate and arriving flow rate estimation model), the proposed R-IQP system has demonstrated its potential for use in practice to predict incident queue length with sufficient reliability under various data availability scenarios.

Chapter 5
Estimating the Incident Impacts onto the Neighboring Local Networks with a Detour Rate Estimation System

5.1 INTRODUCTION

Recognizing that quality detector data may not always be available over most freeway segments, this chapter presents a model for detour rate estimation for impact assessment of time-varying queues from a freeway incident onto its neighboring local traffic. This study has developed a Real-time Detouring Rate Estimation System (R-DRES), which employs the widely used real-time probe speed data as the sole input to a set of off-line calibrated speed-flow models to estimate the resulting traffic queue impacts to neighboring arterials. Such a low-cost but robust system enables the traffic management center to approximate mainline traffic's time-varying detour rate during the incident clearance period and evaluates the necessity of activating proper traffic control strategies.

However, in developing the proposed system, one needs to overcome two major challenges. First, an extensive set of quality archived speed and volume data by day of the week and time of day shall be available for calibrating the robust speed-flow relations under various traffic conditions. Secondly, the applicability of the flow rates predicted with such models for the incident's upstream segments during the clearance operations needs to be verified with a reliable mechanism, due to the day-to-day fluctuation of traffic volume, and differences in drivers' decisions when encountering incidents. Whereas the first challenge has been addressed in Chapter 4, the remainder of this chapter will detail the core logic and modeling process developed to cope with the latter.

Note that the development of the proposed R-DRES is based on the following three primary assumptions:
- Reliable real-time probe speed data is available from various sources (e.g., RITIS, Google Maps, HERE);
- Average probe speed represents the point speed at the subsegment center of the target highway; and
- A set of off-line calibrated yet robust models for the speed-flow relations over different times of a day and days of a week under incident-free conditions are available.

5.2 REAL-TIME DETOURING RATE ESTIMATION SYSTEM (R-DRES)

Figure 5-1 illustrates the process of applying the proposed R-DRES for real-time detouring rate estimation. Specifically, with such a system, one can employ the real-time probe speed data to compute the difference in flow rates between the upstream and downstream segments of an interchange during the incident clearance operations and compare them with the same measurement during the same time period of a typical day but under incident-free condition. The proposed system features its self-evaluation mechanism that employs an embedded well-calibrated macroscopic traffic model to assess the quality of the flow rate data predicted with those speed-flow rate models calibrated off-line from archived data. The entire development process can be decomposed into the following major steps:

- **Step 1**: Collect the following two types of speed data:
  - o The real-time speed data for both upstream and downstream segments of each interchange within the projected maximum queue impact range during the incident clearance period.
  - o The archived speed data over the same time periods of day and days of a week for all these segments within the same projected spatial range but under incident-free scenarios.
- **Step 2**: Smooth the collected real-time/archived speed data and perform necessary data imputation if needed.
- **Step 3**: Estimate the flow rates for each time interval within the incident clearance period for those freeway segments within the incident's maximum impact range, based on the processed real-time probe speed data and the available speed-flow models; conduct the same estimates for flow rates over the same segments and same time intervals with archived speed data under incident-free conditions.
- **Step 4**: Assess the reliability of those flow rates estimated from the speed-flow models and perform the parameter update if deemed necessary. This step is to ensure that the estimated flow rates can reliably reflect the real-time traffic volume fluctuation. The activities executed in this entire step involve the applications of the following four major system components:
  - o A macroscopic traffic flow model to capture the traffic dynamics of the freeway during the incident clearance operations;
  - o An innovative mechanism that adopts the developed macroscopic traffic flow model to perform the quality assessment for the flow rate estimated from the set of speed-flow models;
  - o An efficient algorithm for searching the parameters in the macroscopic traffic model that can best fit the real-time available speed information from probe vehicles; and
  - o An update algorithm for the set of speed-flow models to update their key parameters in real-time when justified to do so.
- **Step 5**: Enhance the robustness of the estimated flow rates for impact assessment with the rolling horizon concept.
- **Step 6**: Compute the flow difference between the upstream and downstream segments of the roadway containing off-ramps (see Figure 5-2), with the following expressions:

$$Q_m^{k',h}(k) = \tilde{q}_{i-1}^{k',h}(k) - \tilde{q}_{i+1}^{k',h}(k) \tag{1}$$

$$\bar{Q}_m^{k',h}(k) = \bar{q}_{i-1}^{k',h}(k) - \bar{q}_{i+1}^{k',h}(k) \tag{2}$$

  where $Q_m^{k',h}(k)$ denotes the real-time estimated difference in traffic volumes between the upstream and downstream segments of interchange m from time interval $k - h$ to time interval k, measured at time interval k'; and $\bar{Q}_m^{k',h}(k)$ denotes the historical flow difference during the same but incident-free period (i.e., estimated from the archived speed).
- **Step 7**: Compute the detouring volume rates based on the flow rate difference between the one measured in real-time and the same measurement but during the incident-free periods, as shown in Eq. (3).

$$DV_m^{k',h}(k) = Q_m^{k',h}(k) - \bar{Q}_m^{k',h}(k) \tag{3}$$

where $DV_m^{k',h}(k)$ denotes the real-time detouring rate at interchange m from time interval $k - h$ to time interval k, measured at time interval k'

Step-1: Collect the speed data
- Real-time speed data from all upstream segments containing off-ramps within the queue impact range
- The same set of speed data from archived data over the same period for its upstream segments containing off-ramps within the queue impact range

Step-2: Probe speed smoothing/imputation

Step-3: Estimate the flow rate using speed-flow model

Step-4: Validation of the estimated flow rate and update of the speed-flow model using macroscopic traffic flow models

| Macroscopic traffic flow models for incident conditions | Search for the parameter set in macroscopic flow models that fit the real-world observation |

| Validate the estimated flow rate from speed-flow model | Update the speed-flow model with the estimated flow rate from macroscopic flow models |

Step-5: Flow rate reliability enhancement by adopting rolling horizon concept

Step-6: Compute the flow difference between upstream and downstream segments

Step-7: Compute the detouring volume

Estimated detouring volume

FIGURE 5-1: *The Process for Detouring Rate Estimation with an Assessment Function From a Well Calibrated Macroscopic Traffic Flow Model*
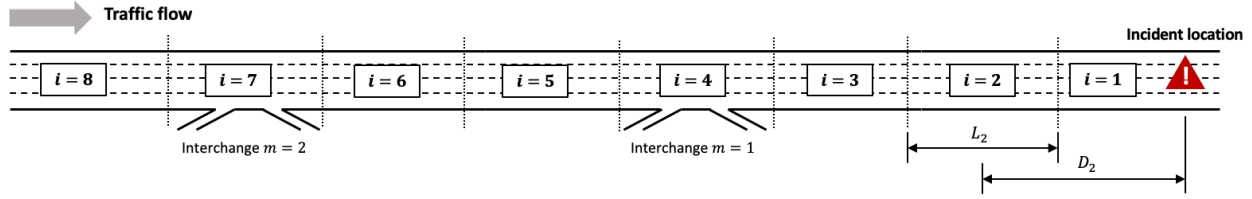
FIGURE 5-2: *Graphical Illustration of a Freeway Segment for Estimating Incident Impacts on the Detouring Rate*

The following sections will first detail the methodology proposed to assess the applicability of the estimated flow rates and the mechanism for an update of the speed flow models (i.e., Step 4 in Figure 5-1), followed by a brief description of the flow rate reliability enhancement by adopting rolling horizon concept (i.e., Step 5 in Figure 5-1). Table 5-1 presents the key variables used in the system development.

**TABLE 5-1:** *Key Variables used in the Development of the Proposed R-DRES*

Notation	Definition
i	Segment index
m	Interchange index
k	Time interval index
h	Number of time steps of each volume difference estimation
$v_i^{k',\,1}(k)$	Processed real-time probe speed of segment i for time interval $k-1$, collected at time interval k'
$\hat{v}_i^{k,\,1}(k)$	Estimated Speed of segment i for time interval k-1, estimated at time interval k' from enhanced METANET
$q_i^{k',\,a}(k)$	Estimated real-time flow rate of segment i from time interval $k-a$ to time interval k, measured at time interval k'
$\tilde{q}_i^{k',\,a}(k)$	Estimated real-time Flow rate of segment i from time interval $k-a$ to time interval k with higher reliability, measured at time interval k'

Methodology for Assessing the Applicability of the Flow Rates Estimated from Off-Line Models

Conceivably, with a reliable speed-flow relation, the real-time and historical flow rate difference between the upstream and downstream of the interchange could be estimated intuitively with the available speed data. However, depending on the traffic impacts by an incident and the nature of day-to-day volume fluctuation, the flow rate information from off-line calibrated models may not always be sufficiently robust to capture the actual flow rates over all roadway segments plagued by the incident-incurred queues, and may consequently affect the reliability of the estimated impacts on the detour rate.

Figure 5-3 illustrates the operational flows of this module, including activities to be executed in each step. It leverages a second-order traffic flow model as a quality control mechanism that integrates with an assessment and update algorithm to ensure that the errors of the estimated flow rate always lie within an acceptable range. In this study, the METANET model (Messmer and Papageorgiou, 1990) has been adopted as the traffic flow model for verifying the speed-flow dynamics due to its efficiency and flexibility under various traffic conditions. The core logic for assessing the predicted flow rates can be specified as follows:

- **Step 4-1**: Obtain $q_i^{k,1}(k)$ estimated by the off-line developed speed-flow models.
- **Step 4-2**: Apply $q_i^{k,1}(k)$ and $v_i^{k,1}(k)$ to METANET, and search for the METANET parameters that can minimize the estimation error for $v_i^{k+1,1}(k+1)$ – the difference between the speed detected by the probing vehicles and that projected with METANET.
- **Step 4-3**: Evaluate whether the estimation error is smaller than a pre-specified threshold, and proceed to the estimation for the next interval; otherwise, go to Step 4-4.
- **Step 4-4**: Estimate the reasonable range of the flow rate, using METANET with a pre-specified set of parameters.
- **Step 4-5**: Update the speed flow model using the flow rate estimated in Step 4-4 for use in future intervals.
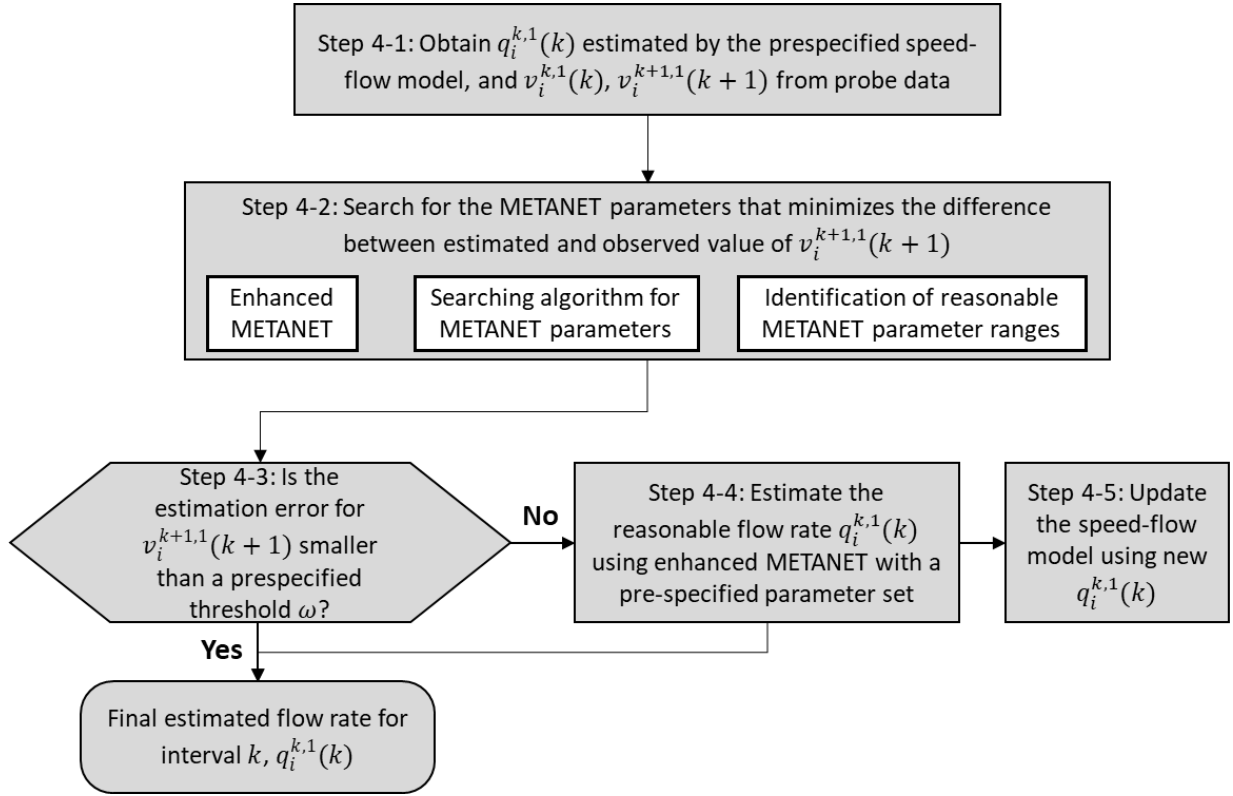
FIGURE 5-3: *Procedures of the Flow Rate Assessment and Update of the Speed-Flow Model*

The above process is grounded in the notion that using the probe speed and flow rate of time interval *k* (estimated by the off-line speed-flow models) as the input to METANET, its projected speed for interval *k*+1 should be within an acceptable range of the probing speed for the same time interval if the input flow rate data from the speed-flow models have the expected reliability. Notably, the output, such as flow rate and speed, from METANET may vary with the selected set of parameters. Hence, given the feasible upper and lower bounds for each of the METNET's key parameters, one can conclude the reliability of the flow rate predicted by the speed-flow rate models, as long as there exist a set of such parameters that enables METANT to produce the predicted speed that is within the acceptable range of the actual speed from probe

vehicles. To execute the above assessment process, the proposed system needs to have the following models:

- An enhanced version of METANET model that can better reflect the freeway's traffic evolution at the freeway interchange under incident scenarios;
- A searching algorithm to find the set of METANET parameters that can minimize the estimation error of the speed predicted for interval $k+1$;
- Specification of the reasonable ranges of parameters in the searching algorithm for METANET to robustly replicate the incident conditions on the target roadway segment.

Enhanced METANET Model

The speed evolution dynamics in the METANET by Messmer and Papageorgiou (1990), is shown in Eq. (4):

$$\hat{v}_i^{k+1,1}(k+1) = v_i^{k,1}(k) + \frac{T}{\tau}\{V[\rho_i^{k,1}(k)] - v_i^{k,1}(k)\} + \frac{T}{L_i}v_i^{k,1}(k)[v_{i-1}^{k,1}(k) - v_i^{k,1}(k)]$$
$$- \phi\frac{T}{L_i}\frac{[\rho_{i+1}^{k,1}(k) - \rho_i^{k,1}(k)]}{\rho_i^{k,1}(k) + \kappa} \tag{4}$$

Note that the convection term in Eq. (4), $\frac{T}{L_i}v_i(k)[v_{i-1}(k) - v_i(k)]$, is to reflect the continuity of traffic conditions between two consecutive freeway segments that are discretized for convenience of model computation. Likewise, the anticipation term, $\phi\frac{T}{L_i}\frac{[\rho_{i+1}(k)-\rho_i(k)]}{\rho_i(k)+\kappa}$, is proposed to capture the perceivable impacts of the downstream segment's traffic conditions–such as congestion–on the speed of drivers in the current segment.

Despite its effectiveness on most freeway segments, the above equation could not fully capture the impact on speed due to the following three traffic dynamics that are specifically prominent at the interchange area upstream of the incident site: 1) the change of speed due to the queue propagation from the downstream; 2) the speed reduction due to the weaving behavior at the interchange; and 3) the speed reduction due to the lane changes prior to the lane blockage location. Hence, this study proposes an enhanced METANET that can better fit the traffic condition both at the interchange area and during the incident by addressing the above three dynamics, as formulated in Eqs. (5)-(7).

$$\hat{v}_i^{k+1,1}(k+1) = \min\left\{v^m, v_i^{k,1}(k) + \frac{T\cdot v_i^{k,1}(k)}{L_i}\omega(\cdot) - \phi\frac{T}{L_i}\frac{[\rho_{i+1}^{k,1}(k) - \rho_i^{k,1}(k)]}{\rho_i^{k,1}(k) + \kappa}\right.$$
$$\left. - \frac{\varphi T}{L_i\lambda_i}\frac{\Delta\lambda \times \rho_i^{k,1}(k)}{\rho_{cr}e^D}v_i^{k,1}(k)^2 - \frac{\theta T\cdot v_i^{k,1}(k)}{L_i\lambda_i(\rho_i^{k,1}(k) + \kappa)}\psi(\cdot)\right\} \tag{5}$$

$$\omega(\cdot) = \begin{cases} [v_{i+1}^{k,1}(k) - v_i^{k,1}(k)] & if\ v_{i-1}^{k,1}(k) - v_{i+1}^{k,1}(k) > a\ AND\ v_{i-1}^{k,1}(k) - v_i^{k,1}(k) > b \\ [v_{i-1}^{k,1}(k) - v_i^{k,1}(k)] & Otherwise \end{cases} \tag{6}$$

$$\psi(\cdot) = \begin{cases} \max\{0, \max[0, v_f - v_i^{k,1}(k)] \cdot \rho_i^{k,1}(k) - \tau\} & if\ v_{i-1}^{k,1}(k) - v_i^{k,1}(k) > c \\ \max\{0, \max[0, v_{i-1}^{k,1}(k) - v_i^{k,1}(k)] \cdot \rho_i^{k,1}(k)\} & Otherwise \end{cases} \tag{7}$$

In Eq. (5), the term $\frac{T \cdot v_i^{k,1}(k)}{L_i}\omega(\cdot)$ models the change in the speed due to the queue propagation from downstream. Conceivably, when the queue from downstream has reached segment i+1, then the speed at segment i+1 would be impacted more significantly by such a speed than by that at segment i-1 as expressed in Eq. (6), where a and b are thresholds used to determine the presence of the queue from the downstream segment.

The term $\frac{\varphi T}{L_i \lambda_i}\frac{\Delta\lambda \times \rho_i^{k,1}(k)}{\rho_{cr}e^D}v_i^{k,1}(k)^2$ is specified to model the speed reduction due to the lane changes taking place ahead of the lane blockage location, where D denotes the distance from the incident location to the center of that probe segment (See Figure 5-1) and φ is the model parameter for the calibration. This term is inherited from the work by Messmer and Papageorgiou (1990) but refines it by further considering the distance to the incident location. The term $\frac{\theta T \cdot v_i^{k,1}(k)}{L_i \lambda_i\left(\rho_i^{k,1}(k)+\kappa\right)}\psi(\cdot)$ is an optional term applied to the interchange segment that captures the speed reduction due to the weavings at the interchange, where τ denotes the threshold of the on/off ramp flows to have a significant impact on the speed due to weaving activities; and θ is a calibrated parameter. Such speed reduction would only be accounted for when the approaching speed is significantly higher, as shown in Eq. (7), where c denotes a threshold over which the weaving activities are viewed to have a significant impact on the mainline's speed; and v_f denotes the free-flow speed.

Searching Algorithms for METANET Parameters

As shown in Figure 5-3, the flow rate estimated based on the probe speed will be verified with the enhanced METANET model. Specifically, the flow rate assessment criterion in this study is whether the METANET model, using a flow rate estimated from the speed-flow model at time interval k, can produce a speed value for time interval k+1 that is close to the ground truth, i.e., observed probe speed. Considering that the METANET model has three major parameters to calibrate, (i.e., ϕ, κ, φ). As such, the flow rate assessment is conducted by searching for a set of parameters that can minimize the difference between METANET-produced speed and the speed from probe vehicles. Such a search process can be done by solving the following optimization problem (OP):

OP 1:

$$Min \sum_i \frac{\hat{v}_i^{k+1,1}(k+1) - v_i^{k+1,1}(k+1)}{v_i^{k+1,1}(k+1)}$$

S.t.

$$Eqs. (5)\text{-}(7)$$
$$\phi^L \leq \phi \leq \phi^U$$
$$\kappa^L \leq \kappa \leq \kappa^U$$
$$\varphi^L \leq \varphi \leq \varphi^U$$

where $\hat{v}_i^{k+1,1}(k+1)$ denotes the speed computed from METANET; $v_i^{k+1,1}(k+1)$ denotes the probe speed; and $\phi^L, \phi^U, \varphi^L, \varphi^U, \kappa^L, \kappa^U$ denote the prespecified lower and upper bounds for the three parameters.

Note that under OP 1, those METANET parameters are decision variables to be optimized with the given predicted flow rate from the speed-flow models and the actual speed from the probing vehicles. If the objective value for OP 1 is greater than a prespecified threshold ω, it indicates that METANET–within the feasible range of its parameters and based on the flow rate obtained from the speed-flow model–fails to generate a reliable speed estimate consistent with that from the real-time detected speed by the probing vehicles. Thus, the set of speed-flow models needs to be updated with any viable update algorithm prior to its use for subsequent time intervals.

Note that OP 1 is highly non-linear and could not be solved with traditional linear programming solution algorithms. Hence, this study applies the method of Stochastic Ranking for Constrained Evolutionary Optimization (Runarsson and Yao, 2000) to perform the parameter search. Ten initial solutions for each optimization case have been randomly generated to avoid being trapped in a local optimum.

To ensure that the searching process is sufficiently comprehensive, and the results are robust, OP 1 will be executed seven times, each treating different parameters as variable(s) and the other parameters unchanged. More specifically, those seven search scenarios are defined as follows:
- **Scenario 1**: only parameter ϕ is the decision variable and keep the remaining two as constants.
- **Scenario 2**: only parameter κ is the decision variable and keep the remaining two as constants.
- **Scenario 3**: only parameter φ is the decision variable and keep the remaining two as constants.
- **Scenario 4**: Parameters ϕ and κ are the decision variables and keep parameter φ as constant.
- **Scenario 5**: Parameters ϕ and φ are the decision variables and keep parameter κ as constant.
- **Scenario 6**: Parameters κ and φ are the decision variables and keep parameter ϕ as constant.
- **Scenario 7**: Parameters ϕ, κ, and φ are all treated as decision variables.

Figure 5-4 demonstrates such a comprehensive searching process for all seven optimization scenarios, where ω denotes a prespecified threshold for the acceptable error. If the value of the objective function for each seven of optimization scenarios is less than such a prespecified threshold, then it can be concluded that the flow rate estimated from the speed-flow model is acceptable. Note that the optimal solutions from scenarios 1-3 can serve as references for the initial solutions for scenarios 4-7 to reduce the likelihood of the search being trapped in local optima. Specifically, for each parameter, a value within its specified range and closest to the optimal solutions from scenarios 1-3 should be selected for the generation of initial solutions in scenarios 4-7. For example, if the optimal value for parameter ϕ from Scenario 1 is between the pre-specified range for Scenario 4, such an optimal value should be adopted in one of the initial solutions for Scenario 4; otherwise, the upper or lower bound of ϕ for Scenario 4 should

be adopted, depending on whether the optimal value from Scenario 1 is larger or smaller than the specified range.
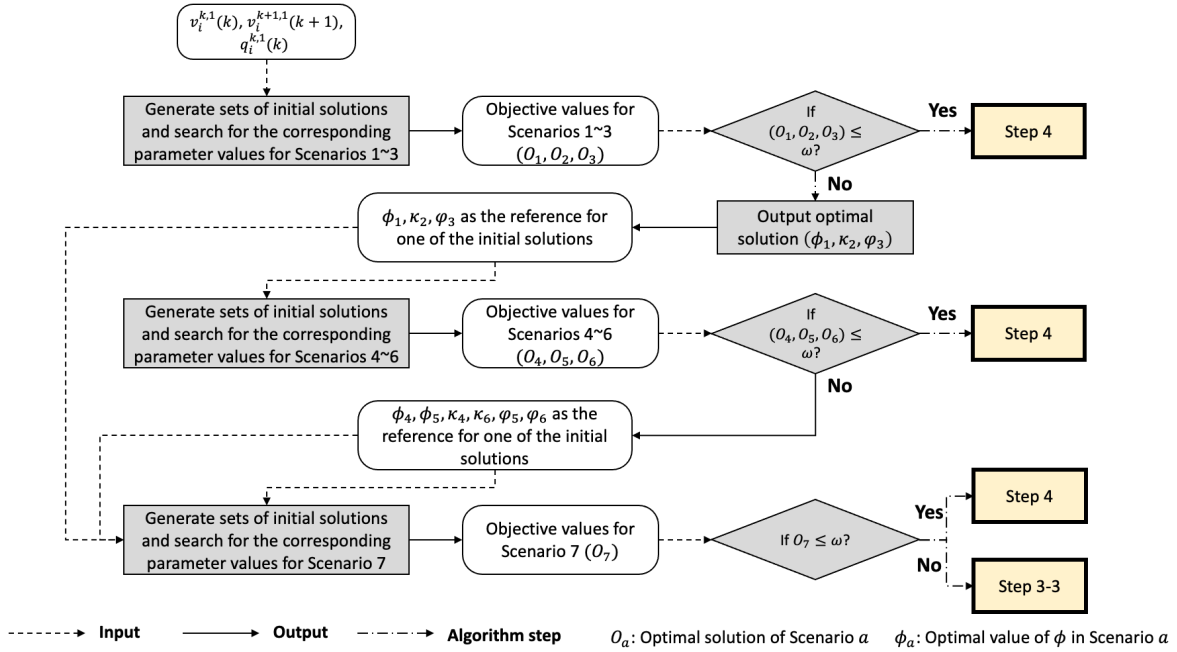

FIGURE 5-4: *The Searching Process to Verify the Flow Rate Estimated with the Speed-Flow Model*

Identification of a Reasonable Range for Each METANET Parameter

The acceptable ranges for each parameter should vary based on the number of parameters specified as decision variables and their designated functions. For example, let ϕ^*, κ^*, and φ^* be the optimal values of the parameters ϕ, κ, and φ, respectively, which were calibrated by minimizing the Mean Absolute Percentage Error (MAPE) using real-world data. Then, the acceptable ranges under each scenario for each parameter can be pre-defined with the following procedures:

- **Step 1**: Determine the tolerance level, denoted by δ, that represents the allowable increase of MAPE in percentage caused by a change in the parameter's value;
- **Step 2**: Conduct sensitivity analysis to identify the maximum change, in percentage, for each parameter that can keep the resulting MAPE within the tolerable range of $\delta\%$. The obtained upper and lower bounds, in percentage, for parameter ϕ are denoted as α^- and α^+, respectively. Likewise, β^- and β^+ are for parameter κ; γ^- and γ^+ are for parameter φ;
- **Step 3**: Compute the reasonable upper and lower bounds for each parameter under Scenarios 1-3. Let $\Theta_k^L(\Theta_k^U)$ be the lower (upper) bound of parameter Θ for optimization Scenario k, where $\Theta \in (\phi, \kappa, \varphi)$, one can specify the feasible upper and the lower bounds for the three major parameters as follows:

$$\phi_1^L = \phi\left(1 - \frac{\alpha^-}{100}\right), \qquad \phi_1^U = \phi\left(1 + \frac{\alpha^+}{100}\right)$$

$$\kappa_1^L = \kappa\left(1 - \frac{\beta^-}{100}\right), \qquad \kappa_1^U = \kappa\left(1 + \frac{\beta^+}{100}\right)$$

61

$$\varphi_1^L = \varphi\left(1 - \frac{\gamma^-}{100}\right), \qquad \varphi_1^U = \varphi\left(1 + \frac{\gamma^+}{100}\right)$$

- **Step 4**: Search the upper and lower bounds for each parameter under scenarios 4-7 with an optimization process. For example, one can identify the upper and the lower bounds for parameters ϕ and κ under Scenario 4 with the following formulations for optimization (*OP 2*):

OP 2:

$$Max \quad \frac{\phi_4^U - \phi_4^L}{\phi^*} \times \frac{\kappa_4^U - \kappa_4^L}{\kappa^*}$$

S.t.

$$\left[1 + \frac{\delta(\phi_4^U - \phi^*)}{\alpha^+\phi^*}\right] \times \left[1 + \frac{\delta(\kappa_4^U - \kappa^*)}{\beta^+\kappa^*}\right] \leq \left(1 + \frac{\delta}{100}\right)$$

$$\left[1 + \frac{\delta(\phi^* - \phi_4^L)}{\alpha^-\phi^*}\right] \times \left[1 + \frac{\delta(\kappa^* - \kappa_4^L)}{\beta^-\kappa^*}\right] \leq \left(1 + \frac{\delta}{100}\right)$$

$$\left[1 + \frac{\delta(\phi_4^U - \phi^*)}{\alpha^+\phi^*}\right] \times \left[1 + \frac{\delta(\kappa^* - \kappa_4^L)}{\beta^-\kappa^*}\right] \leq \left(1 + \frac{\delta}{100}\right)$$

$$\left[1 + \frac{\delta(\phi^* - \phi_4^L)}{\alpha^-\phi^*}\right] \times \left[1 + \frac{\delta(\kappa_4^U - \kappa^*)}{\beta^+\kappa^*}\right] \leq \left(1 + \frac{\delta}{100}\right)$$

where the objective of OP 2 is to maximize the combined allowable range for ϕ and κ. Each constraint in OP 2 aims to ensure that as long as both parameters vary within the specified range, the resulting increase in MAPE should not exceed $\delta\%$. For example, $\left[1 + \frac{\delta(\phi_4^U - \phi^*)}{\alpha^+\phi^*}\right]$ denotes the expected change in the computed speed when increasing ϕ, and the product of two such terms indicate the expected compound change resulting from the adjustments of such two parameters. By the same token, one can develop similar formulations to obtain the acceptable parameter ranges for scenarios 5-6.

For Scenario 7, involving three parameters, one can specify the formulations for the search of their bounds as follows:

OP 3:

$$Max \quad \frac{\phi_7^U - \phi_7^L}{\phi^*} \times \frac{\kappa_7^U - \kappa_7^L}{\kappa^*} \times \frac{\varphi_7^U - \varphi_7^L}{\varphi^*}$$

S.t.

$$\left[1 + \frac{\delta(\phi_7^U - \phi^*)}{\alpha^+\phi^*}\right] \times \left[1 + \frac{\delta(\kappa_7^U - \kappa^*)}{\beta^+\kappa^*}\right] \times \left[1 + \frac{\delta(\varphi_7^U - \varphi^*)}{\gamma^+\varphi^*}\right] \leq \left(1 + \frac{\delta}{100}\right)$$

$$\left[1 + \frac{\delta(\phi^* - \phi_7^L)}{\alpha^-\phi^*}\right] \times \left[1 + \frac{\delta(\kappa^* - \kappa_7^L)}{\beta^-\kappa^*}\right] \times \left[1 + \frac{\delta(\varphi^* - \varphi_7^L)}{\gamma^-\varphi^*}\right] \leq \left(1 + \frac{\delta}{100}\right)$$

$$\left[1 + \frac{\delta(\phi_7^U - \phi^*)}{\alpha^+\phi^*}\right] \times \left[1 + \frac{\delta(\kappa^* - \kappa_7^L)}{\beta^-\kappa^*}\right] \times \left[1 + \frac{\delta(\varphi^* - \varphi_7^L)}{\gamma^-\varphi^*}\right] \leq \left(1 + \frac{\delta}{100}\right)$$

$$\left[1 + \frac{\delta(\phi^* - \phi_7^L)}{\alpha^- \phi^*}\right] \times \left[1 + \frac{\delta(\kappa_7^U - \kappa^*)}{\beta^+ \kappa^*}\right] \times \left[1 + \frac{\delta(\varphi^* - \varphi_7^L)}{\gamma^- \varphi^*}\right] \leq \left(1 + \frac{\delta}{100}\right)$$

$$\left[1 + \frac{\delta(\phi^* - \phi_7^L)}{\alpha^- \phi^*}\right] \times \left[1 + \frac{\delta(\kappa^* - \kappa_7^L)}{\beta^- \kappa^*}\right] \times \left[1 + \frac{\delta(\varphi_7^U - \varphi^*)}{\gamma^+ \varphi^*}\right] \leq \left(1 + \frac{\delta}{100}\right)$$

$$\left[1 + \frac{\delta(\phi_7^U - \phi^*)}{\alpha^+ \phi^*}\right] \times \left[1 + \frac{\delta(\kappa_7^U - \kappa^*)}{\beta^+ \kappa^*}\right] \times \left[1 + \frac{\delta(\varphi^* - \varphi_7^L)}{\gamma^- \varphi^*}\right] \leq \left(1 + \frac{\delta}{100}\right)$$

$$\left[1 + \frac{\delta(\phi_7^U - \phi^*)}{\alpha^+ \phi^*}\right] \times \left[1 + \frac{\delta(\kappa^* - \kappa_7^L)}{\beta^- \kappa^*}\right] \times \left[1 + \frac{\delta(\varphi_7^U - \varphi^*)}{\gamma^+ \varphi^*}\right] \leq \left(1 + \frac{\delta}{100}\right)$$

$$\left[1 + \frac{\delta(\phi^* - \phi_7^L)}{\alpha^- \phi^*}\right] \times \left[1 + \frac{\delta(\kappa_7^U - \kappa^*)}{\beta^+ \kappa^*}\right] \times \left[1 + \frac{\delta(\varphi_7^U - \varphi^*)}{\gamma^+ \varphi^*}\right] \leq \left(1 + \frac{\delta}{100}\right)$$

Update of Speed Flow Models

Should the assessment process (Step 4-3 in Figure 5-3) conclude that the flow rate estimated by the speed flow model is not acceptable, one shall update the speed flow models. The procedures to do so are summarized as follows:

- **Step 1**: Use the METANET model, i.e., Eqs. (5)-(7), to estimate the flow rate with pre-specified values for the parameters (i.e., ϕ^*, κ^*, and φ^*).
- **Step 2**: Check whether the discrepancy between the flow rates, obtained from METANET and the speed-flow model, is due to the classification error, or the estimation error caused by day-to-day traffic variability. Specifically, the following three conditions need to be assessed:
  - If the flow rate estimated from METANET model is within the estimation range of another volume level, it is deemed as a classification error and go to Step 3;
  - If the flow rate estimated from METANET model is within the gap between two estimation ranges from two different classified volume levels, it is also deemed as a classification error and go to Step 4;
  - Otherwise, it is deemed as an estimation error and go to Step 5.
- **Step 3**: Reclassify current traffic conditions to the proper volume level, based on the flow rate information produced from METANET, and then apply the revised volume's associated speed-flow model for the next time interval.
- **Step 4**: Consider the designated volume level from previous n time intervals as references to identify which volume level to be adopted in the next time interval. This can be achieved by using Eq. (8):

$$Y = \sum_{k=k-n}^{k-1} \left\{ \alpha[1 + (1-\alpha) + (1-\alpha)^2 + \cdots + (1-\alpha)^{n-1}] \times \left(\sum_{k=k-n}^{k-1} 1_{\{q(k)\in L_1\}} - \sum_{k=k-n}^{k-1} 1_{\{q(k)\in L_2\}} \right) \right\} \quad (8)$$

where $0 < \alpha < 1$ is the weighting parameter; and L_1 and L_2 denote two different volume levels. Level L_1 should be adopted for the next time interval when $Y > 0$; otherwise, level L_2 should be adopted.

- **Step 5**: Update the speed-flow model to include the estimated flow rate from METANET while maintaining the size of its original covering area in Figure 5-5. Figure 5-5 illustrates an example, where q_M denotes the estimated flow rate from METANET and the original model is formulated as:

63

$$D \le q_M \le 1400 + \left(v_i^{k,1}(k) - 10\right) \times E \tag{9}$$

the updated model will adjust D and E to form a new covering area that can accommodate q_M. This can be achieved by using Eqs. (10)-(11).

$$\hat{D} = D + \left[60 - v_i^{k,1}(k)\right] \times \frac{q_M - 1400}{50} \tag{10}$$

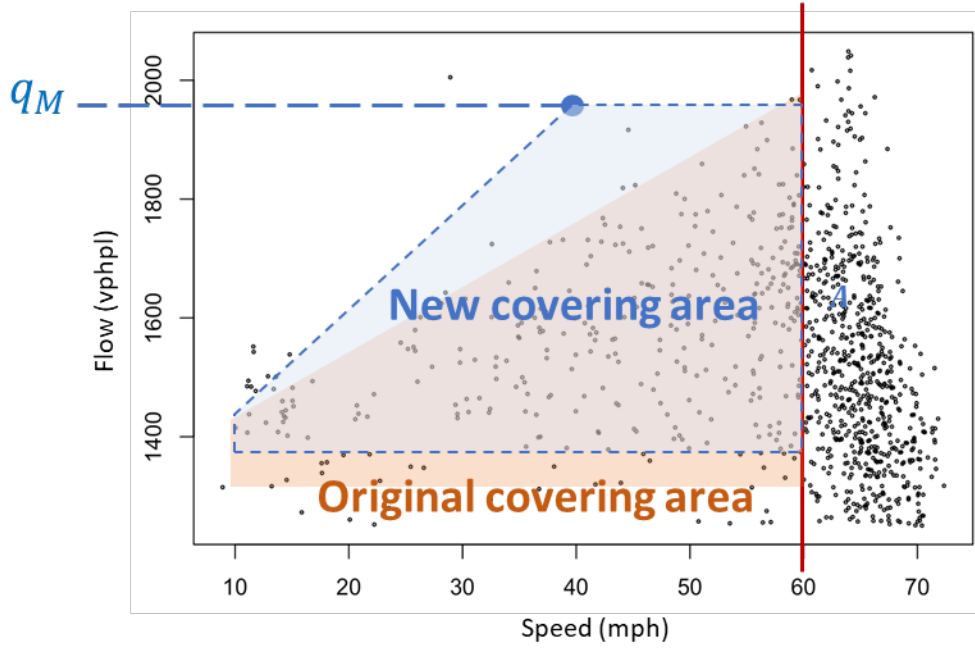$$\hat{E} = \frac{q_M - 1400}{v_i^{k,1}(k) - 10} \tag{11}$$

FIGURE 5-5: *An Example of the Update of the Speed-Flow Relation*

Enhancement of Estimated Flow Rate Reliability using Rolling Horizon Concept

Recognizing that the flow rate estimated with one set of speed data could be unreliable due to either detection error or short-term speed fluctuation, this study adopts the rolling horizon logic to ensure the reliability of flow rate estimation when more data become available (i.e., Step 5 in Figure 5-2). The step-by-step procedures to enhance the reliability of flow rate estimation are summarized below:

- **Step 5-1**: Estimate the set of flow rates from time interval $k - a$ to time interval k, where $a = 2,3,\ldots,h$, based on the developed speed flow models $f(v)$, as shown in Eq. (13):

$$q_i^{k+1,a}(k) = f(\hat{v}_i^{k+1,a}(k)) \tag{13}$$

where $\hat{v}_i^{k+1,a}(k)$ denotes the weighted average speed from time interval $k - a$ to time interval k, using the speed and flow rate information estimated from previous time intervals, as shown in Eq. (14):

$$\hat{v}_i^{k+1,a} = \frac{\sum_{n=0}^{a-1} v_i^{k-n+1,1}(k-n) \times q_i^{k-n+1,1}(k-n)}{\sum_{n=0}^{a-1} q_i^{k-n+1,1}(k-n)} \tag{14}$$

- **Step 5-2**: Estimate the single-interval flow rate from time interval $k - n - 1$ to time interval $k - n$, where $n = 1,2,\ldots,h-1$, using Eq. (15):

<div align="center">64</div>

$$q_i^{k+1, 1}(k - n) = q_i^{k+1, n+1}(k) \times (n + 1) - q_i^{k+1, n}(k) \times n \tag{15}$$

- **Step 5-3**: Enhance the reliability of the single-interval flow rate from time interval $k - n - 1$ to time interval $k - n$, where $n = 1, 2, \ldots, h - 1$, by integrating all estimated flow rates for that interval, as shown in Eq. (16):

$$\tilde{q}_i^{k+1, 1}(k - n) = \frac{\sum_{m=0}^{n} q_i^{k+1-m,1}(k - n)}{n + 1} \tag{16}$$

- **Step 5-4**: Compute reliable flow rate from time interval $k - 2h$ to time interval $k - h$, using the flow rate estimated for every individual time interval from time interval $k - 2h$ to time interval $k - h$, as formulated in Eq. (17)

$$\tilde{q}_i^{k+1, h}(k - h + 1) = \frac{\sum_{n=1}^{h} q_i^{k-h+n+1,1}(k - 2h + n + 1)}{h} \tag{17}$$

Figure 5-6 illustrates an example of applying such procedures for enhancing the reliability of the flow rate estimation, where $h = 5$ (i.e., that is, the estimates are produced per 5 minutes from the probe speed data collected per minute). While the flow rate estimation for time interval $k - 5$ to time interval k, dependent on the estimated results from time $k - 1$ to time k (as shown between the red dashed lines), can be made preliminarily at as early as time $k + 1$, the most reliable estimation will be provided at time $k + 5$ when more data is available.
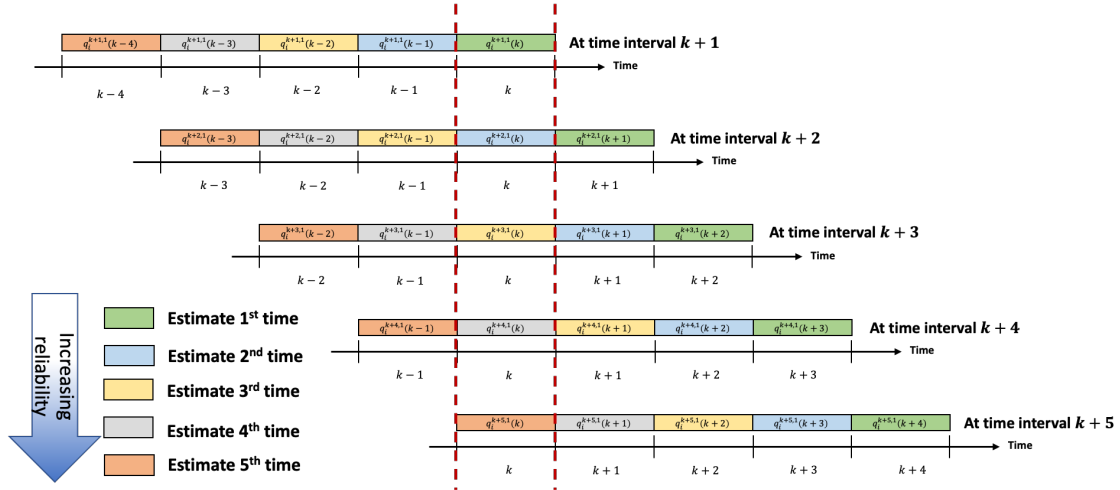
FIGURE 5-6: *Schematic Figure of the Initial Estimation and the Reliable Estimation of the Flow Rates*

5.3 NUMERICAL EXPERIMENTS

The numerical experiments reported in this study focus on two major tasks: 1) calibration of the enhanced METANET and identification of the feasible range for the model parameters; and 2) performance evaluation for the proposed R-DRES. The first task aims to calibrate a set of optimal parameters for the enhanced METANET by using the off-line data collected by available detectors, and then use the set of calibrated parameters to pre-define the feasible range for each parameter used in the flow rate assessment method. In the second task, the developed R-DRES will be applied to two incidents to estimate the detouring rate. The effectiveness of the flow rate assessment process will be based on whether the flow rate estimated from the speed-flow model, but not sufficiently reliable, can indeed be captured by the proposed methodology that employs the METANET model in a reversed computing process. This is followed by a performance

evaluation of the entire proposed system with the two following measures of effectiveness (MOEs):

- **MOE 1**: The differences between the observed total detouring rate and that estimated from the proposed model during the entire incident duration; and
- **MOE 2**: The consistency between the travel time increment on the detouring route and the detouring volume from the mainline.

Calibration of the Enhanced METANET and Identification of the Feasible Parameter Range

Prior to the application of the proposed system, one needs to first specify the parameters embedded in the enhanced METANET and their feasible ranges. The pre-specified parameters were calibrated using traffic data along a 6-mile segment of I-270 Maryland from Exit 16 to Exit 22 to capture the behavioral patterns of the local driving populations. The studied segment was deployed with three roadside sensors to collect speed and flow rate data, each covering a 2-mile sub-segment on the freeway modeled with METANET. The calibration was conducted using 5-minute average speed and flow rate data between 9/11/2022 to 9/17/2022 (an incident occurred on 9/15/2022), with a total of 10,080 records. Table 5-2 presents the calibrated value for each parameter specified in the enhanced METANET.

The feasible range was then identified based on the calibrated parameters, and the tolerance level for the MAPE increase where the change in parameters is set to be 10% (i.e., $\delta = 10\%$). Table 5-3 summarizes the resulting feasible ranges for three major parameters (i.e., ϕ, κ, and φ) under those seven distinct scenarios. With the calibrated parameter values and the feasible ranges for the three major parameters, the performance evaluation then proceeds with data from two real-world incidents.

TABLE 5-2: *Pre-Specified Values for METANET Parameter*

Pre-specified Parameters	
ϕ	48
κ	46 (veh/mile)
φ	1.79
π	15 (mph)
τ	690 (veh/hr)

| Scenario	Changeable parameter(s)	Feasible Range
1	ϕ	$15 \leq \phi \leq 96$
2	κ	$17 \leq \kappa \leq 401$
3	φ	$1.35 \leq \varphi \leq 2.26$
4	ϕ, κ	$32 \leq \phi \leq 71, 32 \leq \kappa \leq 220$
5	ϕ, φ	$31 \leq \phi \leq 73, 1.59 \leq \varphi \leq 2.00$
6	κ, φ	$32 \leq \kappa \leq 223, 1.58 \leq \varphi \leq 2.01$
7	ϕ, κ, φ	$37 \leq \phi \leq 64, 37 \leq \kappa \leq 158, 1.65 \leq \varphi \leq 1.94$

Incidents Information

To evaluate the effectiveness of the proposed model, this study has adopted two incident cases occurring on the southbound of I-95 in Maryland. The observed detour rate was extracted from the Trip Analytics tool of the Regional Integrated Transportation Information System (RITIS) database (CATT, 2023), which provides the routing patterns and origin-destination data from extensive sets of time-stamped "bread-crumb trails" that are created by probe vehicles in the traffic flows. By using this tool, one can collect the routing pattern of those probe vehicles during the incident duration and compare them with that without the incident during the same day of the week and time of day. Such a difference for the entire incident duration would be regarded as the observed detouring rate.

Figure 5-7 illustrates the information of incident Case 1, which occurred on the southbound of I-95 on 12/21/2022, causing 5 miles of the incident queue and 90 minutes of the incident duration. Hence, the three upstream interchanges (i.e., I-95 @ MD 32, I-95 @ MD 175, and I-95 @ MD 100) were taken into consideration to estimate the potential detouring rate. The potential detouring routes for vehicles traveling southbound of I-95 include US-1 on the East side of I-95 and US 29 on the West side. Based on such information, the Trip Analytics tool was then used to collect associated information (see Figure 5-7). The routing patterns of vehicles on two different days (i.e., with and without the incident) traversing through the defined zone and with their travel starting points and ending points outside the defined zone are collected. It can be observed that 100% of vehicles would take I-95 without the incident, while 79.6% of the traffic remains on I-95 with the incident, indicating a 20.4% detouring rate.

Figure 5-8 illustrates the incident information of Case 2. The incident location was on the southbound lanes of I-95, the incident duration was 150 minutes and incurred 3.3 miles of the queue. Hence, considering its impact area, the two upstream interchanges (i.e., I-95 @ MD 175, and I-95 @ MD 100) were used to estimate the potential detouring rate. Similar to Case 1, the potential detouring route for vehicles traveling southbound of I-95 includes US-1 on the East side of I-95 and US 29 on the West side. The routing patterns of vehicles on two different days (i.e., with and without the incident) are collected from the Trip Analytics Tool, as shown in Figure 5-8. Likewise, 100% of vehicles would stay on I-95 without the incident, while 74.0% of the traffic stays on I-95 during the incident, indicating a 26.0% detouring rate.
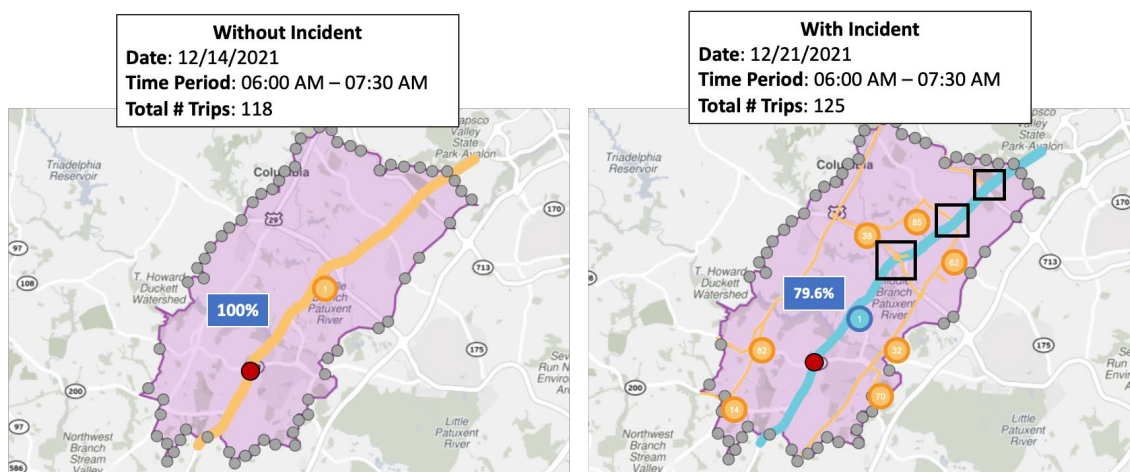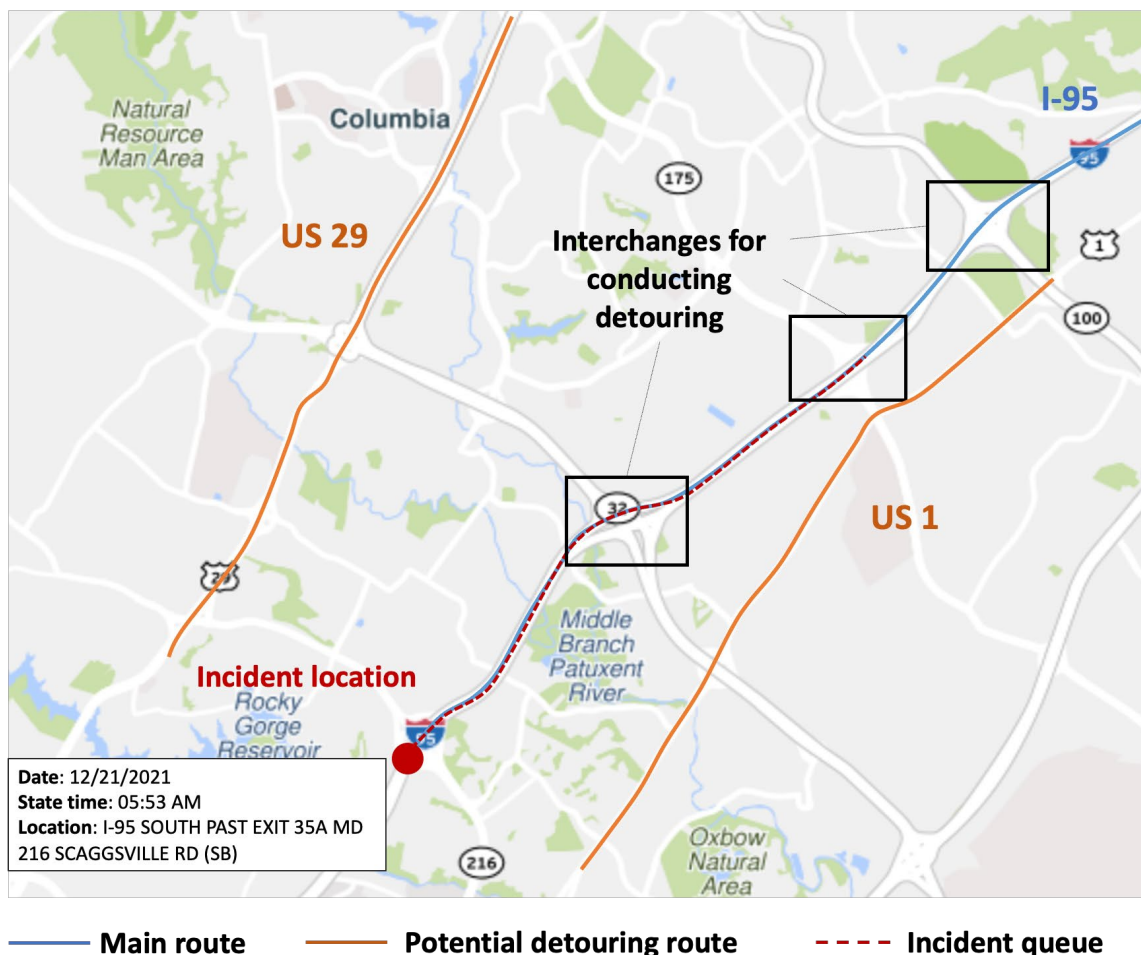
FIGURE 5-7: *Incident Information and Routing Patterns for Incident Case 1*
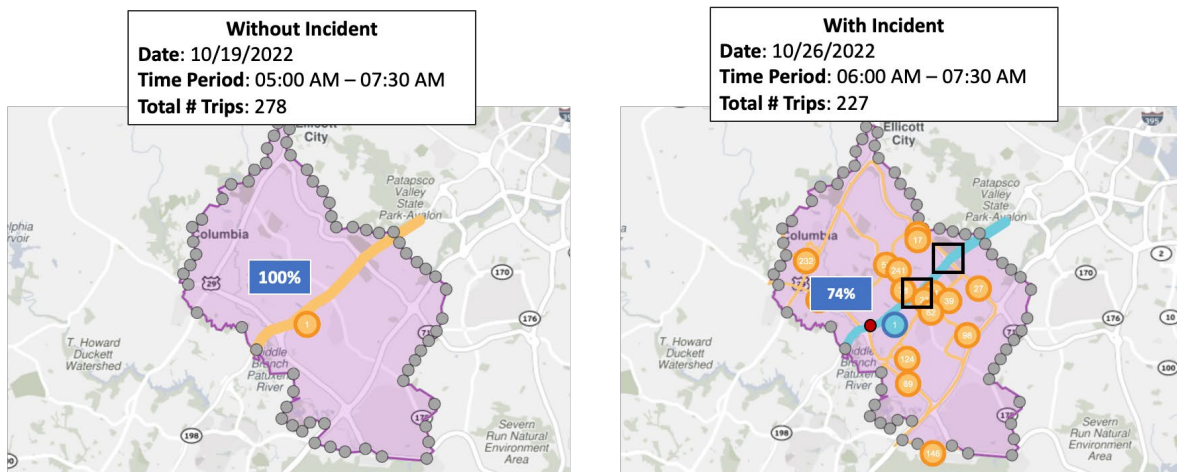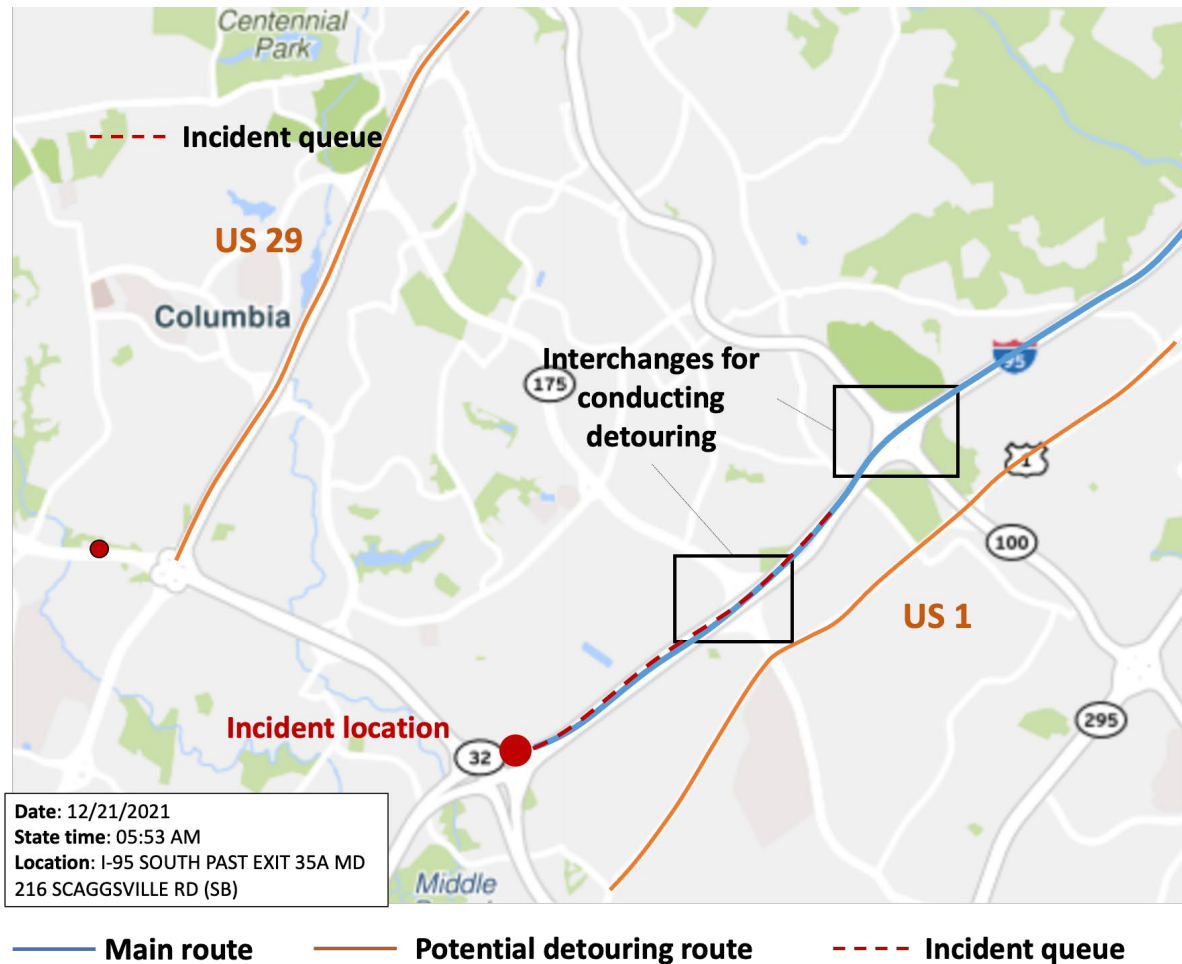
FIGURE 5-8: *Incident Information and Routing Patterns for Incident Case 2*

Verification of the Flow Rate Assessment Function

As for the effectiveness of the proposed R-DRES, the number of unacceptable flow rate estimates detected by the assessment function are summarized in Table 5-4. Note that the speed-

flow relation can indeed capture the traffic conditions of freeway segments under incident-free conditions yielding acceptable flow estimates for all roadway segments in Case 1 and Case 2. In addition, it is also shown that the speed-flow relation performs well in Case 1, resulting in only 0.7% of unacceptable estimates of the flow rate. For Case 2, the unacceptable rate was up to 2.3%, indicating that there were more complex traffic dynamics which cannot be precisely captured with the off-line calibrated speed-flow relations. As such, the update algorithm based on the METANET was triggered more frequently to enhance the reliability of the speed-flow relations.

TABLE 5-4: *Number of Unacceptable Estimates of Flow Rate from the Speed-Flow Models*

|	Case-1 (270 samples)[a]				Case-2 (300 samples)[a]		
	Interchange-1	Interchange-2	Interchange-3	Avg. acceptable rate	Interchange-1	Interchange-2	Avg. acceptable rate
w/o incident[b]	0	0	0	0%	0	0	0%
w/ incident[c]	0	2	0	0.7%	3	4	2.3%

Note:
[a] Total number of sample estimates executed by the models.
[b] The number of unacceptable rate estimations from the speed-flow model during an incident-free period
[c] The number of unacceptable flow rate estimations from the speed-flow model during the incident clearance period.

Figure 5-9 shows the comparison results of the flow rate over time for Interchange 1 (i.e., MD 195 @ I-95). It can be observed that three estimated flow rates (i.e., 96th-98th minute) from speed-flow models are deemed unacceptable based on the assessment results with the METANET model (see orange dots in Figure 5-9). The estimation errors from the speed-flow model are likely due to the sudden speed drop near Interchange 2 caused by the propagation of the incident queue starting from the 93rd minute (as shown in the lower figure of Figure 5-9). However, by updating the speed-flow model with data from those three time periods (96th-98th minute), it is noticeable that the model regains its ability to capture traffic conditions over the remaining time periods.
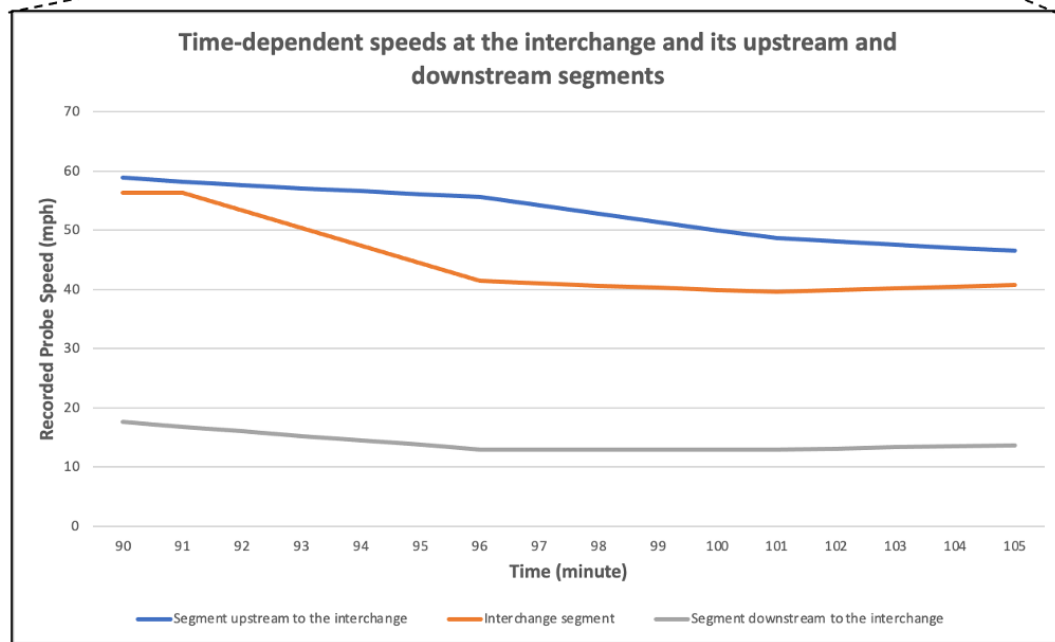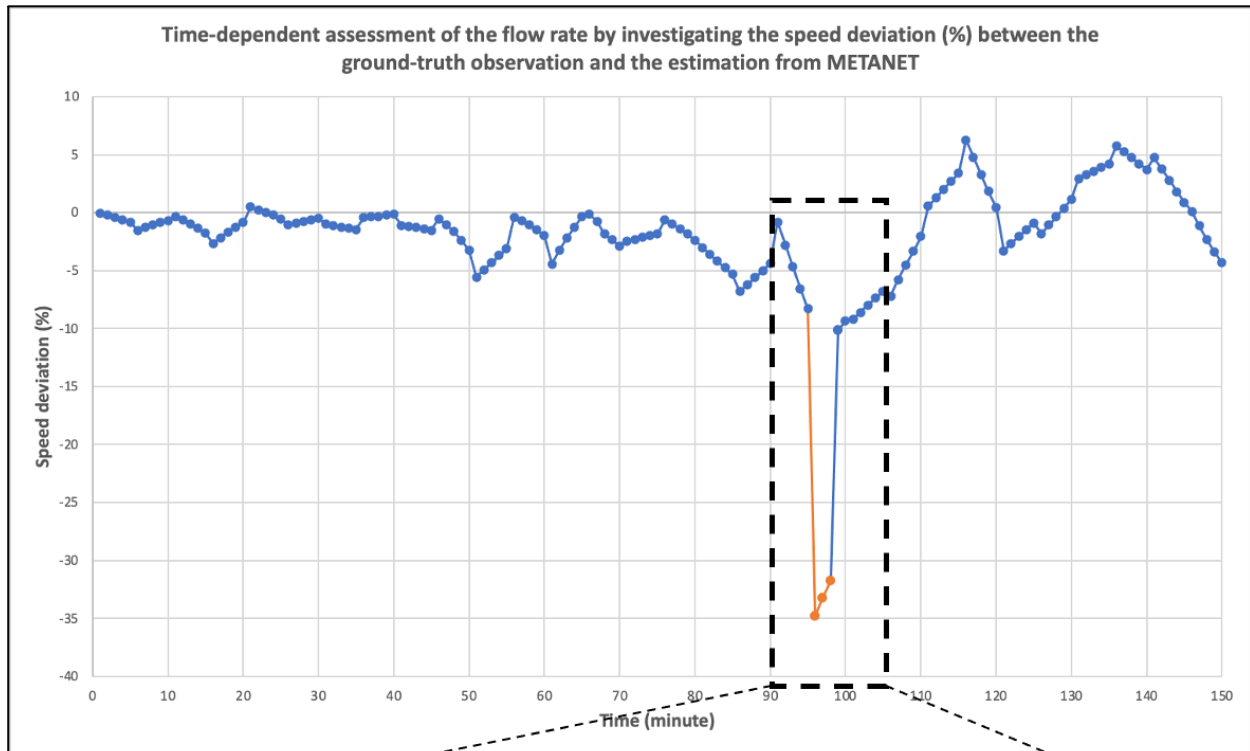
FIGURE 5-9: *Illustration of the Flow Rate Assessment Function from METANET Model*

## Performance Evaluation of the Proposed R-DRES

To evaluate the reliability and accuracy of the detour rate estimation by R-DRES, Table 5-5 summarizes the MOE 1 for Case 1 and Case 2. The estimation results with and without the use of the assessment function are shown to compare their differences. It shows that with the

assessment function with METANET model, the proposed system can provide reliable estimations of the detouring rate, with only a 2.7% and 0.2% difference from the ground-truth detouring rate. In contrast, without using the assessment and performing the model update, the estimation system clearly yields inferior results.

TABLE 5-5: Evaluation results of the detouring rate estimation with MOE-1

	Case 1		Case 2	
Total Inflow (veh)	2,377		4,319	
Ground-truth Detouring Rate (%)	20.4%		26.0%	
With the assessment function or not	Yes	No	Yes	No
Total Detouring Volume (veh)	549	557	1134	917
Detouring Rate (%)	23.1%	23.4%	26.2%	21.2%
MOE-1 (Total Detouring Volume/Total Inflow)	2.7%	3.0%	0.2%	4.8%

To further evaluate the effectiveness of the entire R-DRES system, this study tested whether the detouring flow rate and the increase in the detour route's travel time share the same trend. For Case 1, the travel time on the segment between Exit 15 and Exit 16 of US 29 was collected because it accommodated the most detouring vehicles and locates just upstream of the interchange of US 29 @ MD 216 where the detouring vehicles are likely to get back to I-95 to avoid congestion due to the incident. Likewise, the segment between Exit 16 and Exit 18 of US 29 was collected for Case 2. The McDonald-Kreitman test (McDonald and Kreitman, 1991) was conducted to test if the increment of the travel time on the detouring route and the detouring volume from the mainline share the same trend. The evaluation results in Figure 5-10 show that the trends of the detouring flow from the mainlines are consistent with the evolution of travel time increment on the associated detouring roadway segments, confirming the effectiveness of the proposed R-DRES system in estimating detouring rate.

McDonald-Kreitman test	5th-60th minute	60th-90th minute
Detouring flow	*Increase*	*Decrease*
Travel time increment on the detouring route	*Increase*	*Decrease*

McDonald-Kreitman test	5th-150th minute
Detouring flow	*Increase*
Travel time increment on the detouring route	*Increase*
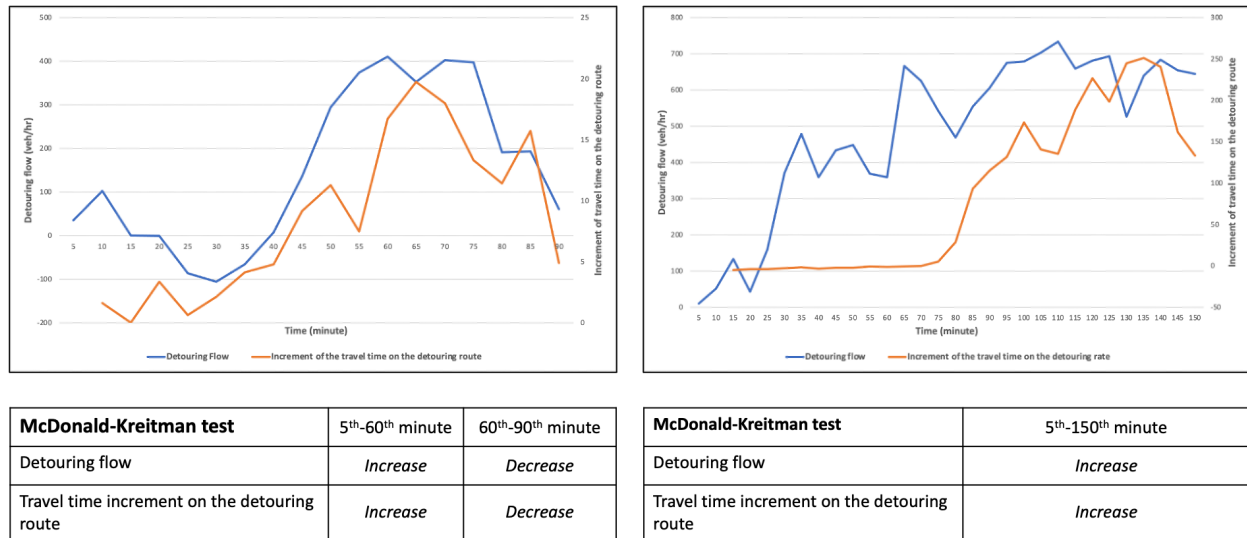
FIGURE 5-10: *Evaluation Results of the Detouring Rate Estimation with MOE-2*

In brief, experimental analyses with data from two real-world incidents have shown that the proposed system offers the potential for use in estimating the detouring rate to neighboring arterials, resulting from time-varying queues due to a freeway incident. Such a system, designed mainly for approximating detouring traffic impacts on neighboring streets without information from traffic surveillance systems, may not yield precise detour flow rate information over time, but its resulting estimates are within the acceptable range and sufficiently robust for traffic control centers to assess the need to active necessary control strategies, especially during the clearance period of severe incidents.

Chapter 6
Conclusions and Recommendations

6.1 CONCLUDING FINDINGS

This phase of the study has finalized the innovative system for real-time prediction of a detected incident's duration and its potential traffic impacts on both the subject freeway and its neighboring local streets due to the queues and resulting detouring off-ramp flows. With such information, highway agencies responsible for incident response and traffic management can inform en-route motorists via any advanced traveler information system or public media of the location and time duration over which the freeway segment will be plagued by nonrecurrent congestion queues. Depending on the severity level of the detected incidents and the estimated traffic impacts, responsible traffic agencies can either concurrently or sequentially respond with appropriate strategies. Some major findings from this study are summarized below:

1. The innovative method of transferability analysis developed in this study has proved its effectiveness in coping with the data insufficient issue, allowing the responsible agency to take advantage of some quality data and well-calibrated models from some regions/districts to generate the estimated clearance time for a detected incident in other areas (e.g., underserved highway networks). More specifically with the developed methodology the extensive set of knowledge-based rules for incident duration prediction, developed for I-495, I-695, I-70, and US 29, can be applied to all major highways which suffer from insufficient incident data for calibrating their own customized prediction models.

2. Although a traffic surveillance system with well-calibrated and properly spaced sensors is most desirable for designing and operating a real-time effective incident response and traffic management system, the speed data from probing vehicles integrated with a set of off-line reliably calibrated models can produce an acceptable approximate of a detected incident's traffic impact range during incident clearance period. Such information is sufficiently reliable for use in advanced traveler information systems and the selection of responsive traffic management strategies.

3. Innovative integration of speed data from real-time probing vehicles and a well-calibrated macroscopic traffic model seems to offer any viable alternative for estimating the detour rate from mainline traffic within the impact boundaries of the incident-incurred queues, and for assessing the resulting impacts to neighboring local networks.

4. This study–with an innovative modeling methodology in artificial intelligence and creative use of available archived traffic data–clearly shows that one can derive essential estimates critical to efficient incident response and traffic management, including the estimated incident clearance duration, the maximum distance of the resulting queue impacts on the main traffic and neighboring local networks.

5. The system, developed in this study for incident response and traffic management, offers an effective alternative for highway agencies to circumvent the need of extensive detector deployment and the demanding maintenance efforts, as well as the associated costs, so long as all essential traffic and incident-related data are properly archived in a reliable database system.

In brief, it is expected that the best use of the developed system with only archived data and real-time probe vehicle information can produce significant benefits to the entire community served by the highway networks, including the reduction in incident-incurred congestion delay, fuel consumption, emissions, potential secondary incidents, balance of traffic conditions between the freeway mainline and its detour routes, and associated costs for maintaining an efficient incident detection, response, and management operation.

6.2 RECOMMENDATIONS FOR FUTURE STUDIES

Although this study has successfully developed an integrated incident management system that with its innovative modeling structure can effectively circumvent the demanding development efforts and extensive data needs for key module calibration, much, however, remains to be done to ensure the sustainable operations of such a system and its reliability as well as accuracy with emerging new technologies. Some of the essential future extensions and enhancements are listed below:

1. A mechanism with state-of-the-art methodology in artificial intelligence for the developed system to automatically update its key parameters, based on the newly available data from daily incident response and operations.
2. Periodical recalibration and update of those off-line calibrated speed-flow relation models under various incident scenarios will be essential so that the evolution of traffic patterns and possible change in driver responses to incident scenarios, reflected, to some extent, in the archived datasets can be properly captured with updated model parameters.

REFERENCES

Abdel-Aty, M., and M. F. Addalla. Modeling Drivers' Diversion from Normal Routes Under ATIS Using Generalized Estimating Equations and Binomial Probit Link Function. Transportation, Vol. 31, No. 3, 2004, pp. 327–348.

Agrawal, R., T. Imielinski, and A. Swami. Mining Association Rules between Sets of Items in Large Databases. Proc., 1993 ACM SIGMOD International Conference on Management of Data, Washington, D.C., Association for Computing Machinery (ACM), 1993, pp. 207–216.

Al-Deek, H., S. Venkata, J. Flick, and A. Khattak. Dynamic Message Sign Deployment and Diversion Behavior of Travelers on Central Florida Toll Roads. Transportation Research Record: Journal of the Transportation Research Board, 2009. 2129: 24–34.

Akçelik, R. 1997. Progression factor for queue length and other queue-related statistics. Transportation Research Record. No. 1555, pp. 99–104.

Ban, X., J.S. Pang, H.X. Liu, and R. Ma. 2012. Continuous-time point-queue models in dynamic network loading. Transportation Research Part B. Vol. 46, no. 3, pp. 360-380.

Biecek, P. and Burzykowski, T. 2020. Explanatory Model Analysis: Explore, Explain and Examine Predictive Models. New York. Chapman and Hall/CRC

Boyles, S., D. Fajardo, and S. T. Waller. A Naive Bayesian Classifier for Incident Duration Prediction. Presented at 86th Annual Meeting of the Transportation Research Board, Washington, D.C., 2007.

Breiman, L. 1984. Classification and Regression Trees. New York: Routledge.

Carlson, R.C., I. Papamichail, M. Papageorgiou, and A. Messmer. 2010. Optimal mainstream traffic flow control of large-scale motorway networks. Transportation Research Part C. Vol. 18, no. 2, pp. 193-212.

Cassidy, M.J. and R.L. Bertini. 1999. Some traffic features at freeway bottlenecks. Transportation Research Part B: Methodological. Vol. 33, No. 1, pp. 25-42.

Cao, J., Md. Hadiuzzaman, T.Z. Qiu, and D. Hu. 2015. Real-time queue estimation model development for uninterrupted freeway flow based on shockwave analysis. Canadian Journal of Civil Engineering. Vol. 42, No. 3, pp. 153-163.

Cao, J., D. Hu, and Md. Hadiuzzaman. 2014. Comparison of Queue Estimation Accuracy by Shockwave-Based and Input-Output-Based Models. 17th International Conference on Intelligent Transportation System. Qingdao, China.

CATT Lab. 2023. Regional Integrated Transportation Information System.

Chatterjee, K., and M. Mcdonald. Effectiveness of Using Variable Message Signs to Disseminate Dynamic Traffic 450 Transportation Research Record 2676(6) Information: Evidence from Field Trials in European Cities. Transport Reviews, Vol. 24, No. 5, 2004, pp. 559–585.

Chang, H. L., and T. P. Chang. Prediction of Freeway Incident Duration based on Classification Tree Analysis. Journal of the Eastern Asia Society for Transportation Studies, Vol. 10, 2013, pp. 1964–1977.

Charnes, A., Cooper, W.W., and Rhodes, E. Measuring the Efficiency of Decision Making Units. European Journal of Operational Research. Vol. 2, 1978, pp.429–444.

Cheng, Q., Z. Liu, J. Guo, X. Wu, R. Pendyala, B. Belezamo, and X. Zhou. 2022. Estimating key traffic state parameters through parsimonious spatial queue models. Transportation Research Part C: Emerging Technologies. Vol. 137.

Cheevarunothai, P., M. Mooney, and Y. Wang. 2007. Statistical and Queuing Analyses of Freeway Incidents in Washington State. 2007 IEEE Intelligent Transportation Systems Conference. Bellevue, USA.

Cortes, C. and V. Vapnik. 1995. Support-Vector Networks. Machine Learning. 20, pp. 273-297.

Chung, Y. Development of an Accident Duration Prediction Model on the Korean Freeway Systems. Accident Analysis & Prevention, Vol. 42, No. 1, 2010, pp. 282–289.

Chung, K., J. Rudjanakanoknad, and M.J. Cassidy. 2007. Relation between traffic density and capacity drop at three freeway bottlenecks. Transportation Research Part B: Methodological. Vol. 41, No. 1, pp. 82-95.

Du, B., S. Chien, J. Lee, and L. Spasovic. 2017. Predicting Freeway Work Zone Delays and Costs with a Hybrid Machine-Learning Model. Journal of Advanced Transportation. Vol. 2017.

El-Basyouny, K., and T. Sayed. Comparison of Two Negative Binomial Regression Techniques in Developing Accident Prediction Models. Transportation Research Record: Journal of the Transportation Research Board, 2006. 1950: 9–16.

Elefteriadou, L., R.P. Roess, and W.R. McShane. 1995. Probabilistic nature of breakdown at freeway merge junctions. Transportation Research Record.

Erera, A.L., T.W. Lawson, and C.F. Daganzo. 1998. Simple, Generalized Method for Analysis of Traffic Queue Upstream of a Bottleneck. Transportation Research Reocrd. Vol. 1646, No. 1, pp. 132-140.

Essien, A., I. Petrounias, P. Sampaio, and S. Sampaio. A Deep-Learning Model for Urban Traffic Flow Prediction with Traffic Events Mined from Twitter. World Wide Web: Internet and Web Information Systems, Vol. 24, No. 4, 2021, pp. 1345–1368.

Farradyne, P.B., 2000. Traffic incident management handbook. Prepared for Federal Highway Administration, Office of Travel Management.

Foo, S., and B. Abdulhai. Evaluating the Impacts of Changeable Message Signs on Traffic Diversion. Proc., Intelligent Transportation Systems Conference, ITSC'06, IEEE, New York, 2006, pp. 891–896.

Garib, A., A. E. Radwan, and H. Al-Deek. Estimating Magnitude and Duration of Incident Delays. Journal of Transportation Engineering, Vol. 123, No. 6, 1997, pp. 459–466.

Geroliminis, N. and A. Skabardonis. 2005. Prediction of arrival profiles and queue lengths along signalized arterials by using a markov decision process. Transportation Research Record. Vol. 1934, No. 1, pp. 116–124.

Giuliano, G. Incident Characteristics, Frequency, and Duration on a High Volume Urban Freeway. Transportation Research Part A: General, Vol. 23, No. 5, 1989, pp. 387–396.

Ghosh, B., J. Dauwels, and U. Fastenrath. 2017. Analysis and prediction of the queue length for non-recurring road incidents. 2017 IEEE symposium Series on Computational Intelligence. Honolulu, Hi, USA.

Golob, T. F., W. W. Recker, and J. D. Leonard. An Analysis of the Severity and Incident Duration of Truckinvolved Freeway Accidents. Accident Analysis & Prevention, Vol. 19, No. 5, 1987, pp. 375–395.

Guan, L., W. Liu, X. Yin, and L. Zhang. Traffic Incident Duration Prediction Based on Artificial Neural Network. Proc., 2010 International Conference on Intelligent Computation Technology and Automation, Changsha, China, IEEE, New York, 2010.

Hadi, M., Y. Xiao, and M. Rojas. Estimation of Diversion Rate During Incidents on Basis of Main-Line Detector Data. Transportation Research Record: Journal of the Transportation Research Board, 2013. 2396: 54–60.

Hadiuzzaman, M. and Z.T. Qiu. 2013. Cell transmission model based variable speed limit control for freeways. Transportation Research Board 91st Annual Meeting. Washington D. C.

Haghani, A., M. Hamedi, R. L. Fish, and A. Nouruzi. Evaluation of Dynamic Message Signs and Their Potential Impact on Traffic Flow. Report No. MD-13-SP109B4C. Maryland State Highway Administration, Research Division, Baltimore, MD, 2013.

Han, K.E., T.L. Friesz, T. Yao. 2013a. A partial differential equation formulation of Vickrey's bottleneck model, Part I: Methodology and theoretical analysis. Transportation Research Part B: Methodologies. Vol. 49, pp. 55-74.

Han, K.E., T.L. Friesz, T. Yao. 2013b. A partial differential equation formulation of Vickrey's bottleneck model, Part II: Numerical analysis and computation. Transportation Research Part B: Methodologies. Vol. 49, pp. 75-93.

Hahsler, M., B. Gru¨n, and K. Hornik. A Computational Environment for Mining Association Rules and Frequent Item Sets. Journal of Statistical Software, Vol. 14, No. 15, 2005, pp. 1–25.

He, Q., Y. Kamarianakis, K. Jintanakul, and L. Wynter. Incident Duration Prediction with Hybrid Tree-based Quantile Regression. In Advances in Dynamic Network Modeling in Complex Transportation Systems, Springer, 2013, pp. 287–305.

He, Z., W. Guan, and S. Ma. A Traffic-Condition-Based Route Guidance Strategy for a Single Destination Road Network. Transportation Research Part C: Emerging Technologies, Vol. 32, No. 4, 2013, pp. 89–102.

He, Z., L. Zheng, W. Guan, and B. Mao. A Self-Regulation Traffic-Condition-Based Route Guidance Strategy with Realistic Considerations: Overlapping Routes, Stochastic Traffic and Signalized Intersections. Journal of Intelligent Transportation Systems, Vol. 20, No. 6, 2016, pp. 545–558.

Hegyi, B. De Schutter, and H. Hellendoorn. 2005. Model predictive control or optimal coordination of ramp metering and variable speed limit. Transportation Research Part C. Vol. 13, no. 3, pp. 185-209.

Hojati, A. T., L. Ferreira, S. Washington, and P. Charles. Hazard Based Models for Freeway Traffic Incident Duration. Accident Analysis & Prevention, Vol. 52, 2013, pp. 171–181.

Hong, J., R. Tamakloe, and D. Park. Estimating Incident Duration Considering the Unobserved Heterogeneity of Risk Factors for Trucks Transporting HAZMAT on Expressways. Transportation Research Record, Vol. 2673, No. 2, 2019, pp. 232-242.

Huchingson, R. D., and C. L. Dudek. Delay, Time Saved, and Travel Time Information for Freeway Traffic Management. Transportation Research Record: Journal of the Transportation Research Board, 1979. 722: 36–40.

Hurdle, V.F. and B. Son. 2001. Shock Wave and Cumulative Arrival and Departure Models: Partners Without Conflict. Transportation Research Record. Vol. 1776, No. 1, pp. 159-166.

Ji, Y. Prediction of Freeway Incident Duration Based on the Multi-model Fusion Algorithm. Proc., 2011 International Conference on Remote Sensing, Environment and Transportation Engineering (RSETE), Nanjing, China, IEEE, New York, 2011.

Jiang, Y. 2001. Estimation of Traffic Delays and Vehicle Queues at Freeway Work Zone. Transportation Research Board. Washington D.C.

Kattan, L., K. Habib, S. Nadeem, and T. Islam. Modeling Travelers' Responses to Incident Information Provided by Variable Message Signs in Calgary, Canada. Transportation Research Record: Journal of the Transportation Research Board, 2010. 2185: 71–80.

Kerner, B.S. 2002. Empirical macroscopic features of spatial-temporal traffic patterns at highway bottlenecks. Physical Review E. Vol. 65, No. 4.

Khattak, A. J., H. M. Al-Deek, and R. W. Hall. Concept of an Advanced Traveler Information System Testbed for the Bay Area: Research Issues. Journal of Intelligent Transportation Systems, Vol. 2, No. 1, 1994, pp. 45–71.

Khattak, A. J., J. L. Schofer, and M. H. Wang. A Simple Time Sequential Procedure for Predicting Freeway Incident Duration. Journal of Intelligent Transportation Systems, Vol. 2, No. 2, 1994, pp. 113–138.

Khattak, A., X. Wang, and H. Zhang. Incident Management Integration Tool: Dynamically Predicting Incident Durations, Secondary Incident Occurrence and Incident Delays. IET Intelligent Transport Systems, Vol. 6, No. 2, 2012, pp. 204–214.

Khattak, A. J., J. Liu, B. Wali, X. Li, and M. Ng. Modeling Traffic Incident Duration Using Quantile Regression. Transportation Research Record: Journal of the Transportation Research Board, 2016. 2554: 139–148.

Khattak, A. J., F. S. Koppelman, and J. L. Schofer. Stated Preferences for Investigating Commuters' Diversion Propensity. Transportation, Vol. 20, 1993, pp. 107–127. https://doi.org/10.1007/BF01307055.

Kim, W., and G. L. Chang. Development of a Hybrid Prediction Model for Freeway Incident Duration: A Case Study in Maryland. International Journal of Intelligent Transportation Systems Research, Vol. 10, No. 1, 2012, pp. 22–33.

Kuwahara, M. and T. Akamatsu. 1997. Decomposition of the reactive dynamic assignments with queues for a many-to-many origin–destination pattern. Transportation Research Part B: Methodologies. Vol. 31, no. 1, pp. 1-10.

Laman, H., S. Yasmin, and N. Eluru. Joint Modeling of Traffic Incident Duration Components (Reporting, Response, and Clearance Time): A Copula-Based Approach. Transportation Research Record, Vol. 2672, No. 30, 2018, pp. 76-89.

Laval, J. A. and L. Leclercq. 2008. Microscopic modeling of the relaxation phenomenon using a macroscopic lane-changing model. Transportation Research Part B: Methodological. Vol. 42, No. 6, pp. 511-522.

Law, A. M., Kelton, W. D., & Kelton, W. D. (2007). Simulation modeling and analysis (Vol. 3). New York: Mcgraw-hill.

Lawson, T.W., D.J. Lovell, and C.F. Daganzo. 1997. Using Input-Output Diagram To Determine Spatial and Temporal Extents of a Queue Upstream of a Bottleneck. Transportation Research Record. Vol. 1572, No. 1, pp. 140-147.

Leclercq, L., et al., Capacity drops at merges: analytical expression for multilane freeways. Transportation Research Record.

Lee, D.A. Noyce, and X. Qin. 2008. Development of Traffic Delay Assessment Tool for Short-Term Closures on Urban Freeways. Transportation Research Record. Vol. 2055, No. 1, pp. 39-48.

Lee, Y., C.-H. Wei, and K.-C. Chao. 2018. Evaluating the Effects of Highway Traffic Accidents in the Development of a Vehicle Accident Queue Length Estimation Model. International Journal of Intelligent Transportation Systems Research. Vol. 16, pp. 26-38.

Li, B., W. Cheng, and L. Li. 2018. Real-Time Prediction of Lane-Based Queue Lengths for Signalized Intersections. Journal of Advanced Transportation. Vol. 2018.

Li, R., and P. Shang. Incident Duration Modeling Using Flexible Parametric Hazard-based Models. Computational Intelligence and Neuroscience, Vol. 2014, 2014, p. 33.

79

Li, R., F. C. Pereira, and M. E. Ben-Akiva. Competing Risk Mixture Model and Text Analysis for Sequential Incident Duration Prediction. Transportation Research Part C: Emerging Technologies, Vol. 54, 2015, pp. 74–85.

Li, X., A. J. Khattak, and B. Wali. Large-Scale Traffic Incident Duration Analysis: The Role of Multi-agency Response and On-Scene Times. Transportation Research Record: Journal of the Transportation Research Board, 2017. 2616: 39–48.

Lighthill, M. J. and G.B. Whitham. 1955. On kinematic waves II. A theory of traffic flow on long crowded roads. Proceedings of Royal Society. Vol. 229, No. 1178, pp. 317-345.

Lin, P.-W., N. Zou, and G. L. Chang. Integration of a Discrete Choice Model and a Rule-based System for Estimation of Incident Duration: a Case Study in Maryland. Presented at 83rd Annual Meeting of the Transportation Research Board, Washington, D.C., 2004.

Ma, X., C. Ding, S. Luan, Y. Wang, and Y. Wang. Prioritizing Influential Factors for Freeway Incident Clearance Time Prediction Using the Gradient Boosting Decision Trees Method. IEEE Transactions on Intelligent Transportation Systems, Vol. 18, No. 9, 2017, pp. 2303–2310.

MDOT. 2023. Internet Traffic Monitoring System (ITMS).

Mehran, B. and H. Nakamura. 2009. Implementing travel time reliability for evaluation of congestion relief schemes on expressways. Transportation Research Record. Vol. 2124, pp. 137-147.

Messner, A., and M. Papageorgiou. 1990. "METANET: A macroscopic simulation program for motorway networks." Traffic Eng. Control 31 (9): 466–470.

Mirchandani, P. and L. Head. 2001. A real-time traffic signal control system: architecture, algorithms, and analysis. Transportation Research Part C: Emerging Technologies. Vol. 9, No. 6, pp. 415–432.

Nam, D. H. and D. R. Drew. 1998. Analyzing freeway traffic under congestion: Traffic dynamics approach. Journal of Transportation Engineering. Vol. 124, no. 3, pp. 208-212.

Newell, G.F. 1968a. Queues with time-dependent arrival rates: I. The transition through saturation. Journal of Applied Probability. Vol. 5, No. 2, pp. 436-451.

Newell, G.F. 1968b. Queues with time-dependent arrival rates: II. The maximum queue and the return to equilibrium. Journal of Applied Probability. Vol. 5, No. 3, pp. 579-590.

Newell, G.F. 1968c. Queues with time-dependent arrival rates: III. A mild rush hour. Jounral of Applied Probability. Vol. 5, No. 3, pp. 591-606.

Newell, G.F. 1982. Applications of queueing theory (second ed.). Chapman and Hall Ltd. New YorkM. Albanese, R. Camus, and G. Longo. 2003. Capacity and Queue Modeling for On-Ramp-Freeway Junctions. Transportation Research Record. Vol. 1852, No. 1, pp. 256-264.

Nie, X. and H. Zhang. 2005. A comparative study of some macroscopic link models used in dynamic traffic assignment. Networks and Spatial Economics. Vol. 5, no. 1, pp. 89-115.

Ozbay, K., and P. Kachroo. Incident Management in Intelligent Transportation Systems. Artech House Inc., Mass., 1999.

Ozbay, K., and N. Noyan Estimation of Incident Clearance Times Using Bayesian Networks Approach. Accident Analysis & Prevention, Vol. 38, No. 3, 2006, pp. 542–555.

Park, H., A. Haghani, and X. Zhang. Interpretation of Bayesian Neural Networks for Predicting the Duration of Detected Incidents. Journal of Intelligent Transportation Systems, Vol. 20, No. 4, 2016, pp. 385–400.

Park, H. J., S. Gao, and A. Haghani. Sequential Interpretation and Prediction of Secondary Incident Probability in Real Time. Presented at 96th Annual Meeting of the Transportation Research Board, Washington, D.C., 2017.

Peeta, S., J. Ramos, and R. Pasupathy. Content of Variable Message Signs and Online Driver Behavior. Transportation Research Record: Journal of the Transportation Research Board, 2000. 1725: 102–108

Peeta, S., and S. Gedela. Real-Time Variable Message Sign-Based Route Guidance Consistent with Driver Behavior. Transportation Research Record: Journal of the Transportation Research Board, 2001. 1752: 117–125.

Pettet, G., S. Nannapaneni, B. Stadnick, A. Dubey, and G. Biswas. Incident Analysis and Prediction Using Clustering and Bayesian Network. Proc., The First IEEE International Conference on Smart City Innovations (IEEE SCI 2017), San Francisco Bay Area, USA, Institute of Electrical and Electronics Engineers (IEEE), 2017.

Persaud, B., S. Yagar, and R. Brownlee. 1998. Exporation of the breakddown phenomenon in freeway traffic. Transportation Research Record.

Pihur, V., Datta, S. & Datta, S. RankAggreg, an R package for weighted rank aggregation. BMC Bioinformatics, Vol. 10, 62, 2009.

PTV Group. 2023. VISSIM Simulation.

Qi, Y., and H. Teng. An Information-based Time Sequential Approach to Online Incident Duration Prediction. Journal of Intelligent Transportation Systems, Vol. 12, No. 1, 2008, pp. 1–12.

Richards, P. I. 1956. Shock waves on the highways. Operations Research. Vol. 4, pp. 42-51.

Runarsson, T. P. and Yao, X. 2000. Stochastic ranking for constrained evolutionary optimization. Vol. 4, No. 3, pp. 284-294.

Sharma, A., D. M. Bullock, and J. A. Bonneson. 2007. Input-output and hybrid techniques for real-time prediction of delay and maximum queue length at signalized intersections. Transportation Research Record, No. 2035, pp. 69–80, 2007.

Sadek, A. W., B. L. Smith, and M. J. Demetsky. Artificial Intelligence Search Algorithms for Dynamic Traffic Routing. Transportation Research Record: Journal of the Transportation Research Board, 1999. 1679: 87–94.

Sadek, A. W., B. L. Smith, and M. J. Demetsky. Artificial Intelligence-Based Architecture for Real-Time Traffic Flow Management. Transportation Research Record: Journal of the Transportation Research Board, 1998. 1651: 53–58.

Sarvi, M., M. Kuwahara, and A. Ceder. 2007. Observing freeway ramp merging phenomena in congested traffic. Journal of Advanced Transportation. Vol. 41, No. 2, pp. 145-170.

Sheu, J.-B., Y.-H. Chou, and L.-J. Shen. 2001. A stochastic estimation approach to real-time prediction of incident effects on freeway traffic congestion. Transportation Research Part B. Vol. 35, pp. 575-592.

Spall, J. C. 1998. An Overview of the Simultaneous Perturbation Method for Efficient Optimization. John Hopkins APL Technical Digest. Vol. 4, pp. 482-492.

Ullman, G.L. and C.L. Dudek. 2003. Theoretical Approach to Predicting Traffic Queues at Short-Term Work Zones on High-Volume Roadways in Urban Areas. Transportation Research Record. Vol. 1824, No. 1, pp. 29-36.

Valenti, G., M. Lelli, and D. Cucina. A Comparative Study of Models for the Incident Duration Prediction. European Transport Research Review, Vol. 2, No. 2, 2010, pp. 103–111.

Vickrey, W. 1969. Congestion theory and transport investment. The American Economic Review. Vol. 39, no. 8, pp. 251-260.

Vlahogianni, E. I., and M. G. Karlaftis. Fuzzy Entropy Neural Network Freeway Incident Duration Modeling with Single and Competing Uncertainties. Computer Aided Civil and Infrastructure Engineering, Vol. 28, No. 6, 2013, pp. 420–433.

Wang, X., S. Chen, and W. Zheng. Traffic Incident Duration Prediction Based on Partial Least Squares Regression. Procedia-Social and Behavioral Sciences, Vol. 96, 2013, pp. 425–432.

Wang, J., C. Haozhe, and Q. Shi. Estimating Freeway Incident Duration Using Accelerated Failure Time Modeling. Safety Science, Vol. 54, 2013, pp. 43–50.

Wang, S., R. Li, and M. Guo, Application of nonparametric regression in predicting traffic incident duration. Transport, Vol. 33, No. 1, 2018, 22-31.

Wang, W., H. Chen, and M. C. Bell. Vehicle Breakdown Duration Modelling. Journal of Transportation and Statistics, Vol. 8, No. 1, 2005, pp. 75–84.

Wei, C. H., and Y. Lee. Sequential Forecast of Incident Duration Using Artificial Neural Network models. Accident Analysis & Prevention, Vol. 39, No. 5, 2007, pp. 944–954.

Weng, J. and Q. Meng. 2013. Estimating capacity and traffic delay in work zones: An overview. Transportation Research Part C: Emerging Technologies.

Won, M., K. Heyonmi, and G. L. Chang. Knowledge-Based System for Estimating Incident Clearance Duration for Maryland I-95. Transportation Research Record. Vol. 2072, No. 14, 2018, pp. 61-72.

Won, M. Development of a Traffic Incident Management Support System. 2019, PhD Thesis, University of Maryland, College Park.

Wu, W. W., S. Y. Chen, and C. J. Zheng. Traffic Incident Duration Prediction Based on Support Vector Regression. Proc., 11th International Conference of Chinese Transportation Professionals (ICCTP 2011): Towards Sustainable Transportation Systems, Nanjing, China, American Society of Civil Engineers (ASCE), 2011, pp. 2412–2421.

Xiong, C., X. Chen, X. He, X. Lin, and L. Zhang. AgentBased En-Route Diversion: Dynamic Behavioral Responses and Network Performance Represented by Macroscopic Fundamental Diagrams. Transportation Research Part C: Emerging Technologies, Vol. 64, 2016, pp. 148–163.

Yang, G., Z. Tian, H. Xu, and D. Wang. 2016. Queue length estimation at metered freeway-to-freeway connectors. Journal of Advanced Transportation. Vol. 50, No. 8, pp. 1912-1924.

Yi, H. and T. Mulinazzi. 2007. Observed distribution patterns of on-ramp merge lengths on urban freeways. Transportation Research Record.

Yuan, K. V.L. Koop, and S.P. Hoogendoorn. 2017. A Microscopic Investigation Into the Capacity Drop: Impacts of Longitudinal Behavior on the Queue Discharge Rate. Transportation Science.

Zhang, Z, J. Liu, X. Li, and A. J. Khattak. Do Larger Sample Sizes Increase the Reliability of Traffic Incident Duration Models? A Case Study of East Tennessee Incidents. Transportation Research Record, 2021.

Zou, Y., K. Henrickson, D. Lord, Y. Wang, and K. Xu. Application of Finite Mixture Models for Analysing Freeway Incident Clearance Time. Transportmetrica A: Transport Science, Vol. 12, No. 2, 2016, pp. 99–115.

Zhao, X., R. Li, and X. Yu. Incident Duration Model on Urban Freeways Based on Classification and Regression Tree. Proc., 2009 Second International Conference on Intelligent Computation Technology and Automation, Changsha, Hunan, China, IEEE, New York, 2009.

Zhu, W., Z. Zeng, Y. Wang, and Z. Pu. Predicting Incident Duration based on Spatiotemporal Heterogeneous Pattern Recognition. Presented at 96th Annual Meeting of the Transportation Research Board, Washington, D.C., 2017.